NASA-CR-195,367

Advanced Turbine Technology
ATTAP
Applications Project

DOE/NASA 0336-4
NASA CR-195367
EDR 16624

1991 Annual Report

Allison
Gas Turbine Division
General Motors Corporation
P.O. Box 420
Indianapolis, Indiana 46206-0420

December 1992

Final

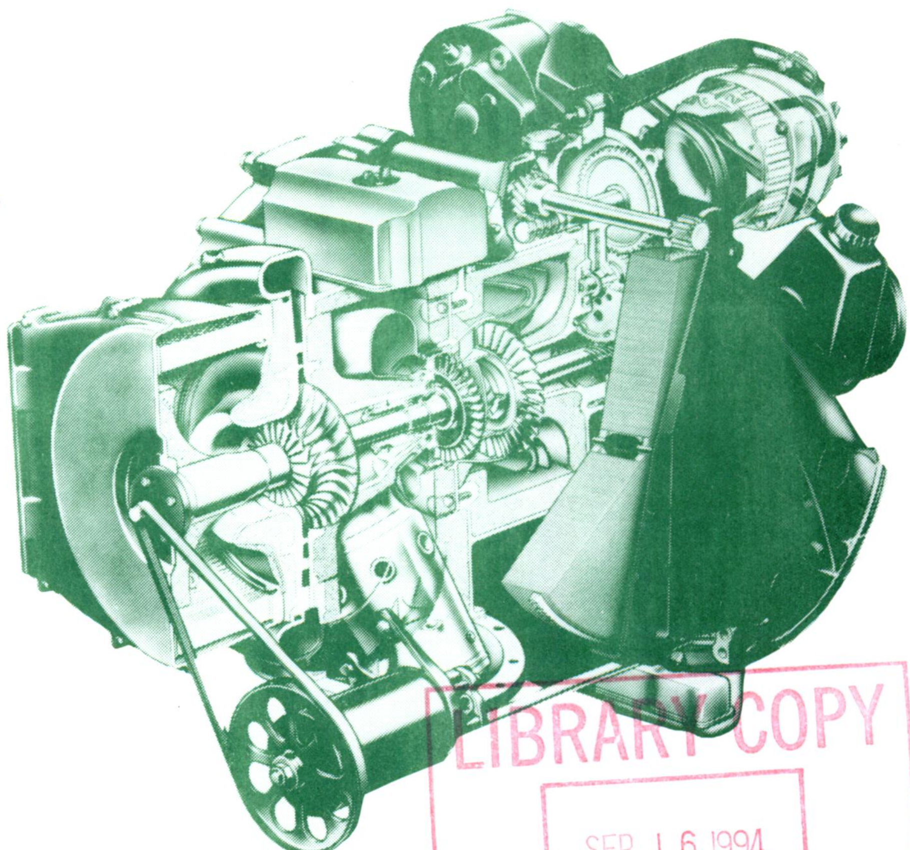

Prepared for
National Aeronautics
and Space Administration
Lewis Research Center
Cleveland, Ohio 44135
Contract DEN 4-336

For U.S. Department of Energy
Conservation and Renewable Energy
Office of Transportation Technologies

NOTICE

DOE/NASA 0336-3
NASA CR-189142
EDR 16624

Advanced Turbine Technology
ATTAP
Applications Project

1991 Annual Report

Allison
Gas Turbine Division
General Motors Corporation
P.O. Box 420
Indianapolis, Indiana 46206-0420

December 1992

Final

Prepared for
National Aeronautics
and Space Administration
Lewis Research Center
Cleveland, Ohio 44135
Contract DEN 3-336

For U.S. Department of Energy
Conservation and Renewable Energy
Office of Transportation Technologies

FOREWORD

This report presents a technical summary of work accomplished on the Advanced Turbine Technology Applications Project (ATTAP) under NASA contract DEN3-336 for calendar year 1991. The report is set up and arranged per the original Work Breakdown Structure (WBS). Only WBSs with activity in 1991 are reported herein.

This technology project is funded by the U.S. Department of Energy, Energy Efficiency & Renewable Energy, Office of Transportation Systems, Office of Propulsion Systems, Advanced Propulsion Division. Project management and technical direction are provided by the NASA Lewis Research Center (LeRC), Aeronautics Directorate, Propulsion Systems Division, Terrestrial Propulsion Office.

The overall intent of the ATTAP is to bring the automotive gas turbine engine to a technology state at which industry can make commercialization decisions. Key to this goal is the development and demonstration of structural ceramic component technology as the critical high risk/high payoff element in this type of engine. Such ceramic technology is the prime ATTAP focus. Automotive gas turbine attractions include the following potential advantages:

- Significantly increased fuel economy
- Ability to meet Federal emission standards with untreated exhaust
- Ability to operate on a wide range of alternate fuels
- Inherently smooth, low-vibration operation

General Motors (GM) is addressing the ATTAP with a team that draws on:

- The extensive ceramic design, analysis, and materials data base and expertise in place at the Allison Gas Turbine Division (Allison)
- The substantial experience, design and test capabilities, automotive gas turbine technology and hardware, and test vehicle resources that were developed under GM funding as background to this project and are in place at GM's Advanced Engineering Staff (AES)
- The infrastructure of expertise and resources in place in the American ceramics industry and the working relationships between the industry and Allison
- The unique capabilities and resources existing at universities and at national laboratories, such as the High Temperature Materials Laboratory (HTML) at the Oak Ridge National Laboratory (ORNL)

In this arrangement, Allison serves as prime contractor. Major ceramics industry development subcontractors to date are: The Carborundum Company (CBO), Corning Inc., Manville Corp, Ceramics Process Systems (CPS), and Norton/TRW Ceramics (N/TRW). A major ceramic component supplier is the Kyocera Industrial Ceramics Corporation.

TABLE OF CONTENTS

LIST OF ILLUSTRATIONS

LIST OF ILLUSTRATIONS (cont)

LIST OF ILLUSTRATIONS (cont)

LIST OF TABLES

SUMMARY

ATTAP activities during the past year included test-bed engine design and development, ceramic component design, materials and component characterization, ceramic component process development and fabrication, ceramic component rig testing, and test-bed engine fabrication and testing. Although substantial technical challenges remain, all areas exhibited progress.

Test-bed engine design and development included engine mechanical design, combustion system design, alternate aerodynamic designs of ceramic gasifier scrolls, and engine system integration aimed at upgrading the AGT-5 from a 1038°C (1900°F) metal engine to a durable 1371°C (2500°F) structural ceramic component test-bed engine. A finite element method (FEM) analysis of the regenerator seals was completed, and a seal design optimization experiment conducted, leading to redesign of the regenerator seals. Two types of insulating hot crossarm inserts were designed for seal leaf thermal gradient reduction. Combustion system design/development included testing three diffusion flame combustor modifications. One combustor modification test with methanol successfully passed current federal emissions standards using the transient urban driving cycle. In addition, the first low emission combustor design underwent FEM analysis and a preliminary design review. In the aerodynamics area, an advanced concept scroll was analytically modeled, fabricated, and the flow characteristics were subsequently measured. Engine control developmental efforts included completion of initial testing, debugging, and usage of the EDM-800 controller in a turbine vehicle.

ATTAP-defined ceramic and associated ceramic/metal component design activities completed include: the ceramic gasifier turbine static structure, the ceramic gasifier turbine rotor, ceramic combustors, the ceramic regenerator disk, the ceramic power turbine rotors, and the ceramic/metal power turbine static structure. Ceramic combustor efforts included construction of 2-D finite element models to calculate component temperatures, deflections, stress profiles, and the resulting Probability of Survival (POS) for N/TRW and CBO combustors. Each of the combustor configurations met the minimum POS at maximum power steady-state operating conditions, limited by the stress concentration at the edge of the primary air holes. When ultimately tested, an "as manufactured" silicone carbide combustor failed due to elevated through-wall thermal gradients. This was corrected by reducing wall thickness. The design of an advanced concept gasifier scroll, utilizing independent ceramic mount rings to eliminate thermal stresses, was completed.
2-D finite element structural analysis showed acceptable POS for the scroll and mount assembly using N/TRW siliconized SiC. A full scale polycarbonate prototype of the scroll was subsequently used for cold flow aerodynamic tests as well as for mold development by a ceramic vendor. 26-bladed gasifier rotor designs, intended to increase efficiency and test Foreign Object Damage (FOD) tolerance, were completed. FEM analyses were performed for rotors using CPS's CM200, N/TRW's NT154, and Kyocera's SN252 materials. A 3-D FEM cold proof spin test analysis showed that a larger blade root fillet was needed in the leading edge region. This larger fillet was incorporated into the N/TRW and Kyocera rotors. Polycarbonate prototypes of the 26-bladed rotor (full size) and a ten times size blade root fillet were generated to aid in rotor construction.

The materials and component characterization efforts included the testing and evaluation of seven candidate ceramic materials and three components being developed for use in the ATTAP. Material characterization focused on microstructural, density, fracture toughness, and flexural strength evaluations of various candidate ceramic materials. Fracture surface analysis was also used to determine the nature and location of the strength-controlling defects. In addition, the time-dependent strength and oxidation resistance characteristics were evaluated for selected materials.

Ceramic component process development and fabrication proceeded for the gasifier turbine rotor, gasifier turbine scroll, gasifier turbine vanes and vane platform, extruded regenerator disks, and thermal insulation. Major ceramic industry development subcontractors are: CBO,

Manville Corp., Corning Inc., CPS, and N/TRW. Characterization of CBO's α-SiC material showed significant improvements in the current generation of slip cast sintered material relative to previously evaluated material. Improvements in the slip casting process included the use of powder beneficiation, particle size optimization, and high shear mixing. Manville concentrated on the development and fabrication of ceramic thermal insulation for the test rigs and engines. Fifteen pressure slip cast GN-10 Si_3N_4 tensile specimens from GCC were also characterized. The material was evaluated at the ORNL HTML. CPS addressed the fabrication of CM200 sialon gasifier turbine rotors using their Quickset injection molding process. N/TRW developed both gasifier turbine rotors (fabricated by pressure slip casting NT154 and NT164 Si_3N_4) and turbine scrolls (fabricated of slip cast NT230 SiC). A cooperative effort between N/TRW and CPS focused on co-developing NT154 Si_3N_4 vane platforms utilizing the Quickset injection molding process. Kyocera provided SN252 Si_3N_4 first-stage power turbine rotors and SN235 Si_3N_4 second-stage power turbine rotors. The second-stage rotor was constructed using Kyocera's new forming process.

Component rig activities included the development of both rigs and the necessary test procedures, and conduction of rig testing of the ceramic components and assemblies. All ceramic components are rig proof tested prior to engine test-bed installation. Two significant milestones were reached in 1991. High temperature capability of ceramic static and rotating components was demonstrated with an all-ceramic gasifier assembly that successfully completed a 100 hour durability test. The majority of the test time was under the ATTAP durability schedule with peak conditions of 1371°C (2500°F) at 100 percent speed. The potential for long-term rotor durability was demonstrated with a ceramic gasifier rotor that reached a total of 1000.7 test hours under severe operating conditions. Additional proof tests were run on three other ceramic scroll assemblies and four gasifier rotors. Regenerator rig tests included the evaluation of a Corning extruded aluminum silicate sample. Tests of metal regenerator candidate materials included Inco Alloys In 6262 and Plansee PM2000 samples.

Table I.
Total test hours.

	Test hours		
	Pre-1991	1991	Cumulative
Engine test hours	1592	128	1720
Hot rig test hours	852	719	1571
Totals	2444	847	3291

Test-bed engine fabrication, testing, and development supported improvements in ceramic component technology that will permit the achievement of both program performance and durability goals. Both long-term cyclic and steady-state engine tests are being performed. Test-bed engine activities included completing the shakedown testing of a compressor rig, fabricating and assembling static inlet guide vanes, and fabricating a compressor shroud with wear pegs for an impeller tip clearance test. Five different burner configurations were tested on both DF-1 and M85 fuels. Total test time in 1991 is shown in Table I.

INTRODUCTION

This is the fourth of a series of annual reports documenting work performed on the ATTAP. This work is being conducted by a team directed by GM, with significant activities underway at GM's Allison Gas Turbine Division (which serves as prime contractor), at GM's AES located at the General Motors' Technical Center, and at the several domestic ceramic suppliers who are under development subcontracts. The U.S. Department of Energy (DOE) sponsors this work, which is managed and technically directed by NASA-Lewis Research Center under contract DEN3-336.

GOAL AND OBJECTIVES

ATTAP is intended to advance the technological readiness of an automotive ceramic gas turbine engine based on efforts begun in the Automotive Gas Turbine (AGT) Project, a DOE/NASA program executed between 1979 and 1987. This AGT project successfully demonstrated the feasibility of using structural ceramic hot-section components in automotive-sized gas turbine engines. Specifically, ATTAP aims to develop and demonstrate the technology of structural ceramics that have the potential for competitive automotive engine life cycle cost and for operating for 3500 hr (automotive engine life) in a turbine engine environment at temperatures up to 1371°C (2500°F). Project objectives are the following:

- Enhance the development of analytical tools for ceramic component design using the evolving ceramic properties data base
- Establish improved processes for fabricating advanced ceramic components
- Develop improved procedures for testing ceramic components
- Evaluate ceramic component reliability and durability in an engine environment

PROGRAM SCHEDULE AND CONTENT

Figure 1 shows the scheduled activities in the 61-month program. Materials assessment occurred at the initiation of ATTAP and resulted in the targeting of ceramic component technology goals and the identification of materials, processes, and manufacturers to address those goals. The materials assessment was updated in Year 3 and will be updated in Year 5, at which time the state of the art will be reassessed for each component and required technology improvements will be redefined. The identification and evaluation of materials, processes, and manufacturers are ongoing, continuous activities in ATTAP, and promising candidates are integrated into the program as merited. Similarly, those technologies and/or ceramic component suppliers which do not productively evolve to address program goals are truncated from ATTAP.

Reference Powertrain Design (RPD) activities include the preliminary design of a powertrain system which could meet performance, cost, and reliability design goals. Such a design was executed at the beginning of ATTAP using a high temperature derivative of the AGT-5 automotive gas turbine engine. The RPD was updated in Year 3 to reflect current ceramic component technology and goals, and will be updated again in Year 5 to provide a cost estimate of such a powertrain in production.

Test-bed engine development, shown in Figure 1 as an intermittent activity, includes those efforts aimed at ensuring the availability and functionality of the AGT-5 gas turbine engine as the test-bed for the high temperature ceramic components. Although engine development is not a primary focus of ATTAP, these activities

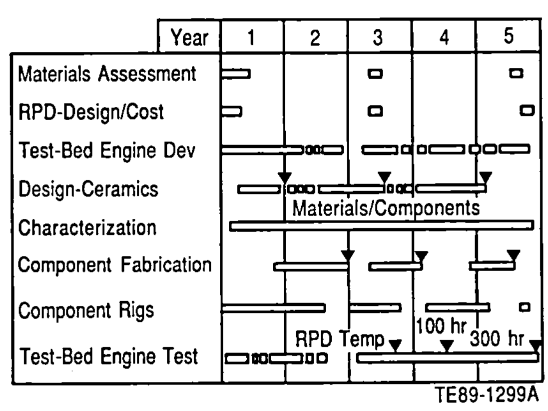

Figure 1. ATTAP schedule.

recognize the need for continuing evolution of the engine to handle the power and thermal loads, as well as design changes resulting from the integration of a high temperature flow path.

Central to the logic of Allison's ATTAP approach is an iterative component development cycle. Three such cycles are shown in Figure 1 and include the design/fabrication/characterization/rigs/engine test sequences of activities. These three development cycles reflect anticipated improvements in ceramic materials and the associated component processing technologies, and the incorporation of laboratory characterization data and rig/engine test results into succeeding designs. The initial design activity, shown with a milestone at the end of Year 1, featured then-current monolithic ceramic technology in the design of the gasifier turbine stage of the AGT-5 engine for 1371°C (2500°F) turbine inlet temperature (TIT) plus other required hot flow-path pieces. The second design phase incorporated toughened monolithic materials, used in the same gasifier stage components. The third phase will incorporate advanced (e.g., from Oak Ridge's Ceramic Technology for Advanced Heat Engines [CTAHE] project) materials and processes as they become available. Additionally, these succeeding design phases include other necessary ceramic components in the high-temperature test-bed engine, notably power turbine flow-path pieces. Component fabrication includes those process development activities executed by ceramic suppliers that result in the fabrication of engine-usable components. Characterization involves those laboratory activities both at suppliers and at Allison which measure and define the various properties and qualities of ceramic materials in both test bar form and in components. Examples are microstructural evaluation and measurements of density, strength, oxidation resistance, toughness, etc. Included are the development and application of nondestructive evaluation (NDE) techniques.

Component rig activity includes the development of rigs for component verification and testing (e.g., hot gasifier turbine rigs) as well as the actual testing activities. Test-bed engine test includes those testing activities associated with test-bed engine development plus the verification and development testing of the ceramic components. Note that each of the three component development cycles begins with design, followed by component fabrication, characterization, then rig testing, and finally engine testing. This rigorous development process, shown in Figure 2, is iterative between the users and the ceramic supplier community and ensures developing an understanding of the behavior of components in service and the continuous identification of areas for improvement.

TEST-BED ENGINE AND RPD

Figure 3 shows the automotive gas turbine engine being used as the ceramic component development test-bed for the ATTAP. This GM-developed engine, the AGT-5, is a two-shaft, regenerative configuration with axial-flow gasifier and power turbines. The engine produces approximately 110 hp at its original full-power TIT of 1038°C (1900°F).

The emissions and alternate fuels goals are considered achievable based on demonstrated GM experience. For example, the AGT100 (from AGT Project) engine's combustion system has displayed laboratory steady-state emissions of oxides of nitrogen (NO_x), CO, and unburned hydrocarbons (UHC) well within current Federal Emissions Standards using diesel fuel, jet fuel, and methanol. The AGT-5 engine has successfully run on dry powdered coal. Although such systems have demonstrated the potential for low emission/alternate fuel gas turbine combustion, much work remains to achieve a fully-functional system suitable for automotive application. Such efforts are outside the scope of ATTAP. The definition of power plant cost and reliability goals, in addition to performance, is included in ATTAP.

CRITICAL COMPONENTS

Consistent with the strong ATTAP emphasis on ceramic component technology is the focus on specific gas turbine components as development/demonstration targets. Four ceramic components and the engine insulation have been identified as critical development components because: (1) their functional success is critical to the viability of the ceramic automotive gas turbine engine, and (2) each requires some

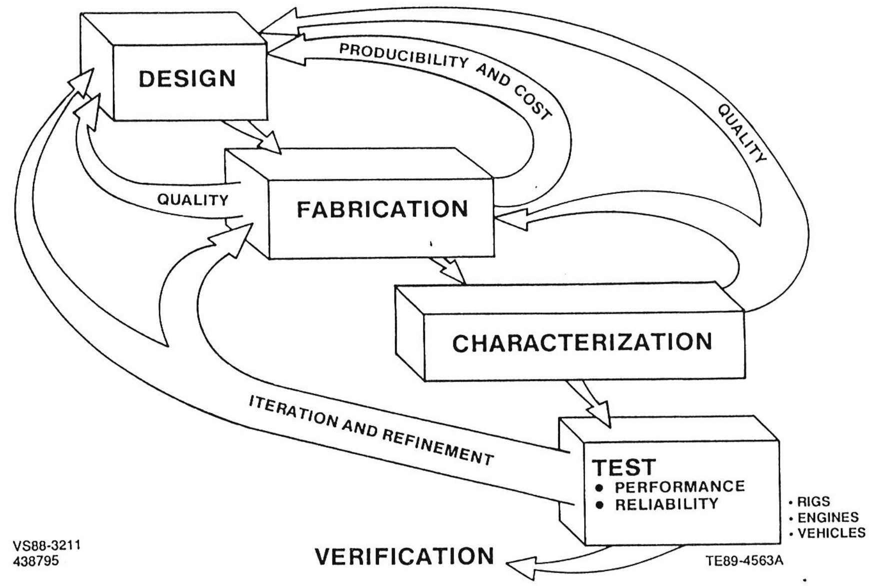

Figure 2. Ceramic component development cycle.

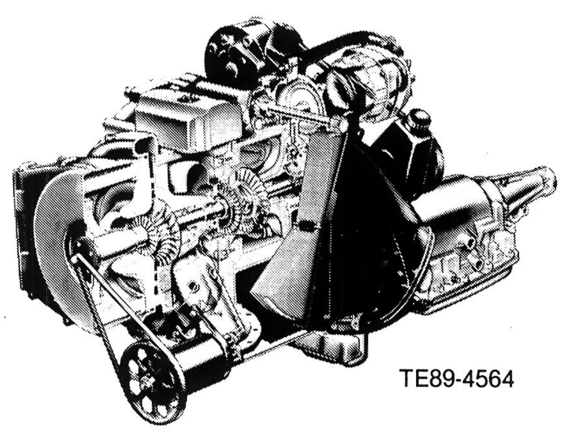

Figure 3. ATTAP test-bed engine--AGT-5.

further technological development to be proven reliable and durable in the automotive engine environment, as well as cost effective. These critical elements, shown in Figure 4, are the following:

- gasifier turbine rotor
- gasifier turbine vanes
- gasifier turbine scroll
- regenerator disks
- thermal insulation

For each component, specific areas and parameters requiring improvement have been identified and quantified where possible.

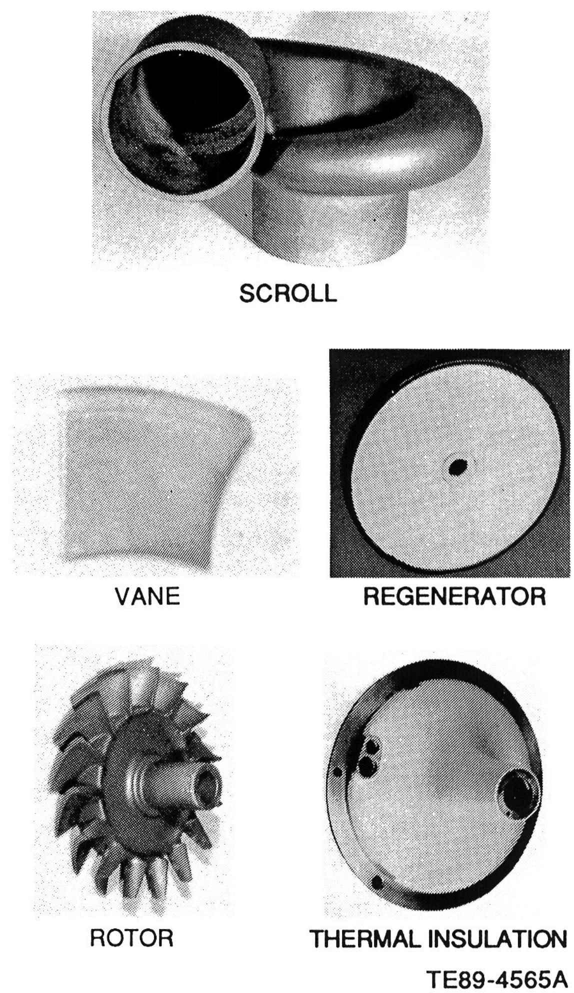

Figure 4. Ceramic components selected for development.

I. ENGINE/POWERTRAIN DESIGN AND DEVELOPMENT, ANALYSIS, AND MATERIALS ASSESSMENT

1.2 REFERENCE POWERTRAIN DESIGN (RPD)

An RPD was completed at the outset of ATTAP in order to ensure that the AGT-5 type power plant has the potential to fulfill the overall goals that underlie the DOE's sponsorship of automotive gas turbine technologies. This original RPD was a preliminary engineering design of a powertrain system that integrates with vehicle characteristics to provide a system with the potential for meeting not only performance, but also cost and reliability goals. Specific performance goals are the following:

- 30% improvements in fuel economy over the reference 1988 Pontiac Grand Am equipped with a 2.5 ℓ, 4-cylinder, spark-ignition engine over the combined Federal Driving Cycle
- competitive vehicle drivability and performance with the reference 1988 Grand Am
- gaseous emissions and particulate levels less than the following (based on diesel fuel No. 2):
  NO_x = 0.249 gm/km (0.4 gm/mile),
  HC = 0.255 gm/km (0.41 gm/mile),
  CO = 2.11 gm/km (3.4 gm/mile),
  particulates = 0.129 gm/km (0.2 gm/mile)
- ability to use a variety of alternate fuels

The RPD was partially updated in 1991 to reflect the current state of the art in automotive turbine development.

Table II shows the results of the current RPD performance simulation, based on the AGT-5-type engine, versus the baseline reference vehicle.

Thus the RPD gas turbine equivalent vehicle exceeds critical fuel economy and performance goals.

1.4 TEST-BED ENGINE DESIGN AND DEVELOPMENT

The overall objective of this task is to perform the required preliminary and detail design activities to ensure that the AGT-5 ATTAP rig(s) and test-bed engine(s) can accept improved ceramic components and operate at the higher temperatures permitted by improved ceramics. Design activities are based on the RPD operating conditions. Specifically, efforts are concentrated in the following four areas:

- mechanical
- combustion systems
- alternate flow paths
- engine system integration

1.4.1 Mechanical

Objective/Approach

The objective of the mechanical design and development activity is to upgrade the AGT-5 from a 1038°C (1900°F) metal engine to a durable 1371°C (2500°F) structural ceramic component test-bed engine.

Table II.
Comparison of the 1991 RPD vehicle performance to baseline Grand Am.

	Baseline--2.5 ℓ spark-ignition	1991 RPD--turbine
0-96.5 kmph (60 mph) time--sec	13.5	13.3
Composite fuel economy-- ℓ /100 km (miles/gal)	7.66 (30.7)	4.46 (44.2)

Accomplishments/Results

- Performed initial design, fabrication and cold flow testing of redesigned regenerator seals.
- Conducted regenerator seal design optimization experiment, leading to completed detail redesign of the regenerator seals.
- Conducted thermal and mechanical finite element modeling (FEM) for analysis of regenerator seal system thermal gradients and stress.
- Designed two types of insulating hot crossarm inserts for seal leaf thermal gradient reduction.
- Completed redesign of the regenerator wearface system.
- Analyzed gearbox noise data from current metal AGT-5 engine and correlated the noise data with a finite element shaft dynamics model. Although the noise data is too sparse to form a firm conclusion, it appears likely that an excitation frequency twice the power turbine speed is exciting a power turbine shaft bending mode.
- Designed a nylon insert to limit the amplitude of shaft vibrations.

Discussion

Redesigned Regenerator Seal System. During 1991, the regenerator seal system was redesigned. The goal of this redesign was to increase seal durability for the 1371°C (2500°F) TIT conditions, while increasing sealing capability and reducing the seal system cost.

An initial seal design was fabricated and tested in a cold-flow seal testing fixture. Preliminary results of this cold flow testing of the redesigned seals indicated cold leakage reductions of greater than fifty percent when compared to current regenerator seal system cold leakage.

With the high initial success of the redesigned seal system, a seal design optimization experiment was set up using General Motors' DEXPERT Design of Experiments system. DEXPERT was utilized to set up a full-factorial experiment of four seal design parameters (e.g., seal thickness, seal preload, etc.)--for 81 experimental combinations. Three of the tested design parameters were found to have a significant effect on the leakage characteristics of the seal. The results of this study were used to optimize the redesigned seals, and detail seal designs were then completed.

Once this seal detail mechanical design was completed, thermal and mechanical finite element method (FEM) models were used to determine the seal system's projected thermal gradient, stress, and deflection characteristics. This analysis was to verify that the redesigned seal system will have acceptable stress levels and sealing ability during 1371°C (2500°F) TIT operation. FEM revealed an unacceptable thermal gradient for the system in the hot crossarm region, leading to predicted thermal stresses above the yield point of the seal material. Incidents of thermal buckling of the seal leafs of the current seal system often occur after full RPD temperature operation. Further analysis was used to develop the specification for maximum thermal gradient of 260°C (500°F) ΔT_{leaf}. With the leaf thermal gradient held below that level, leaf stresses are projected to be well under the yield limit of the seal material, and thermally induced deflections will not unseat the seal.

In order to satisfy the maximum leaf thermal gradient specification in the hot crossarm region, an insulating insert design was developed. Two-dimensional finite element heat transfer models of the hot crossarm region were built for two different insulating insert designs. Using the finite element models, both designs were found to be capable of satisfying the maximum leaf thermal gradient specification. Scaled down test inserts were fabricated showing acceptable manufacturability of the insert system. The insulating insert design concept was then integrated into the redesigned regenerator seal system.

Since the redesigned seal system uses a straight crossarm (different than the current "V" crossarm design), a complete redesign of the regenerator wearface system was necessary. Design for Manufacturability and Assembly (DFMA) principles were followed in the wearface redesign, and the new wearface system has a significantly reduced part count and greatly increased ease of assembly. Pressure balance analysis was conducted, leading to the completed detail design of the revised regenerator wearface system.

Gearbox Noise. Noise data were taken from the original AGT-5 gearbox. The test consisted of keeping the gasifier speed constant and increasing the output shaft speed. This data provided the frequency and amplitude content of the noise for each output shaft speed.

A frequency analysis revealed the noise, whose amplitude is above 80 dB, to be synchronous with shaft speed indicating that the power turbine may be the source of the noise.

To correlate this data with shaft natural frequencies, a finite element analysis of the power turbine was conducted to determine shaft natural frequencies. The second natural shaft/bearing system frequency, with a mode shape showing a stationary rotor and a bending shaft, was calculated to be approximately equal to the test data results (Figure 5).

The motivation for undertaking this analysis lies in concerns of what will happen when ceramic components are installed. A finite element analysis was undertaken for the ceramic power turbine and a similar second-order power turbine mode was calculated to have approximately the same frequency as the test power turbine. Since reducing the natural frequency of this bending mode could shift to a first-order power turbine excitation, a possible solution is to try to limit the amplitude of vibration. This will be evaluated by adding a nylon insert between the shaft and the pinion at the location of maximum displacement as seen in Figure 5.

Air to Fuel Heat Exchanger. A feasibility study of an air to fuel heat exchanger for the regenerative AGT-5 engine was completed. Approximately five to seven percent of the hot gas stream would be bled from the flow path between the power turbine and the regenerator for use in the heat exchanger. The primary application would be to preheat methanol fuel for premixing combustors. Ideally, enough heat should be transferred to vaporize the fuel.

To avoid two phase flow at certain operating conditions, the fuel would be maintained above its critical pressure. This would require a change from the current variable speed fuel pump to a fuel system with a high pressure pump and a mass flow controller at the fuel nozzle. Pressure in the fuel line would be maintained at about 1200 psi and flash vaporization would occur in the combustor fuel preparation zone.

The large heat of vaporization of methanol makes it more difficult to vaporize than other commonly used fuels. By employing flash vaporization, the fuel preparation zone could be shortened. Another advantage would be an increase in fuel economy due to the recovery of waste heat.

In a premixing combustor with variable geometry, the fuel/air ratio in the reaction zone can be reduced to account for the increased energy content of the fuel and maintain constant flame

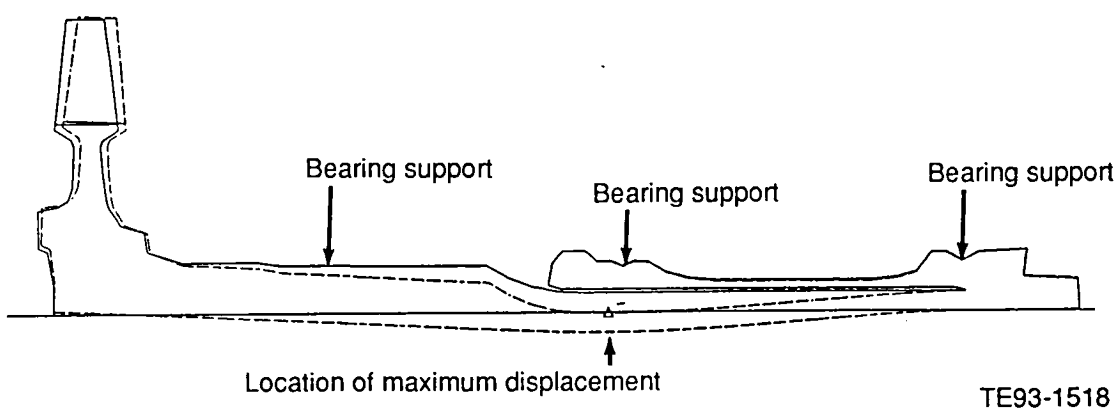

Figure 5. Power turbine shaft displacement—stationary rotor and bending shaft.

temperature. Therefore, NO_X emissions would not increase as they would if fuel preheat were employed in a diffusion flame combustor.

Prior to the study it was hoped that five to seven percent bleed could be tolerated without significantly depressing the combustor inlet temperature. However, the results show a drop of more than five degrees in the combustor inlet temperature for every percent of air bled. In fact, at low power the energy lost from the combustor inlet air actually exceeds that recovered in the fuel. Fuel turndown over the load range is so large that if the heat exchanger is designed to vaporize the fuel at high power, fuel and air flows in the exchanger become unbalanced at low power. At low power, the fuel rapidly reaches turbine exit temperature in the heat exchanger and very little energy is transferred.

Since the driving cycle is very heavily weighted towards low power, a negative heat recovery at this condition would seem to outweigh the advantage of shortening the combustor fuel preparation zone via flash vaporization. Based on this analysis, preheating the fuel was discarded as a viable option.

Fuel Nozzles. An experimental simplex airblast fuel nozzle supplied by Delavan was tested on the atmospheric spray stand. Airblast fuel nozzles use combustor pressure drop as the energy source for atomization as opposed to the air pump used by the standard AGT-5 air assist nozzle. The airblast nozzle demonstrated good atomization at idle and design point simulated conditions, but atomization was worse than that of the standard nozzle at start conditions. These are typical airblast characteristics. Performance on the atmospheric stand was encouraging enough to warrant engine testing where the ability to achieve ignition at cranking conditions will be determined. If reliable lightoff is obtained with the airblast nozzle, then the air pump requirement would be eliminated during starting as well as at load. Otherwise, Delavan will add air assist capability to the nozzle for starting.

Poppet Valve Design. In late 1990, a preliminary finite element structural analysis of the original AGT-5 low emissions poppet valve combustor (Version I) was completed. The analysis predicted unacceptable inner liner stresses at the high power operating condition. The combustor geometry was subsequently modified to incorporate backside convective cooling of the inner liner up to the poppet valve throat (Figure 6). A detailed 2-D axisymmetric finite element model of the Version II geometry was then generated (Figure 7), and a structural analysis initiated. Concurrently, the poppet valve combustor design was reviewed with the ODS alloy fabricator.

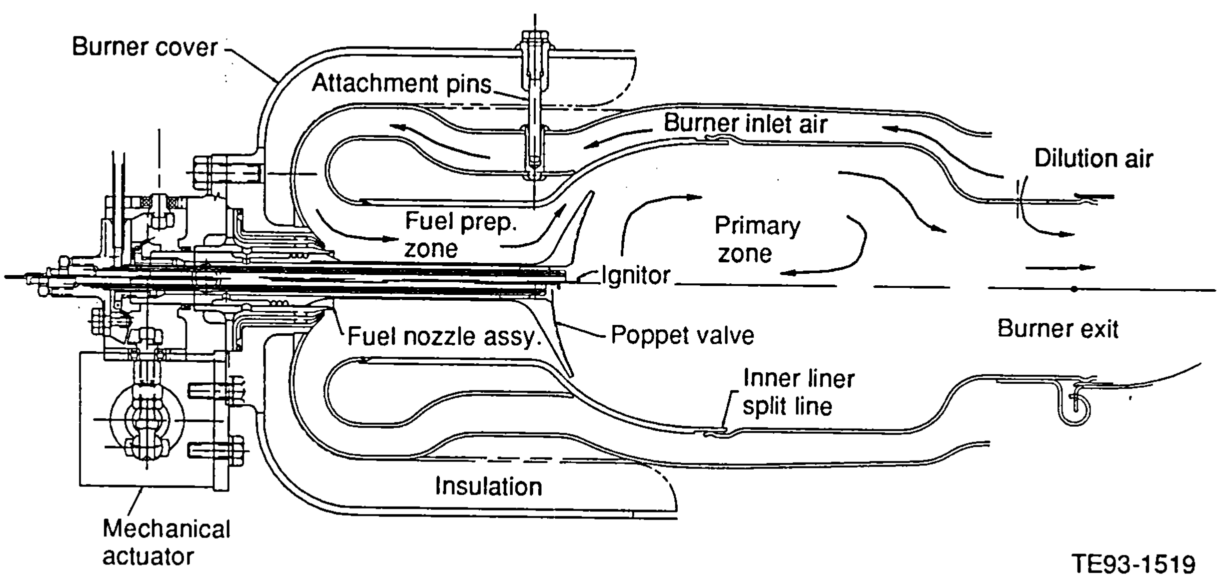

Figure 6. ATTAP AGT-5 low emissions combustor poppet valve Version I.

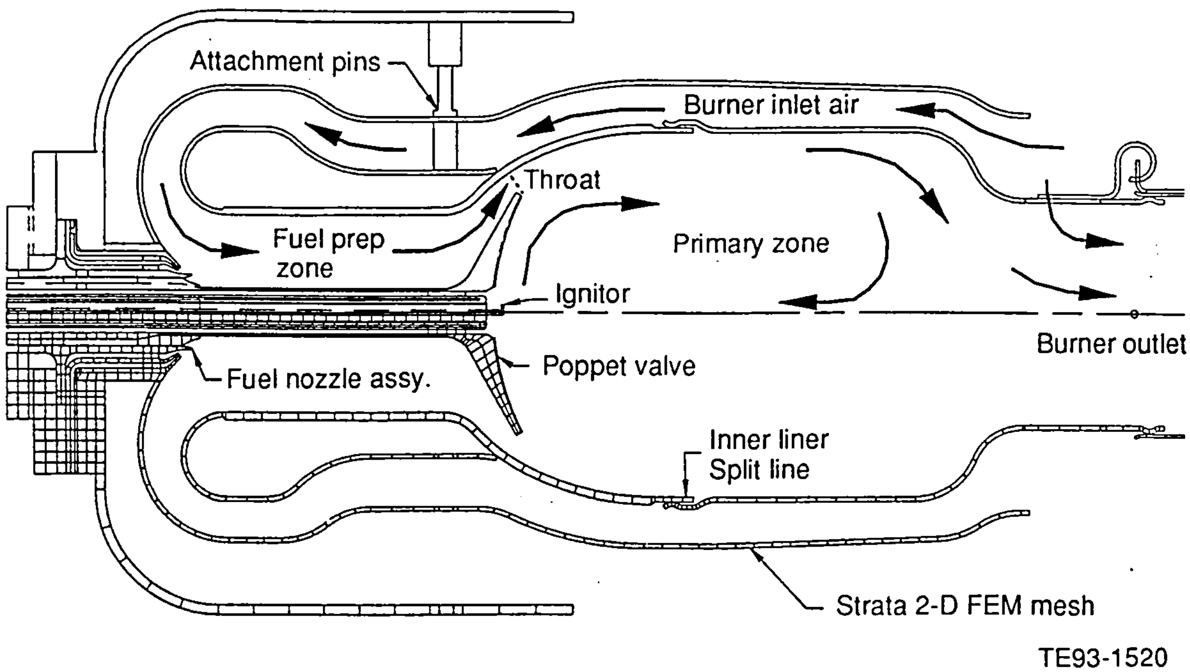

Figure 7. ATTAP AGT-5 low emissions combustor poppet valve Version II.

The vendor's response to the manufacturability question was favorable; however, it was suggested that the inner liner split line be shifted axially forward to coincide with the valve throat. The shift minimizes the liner thermal stress induced by a hot-to-cold wall transition. Additional modifications addressing the ignitor and actuation system are being incorporated into the Version III poppet valve combustor design. The combustor finite element structural analysis will be pursued upon completion of all proposed design modifications.

1.4.3 Alternate Flow Paths

Objective/Approach

Turbine aerodynamic development efforts are required to upgrade the existing 1038°C (1900°F) metal AGT-5 test-bed flow path to meet the requirements of the 1371°C(2500°F) RPD operating conditions. Activities during 1991 focused on developing a low cost gasifier scroll and flow testing RPD size turbomachinery.

Accomplishments/Results

- Completed two detailed flow tests of the advanced concept gasifier scroll.
- Measured pressure drop of the scroll to be half the pressure loss of the existing gasifier scroll.
- A CFD (computational fluid dynamics) model of the advanced concept gasifier scroll qualitatively matched the measured data; however, computer CPU requirements and convergence problems restricted use of the CFD model as a design tool.
- Released new aerodynamic geometry of the scroll for design.
- Flow tested and calibrated five gasifier scrolls for future engine builds.
- Flow tested one gasifier rotor.

Discussion

An aluminum model of the advanced concept gasifier scroll was constructed and detailed cold flow measurements were taken at the scroll exit. The total pressure loss was measured using 180 measurement locations to survey the exit of the aluminum model. There were a total of fifteen circumferential measurement locations. Twelve radial positions were used to map the hub to tip span at each circumferential location. The advanced concept scroll pressure loss was found to be less than half the loss of the present gasifier scroll. Based on the aluminum model, a preliminary ceramic advanced concept gasifier scroll was designed and procured. The preliminary ceramic scroll was also flow tested under the same conditions as discussed above. The geometry of the ceramic scroll was originally designed to match the aluminum model, but the shape was altered for vendor fabrication limitations. The internal geometry of the ceramic piece had several undesirable aerodynamic features, which led to an increase in the pressure drop:

Mass averaged pressure loss

Component	Total pressure loss ratio
Existing ceramic gasifier scroll	1.0
Advanced concept gasifier aluminum scroll model	0.43.
Ceramic advanced concept gasifier scroll	1.85

Five RPD size gasifier scrolls were instrumented with static throat taps and flow tested on a flow bench. During the test, the engine condition Reynolds number and expansion ratio (inlet total pressure to exit static pressure) were matched. The throat static pressure, exit static pressure and mass flow rate were recorded during the test. At equal expansion ratios, an eight percent variation was found in equivalent mass flow rates. The flow difference may be due to casting changes and initial casting problems.

An RPD size gasifier rotor was tested on the same flow bench used to test the gasifier scrolls. The rotor flow rate and expansion ratio were measured. The flow rate of the scroll and rotor were matched with a turbine component efficiency predictor program.

1.4.4 Engine System Integration

Objective/Approach

Development efforts on automatic control systems (control software and control hardware) are required to integrate ceramic components and 1371°C (2500°F) temperature capabilities into the AGT-5 test-bed engines and associated rigs.

Accomplishments/Results

- Completed initial testing/debugging of first EDM-800 controller in a turbine vehicle.
- Built and tested second set of EDM-800 I/O boards.
- Software written, tested, and verified for variable burner geometry (VBG).
- Stepper motor VBG actuator and driver investigated, received, and tested.
- Magnetoresistive sensor circuits included in new EDM-800 I/O board design.
- New magnetoresistive and hall effect sensor parts, including high temperature versions, assembled and tested.
- Turbine powered Camaro modified for methanol usage.
- Optical N_1 (N_1 = gasifier turbine shaft speed [rpm]) sensor fabricated.

Discussion

Engine Control. The Chevrolet Caprice, the latest turbine powered vehicle, has been checked out electronically and mechanically. During this time, many control and electrical systems issues were resolved. Testing involved a static check-out of all the computer input/output and electrical circuits followed by a vehicle test drive. No significant flaws were found and the control system seems to be working well. Additional test plans include: Emissions, Fuel economy, Performance, Driveability, Component Testing and Evaluation, and Powertrain Development.

Switching the Z28 Camaro over to run on methanol involves a change in many control program parameters and some engine hardware. When the changeover is complete, the lightoff is similar to Diesel fuel at room temperature. Most of these program changes are handled with a software assembly switch. The EDM-800 controller is the new generation of controllers that are replacing the old function control module (FCM) controller. The EDM, like all controllers, uses an input/output (I/O) board to condition the signals between the computer and the outside world. There are now two boards in use and more have been ordered. The new boards will incorporate the latest changes and updates required to correct previous problems, incorporate new sensors such as the magnetoresistive sensors, and drive new devices such as the VBG actuator. New signals include: pulse width modulated signals to the step motor driven VBG actuator, position feedback voltages from the actuator to the EDM, and barometric pressure sensor signal to the EDM.

The new equipment ordered consists of new I/O boards, a VMS-2000 laptop computer, and a standard laptop computer. The I/O boards mentioned above are required so that all the rigs and engines can be converted to the EDM-800 controllers. The VMS-2000 is a faster machine than the VMS-1000 currently in use. The VMS-1000 will still be used, but the VMS-2000 can compile programs about five times faster and update screen parameters much faster. The VMS-2000 is designed for rugged vehicular usage and will be installed in the Caprice turbine vehicle. For the test cells, a laptop computer will be used since it costs much less and does not have to meet the harsh demands of a vehicle. The laptop will provide practically all the same functions and speed as the VMS-2000.

Magnetoresistive (MR) sensors have significant advantages over conventional magnetic pickups for sensing shaft speeds. Among the advantages is a 10:1 increase in signal amplitude that is speed independent. The goal is to replace all four of the magnetic pickups used in an installation with custom designed MR sensors that are smaller and have superior performance at competitive prices. However, few MR sensors are available as end user products and most can not handle the high temperatures that may be encountered in the engine gearbox and transmission. Prototype and production components are available for use in making prototype sensors. 100°C chips are readily available from manufacturers, but 200°C chips are available only in very limited quantities.

The magnetoresistive sensor parts have been received from the various manufactures and a housing has been made. The parts consist of (1)sensor chip, (2) samarium cobalt magnet, (3) sensor housing, and (4) miscellaneous wires. These prototype chips are capable of operation up to 120°C. Therefore, they can not be used in the transmission or the gearbox.

Due to the temperature limitations of the first MR chips, a Hall effect-type chip was suggested by one of the manufacturers. They can withstand higher temperatures, but their performance was not up to the standards set by the MR chips. The signal amplitude was low and Hall effect-chips are therefore no longer under consideration.

The VBG will use a stepper motor driven actuator. The actuator has been ordered so that work on controlling the motor can begin. An in-house driver has been identified and will be used allowing a much faster implementation of this technology. Although the VBG software routine is working through the calculations accurately, this does not confirm that the calculations will match the actual airflow. They have not yet been compared to actual engine data although the calibration tables are based on prior work concerning AGT-5 airflow measurements. In addition, variability between builds could also effect the actual airflow.

The VBG actuator has been received and is being tested for performance along with its electronic driver. Position commands given from the EDM-800 controller are translated into voltage pulses, driving the step motor actuator. The pulse frequency is proportional to motor speed. Current and voltage limits and the upper frequency that the driver can deliver determine the limit on motor speed. In order for the VBG to be effective, the actuator must have a slew rate of 5 in/sec.

A new optical sensor can be assembled from low cost off-the-shelf components giving better performance than either magnetic pickups or old design optical sensors. This new sensor has superior characteristics including a very high bandwidth so the signal will not diminish at the highest gasifier speeds. It is designed to give six pulses per revolution which will be used to calculate the N_1 speed.

II. CERAMIC COMPONENT DESIGN

2.1 DESIGN ACTIVITIES

The AGT-5 ATTAP test-bed engine is a two shaft regenerative engine modified to operate at RPD operating conditions, specifically at 1371°C (2500°F) turbine inlet temperature. Engine operation at this TIT requires heat resistant structural ceramic materials in the engine hot section. The overall objective of the ceramic component design activity is to create ceramic component designs that permit successful operation of the AGT-5 engine at the RPD operating conditions.

Specifically, the objectives of this activity are to do the following:

- Complete designs of the defined ATTAP ceramic development components. Turbine components include the gasifier scroll, gasifier vane(s) and vane platform, gasifier vane retaining ring, and the gasifier rotor
- Complete designs of associated ceramic and metal components necessary to permit evaluation of the ATTAP development ceramic components in rig and engine environments at RPD operating conditions. Included are the combustor body (ceramic) and associated components, two power turbine rotors (ceramic) and associated components, two power turbine rotor blade tip shrouds (ceramic), and the two power turbine nozzle assemblies and associated components
- Prepare and present design reviews of selected components
- Incorporate into the ceramic design activity "simultaneous engineering" which integrates component performance and reliability and related design activities, and component vendor fabrication technology development, to enhance the successful manufacture of cost-effective components

The overall approach utilized to design the AGT-5 ATTAP test-bed ceramic components includes the following steps:

- Establish operating conditions(s) and reliability goals for ceramic engine components
- Prepare conceptual designs of components
- Complete detailed linear elastic, fast fracture probabilistic design analyses based on: certified material characteristics, i.e., two parameter characteristic strength and Weibull parameters generated from test bar fracture data; and design reliability goals established from engine system reliability goals
- Iterate design configuration, materials, and operating requirements to achieve satisfactory preliminary component design
- Iterate component design details with ceramic manufacturer(s) to correlate component requirements with processing capabilities
- Finish design layout and detail drawings

After progressing through further steps of the development cycle, the design is reviewed for component performance, cost, and reliability and is updated or modified to achieve overall design goals.

In addition to the ceramic components requiring considerable development under ATTAP (i.e., the gasifier turbine assembly, regenerator disks, and engine insulation), the engine assembly also includes a ceramic combustor assembly and selected ceramic power turbine components (rotors and shrouds). The gasifier turbine static structure, shown in Figure 8, consists of a scroll that guides the gas flow from the combustor to the turbine vane (nozzle) row. This row consists of loosely mounted vanes to accelerate the flow to rotor inlet conditions. A retaining ring surrounds the scroll outer shroud and covers slots within this shroud through which the vanes are inserted into the gas path. A vane platform forms the inner gas path boundary and positions the hub end of the vanes within machined pockets contained in this structure. The gasifier turbine rotor completes the gasifier turbine assembly. The gasifier turbine static structure is

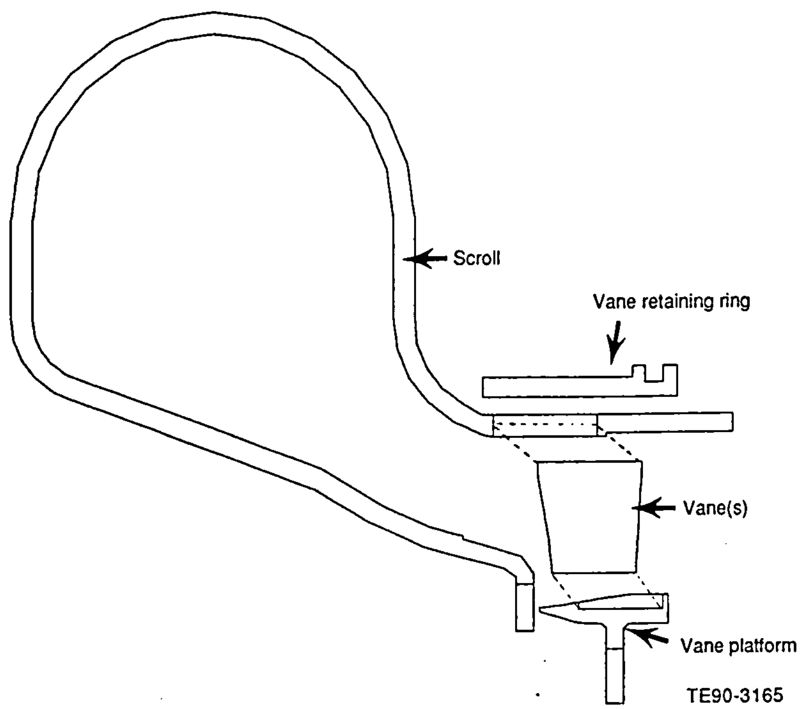

Figure 8. Gasifier turbine static structure.

mounted to the engine by a combination insulating/locating subassembly, which inhibits heat flow from the gas path into the engine structure. Cross key features accurately locate the static structure relative to the rotor blade tips while allowing free movement between ceramic and metallic components for thermal expansion.

The power turbine vane assemblies are attached to the engine housing by a bolted flange which maintains concentricity between the vane assemblies and the power turbine rotors. The ceramic rotor tip shrouds are radially located in the vane assemblies by cross keys. The power turbine rotors are individually attached to metal shaft segments, which are bolted together to form the turbine rotor assembly.

Overall engine design requirements for the turbine and combustor are as follows:

- Duty cycle: 100,000 miles life of which 55,000 miles operate on an urban cycle and the remainder (45,000 miles) is considered highway operation
- 3,500 hr life
- 12,000 starts
- 33,600 low cycle fatigue (LCF) cycles
- Maximum gasifier turbine inlet temperature of 1371°C (2500°F)
- Rotor containment at maximum burst speeds
- Adherence to automotive environmental, maneuver, and attitude requirements
- Reliability goals to have fewer than 0.25 major engine system failures in 100,000 miles

Detail designs and analyses of the turbine assemblies are described in the following subsections. The POS design goal for each ceramic engine component is based on the number of failure sites for that component in relation to the total number of failure sites in the complete engine assembly. The POS design goal for each ceramic component is also listed in the subsections describing that component.

2.1.1 Combustor

Objective/Approach

This activity is focused on designing structural ceramic combustor components that meet performance, mechanical strength and POS, and dimensional criteria for operating in the AGT-5 hot gasifier rig(s) and test-bed engine(s) at RPD conditions. Efforts include the construction of 3-D finite element models to calculate component temperatures, deflections, stress profiles, and the resulting POS. Activities during 1991 focused on the completion of the combustor design to be utilized with the advanced concept scroll and on a failure analysis of the CBO α-SiC diffusion flame combustor.

Accomplishments/Results

- The design of a ceramic combustor body for the advanced concept scroll was completed for N/TRW's NT230 and CBO's α–SiC materials.
- A 3-D FEM thermal and stress analysis of the N/TRW combustor body was completed for two different combustor domes and two different dilution zone flow assumptions.
- Results of the analysis indicated that the higher flow combustor dome was needed to reduce reaction zone temperatures to prevent exceeding the temperature limits of NT230.
- The predicted probability of survival of the NT230 combustor is acceptable for both dilution zone flow assumptions with the high flow dome.
- Generated 2-D axisymmetric finite element models of the CBO α-SiC diffusion flame combustor with "as-designed" 4 mm and "as-manufactured" 6.25 mm thick walls.
- Completed steady-state and transient structural/POS analyses of the diffusion flame combustor with 4 mm and 6.25 mm thick walls operating under nominal and simulated fuel spray impingement conditions.
- Completed a steady-state structural/POS analysis of a 3 mm "thin wall" ceramic diffusion flame combustor.
- Each of the combustor configurations examined has a predicted minimum POS at the max power steady-state operating condition.
- A stress concentration at the edge of the primary air holes represents the POS limiter for all combustor configurations. A methodology has been developed to incorporate this stress concentration in the 2-D axisymmetric finite element POS analyses.
- The 6.25 mm "as-manufactured" combustor wall thickness results in elevated through-wall thermal gradients and an associated 75% increase in stress relative to the 4 mm design.
- Predicted stress at the primary hole O.D. for the 6.25 mm thick wall combustor matches the measured fracture stress (42.6 ksi) (see Section 3.1.3 Failure Analysis) when the appropriate stress concentration factor is applied.
- Fuel spray impingement results in extreme local thermal gradients and associated thermal stresses for both the 4 mm and 6.25 mm thick wall combustors.
- The fuel spray impingement analyses predict ceramic failures at the I.D. corner of the primary air holes for both combustor wall thicknesses.
- Based upon predicted stresses and the observed failure origin, it is concluded that the ceramic combustor failure resulted from the "as-manufactured" 6.25 mm wall thickness rather than from fuel spray impingement.
- A reduction in the ceramic combustor wall thickness from 4 mm to 3 mm improves the minimum POS from 0.9544 to 0.9925.

Discussion

A new ceramic combustor body was needed to mate with the advanced concept scroll. Due to the combustor body's asymmetric shape a 3-D finite element model (Figure 9) was needed to accurately predict temperature and stress profiles. Two different thermal boundary conditions were analyzed, one for the standard dome, another for a dome with increased flow to reduce gas temperatures. Two different dilution air mixing scenarios were analyzed, one with instantaneous uniform mixing of the dilution air, another with two of the five dilution air jets attached to the wall. The attached flow condition is considered the worst case as the cool dilution air jets create a cold spot resulting in the largest thermal gradients. Steady-state maximum power was chosen as the design point because the 2-D analysis of the standard combustor body had previously indicated that

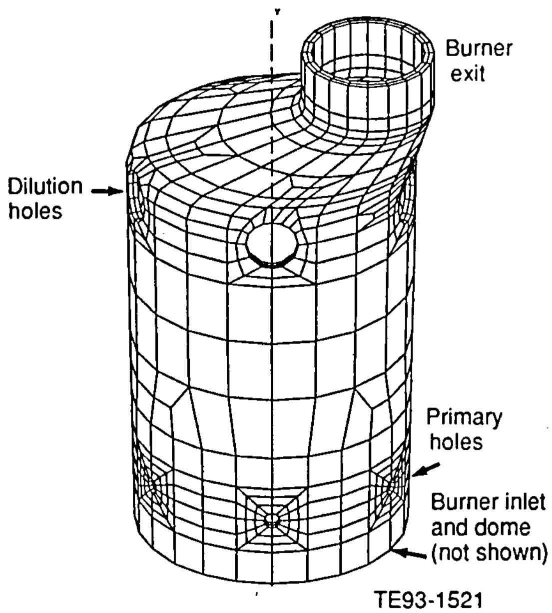

Figure 9. 3-D finite element mesh of the advanced concept scroll combustor body.

steady-state maximum power is the worst case condition for combustor bodies.

Figure 10 shows the temperature distribution for the standard dome and uniform mixing of the dilution air. The maximum wall temperature of 1800°C (3270°F) is well beyond the NT230 maximum use temperature of 1400°C (2550°F). By using the high flow combustor dome with the resulting lower reaction zone temperatures, the maximum wall temperature was reduced to 1388°C (2530°F). Figure 11 shows the predicted temperature distributions at steady-state maximum power with the high flow dome for both uniform and attached dilution flow conditions. Figure 12 shows the maximum principal stress distribution around the primary holes for both dilution flow conditions. For the uniform dilution flow condition, the maximum stress is at the primary holes. Figure 13 shows maximum principal stress distributions at the dilution holes and exit for both dilution flow conditions.

For the attached dilution flow condition, the maximum stress is in a cold island created by the attached dilution flow in the transition region. The uniform flow case has the highest POS of 0.9992 which is well above the goal POS of 0.9752. The attached flow case has a

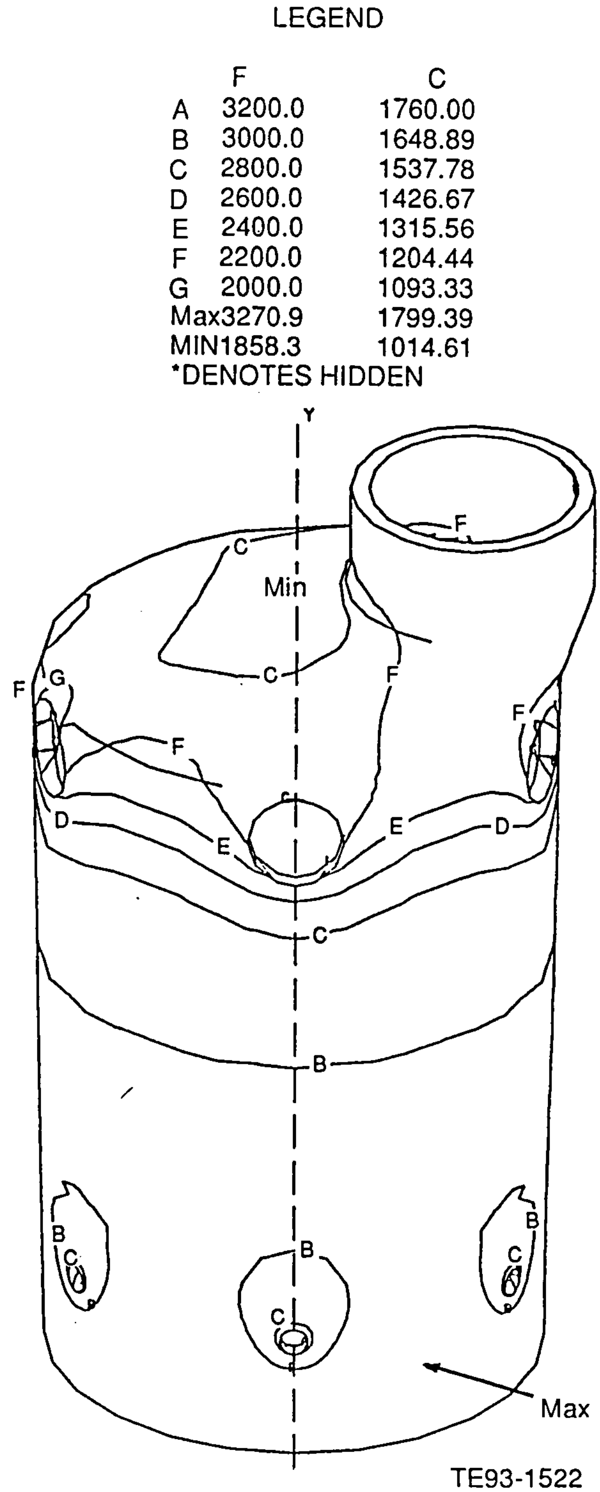

Figure 10. Steady-state maximum power temperature distribution with the standard dome and attached dilution flow.

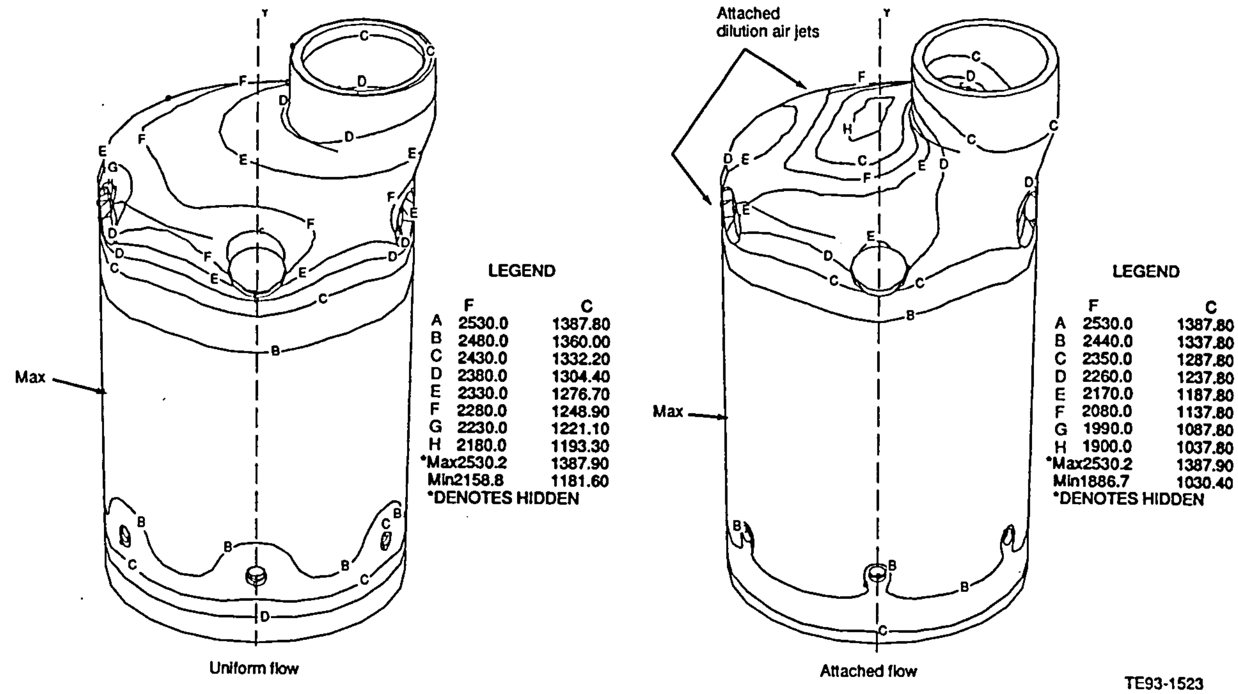

Figure 11. Comparison of steady-state maximum power temperature distributions for the uniform mixing and attached dilution flow conditions with the high flow rate dome.

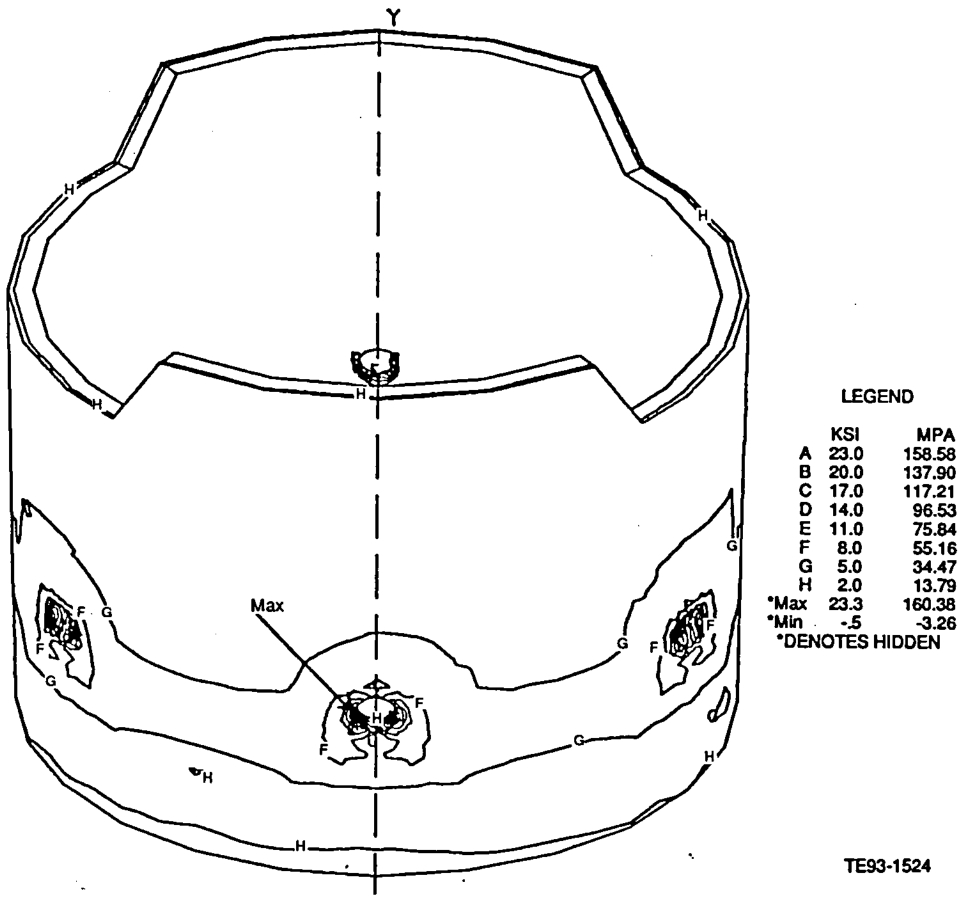

Figure 12. Steady-state maximum power maximum principal stress distribution around the primary air holes with the high flow rate dome.

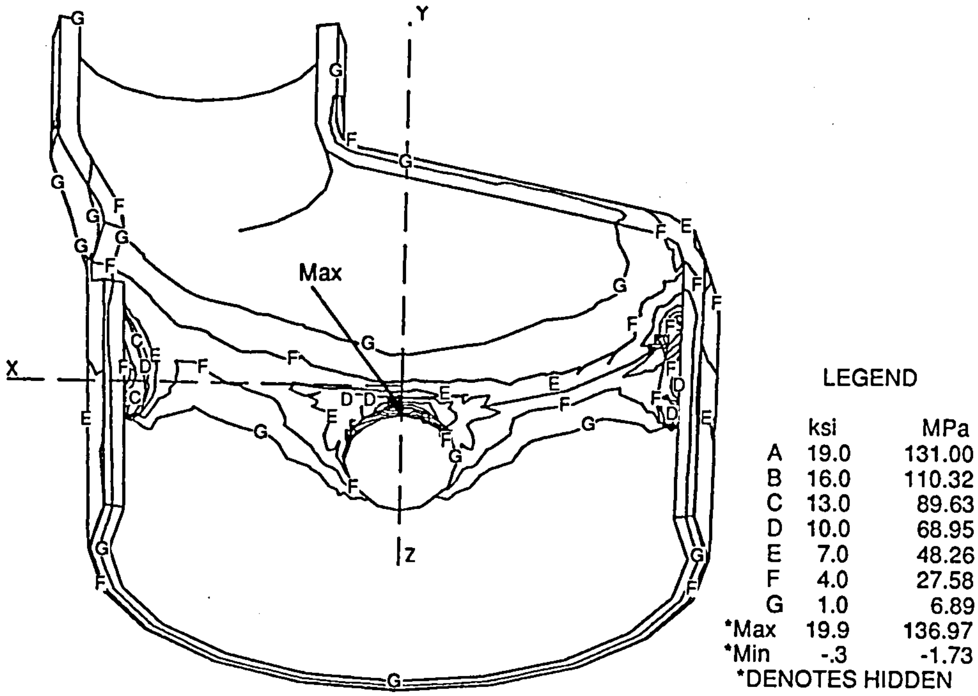

Uniform flow

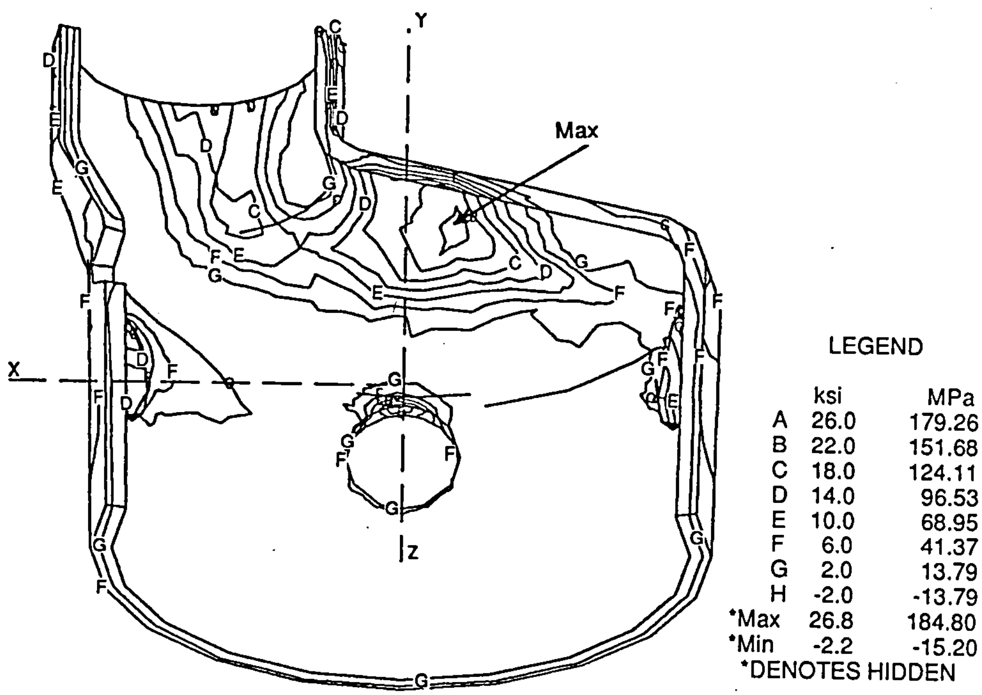

Attached flow

TE93-1525

Figure 13. Comparison of steady-state maximum power maximum principal stress distributions for the uniform mixing and attached dilution flow conditions with the high flow rate dome.

lower POS of 0.9583, which is slightly below the goal POS, but is acceptable for development testing. The attached flow condition is considered a worst case condition with the actual conditions being between the uniform and attached dilution flow conditions. Table III summarizes the thermal, stress, and POS results of the FEM analysis for the NT230 combustor body.

As a result of the analysis, some minor changes were made to the design before prints were sent to CBO for process development and component deliverables with α-SiC. The changes were made to reduce stresses in the transition zone between the dilution holes and the exit. The center line of the dilution holes was lowered slightly to reduce the likelihood of dilution flow attaching to the wall. In addition, the number of dilution holes was changed from five to six. This creates opposing jets which promotes better mixing. The smaller holes also position the top of the holes lower, further distancing the dilution jets from the combustor wall. Figure 14 show a comparison of the two combustor body designs.

Table III.
Summary of thermal and stress analysis of the advanced concept scroll combustor body.

	Max Temp. °C (°F)	Max Stress MPa (ksi)	POS
Standard dome	1800 (3270)	--	--
High flow dome uniform flow	1388 (2530)	160 (23.3)	0.9992
High flow dome attached flow	1388 (2530)	185 (26.8)	0.9583

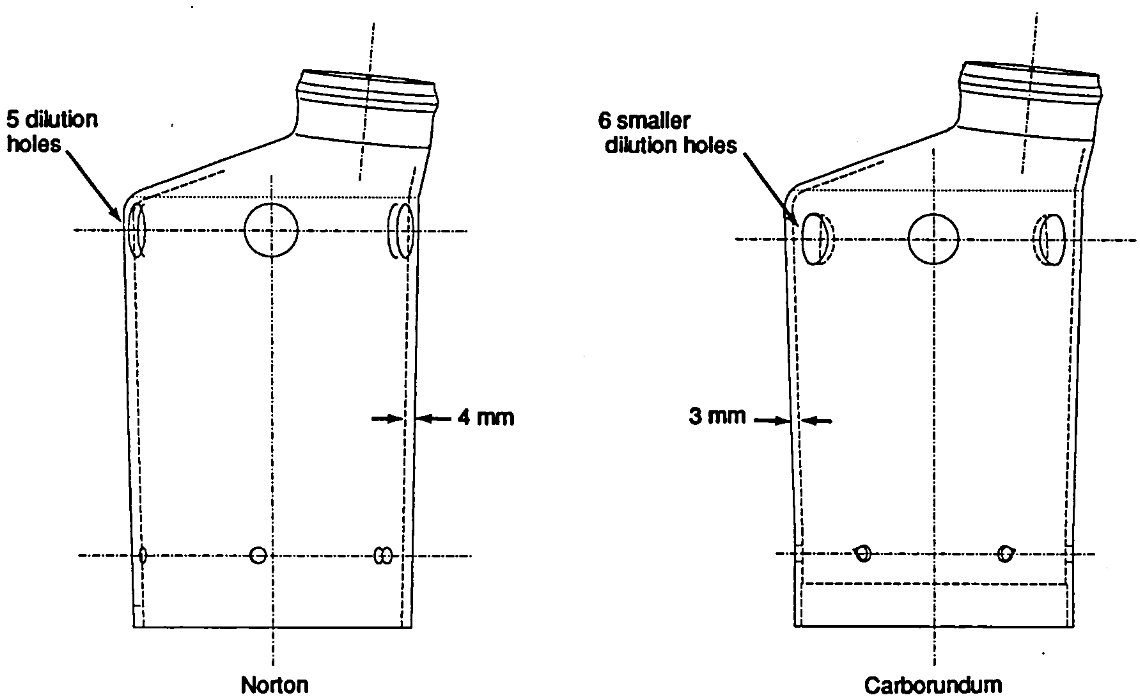

Figure 14. Comparison of the N/TRW and CBO advanced concept scroll combustor bodies.

Six combustor bodies were manufactured by CBO. The first five components were fabricated with an out-of-spec wall thickness of 6.25 mm due to vendor tooling and shrinkage difficulties. The final combustor body was manufactured with the design spec 4 mm wall thickness. Initial testing of the first ceramic diffusion flame combustor (6.25 mm thick wall) resulted in a ceramic failure. A fractographic analysis of the ceramic combustor identified the primary failure origin at the outside edge of a primary air hole. The failure stress was 42.6 ksi as indicated by the fracture mirror radius.

Upon review of the previous analytical results, it was determined that this local stress was significantly higher than predicted. Two scenarios put forth to explain this elevated stress are increased wall thickness and fuel spray impingement on the combustor wall I.D. In order to explore these scenarios, a 2-D axisymmetric finite element analysis comparing the 4 mm and 6.25 mm thick wall diffusion flame combustors was initiated. Steady-state and cold start transient structural/POS analyses have been completed for each of the following four combustor configurations:

1. 4 mm wall thickness/nominal boundary conditions
2. 6.25 mm wall thickness/nominal boundary conditions
3. 4 mm wall thickness/simulated fuel spray impingement
4. 6.25 mm wall thickness/simulated fuel spray impingement

A comparison of maximum power steady-state temperatures for configurations No. 1 and No. 2 are illustrated in Figure 15. Corresponding temperatures for configurations No. 3 and No. 4 are illustrated in Figure 16. Maximum principal stresses (no K_t effect) for the 4 mm versus 6.25 mm wall thickness combustors operating under nominal and fuel spray impingement conditions are shown in Figures 17 through 20, respectively. In order to complete the structural/POS analyses, it was necessary to develop a methodology to account for local stress concentrations around the primary air holes (failure site). Unfortunately, the stress concentration factor[1,2] applies only to calculated nominal stress, not to probability of survival. It was therefore proposed that a corrected POS be generated for a given nominal stress distribution by utilizing a modified Weibull characteristic strength.

The modified value is equal to the standard characteristic strength divided by the local stress concentration factor. In an axisymmetric finite element analysis, the corrected POS is obtained by varying Weibull material properties (volume and surface characteristic strength) for all elements in the region of the stress concentration. Based upon the Peterson correlation for a biaxially stressed infinite plate (large radius cylinder) with an infinite row of circular holes (holes orientated in the circumferential direction), the appropriate stress concentration factor for the combustor primary air holes was calculated to be 2.1.

These plots indicate that the minimum probability of survival occurs at maximum power steady-state for all analyzed configurations. Based upon predicted peak stress locations (O.D. versus I.D.), it was concluded that the ceramic combustor failure resulted from the increased "as-manufactured" wall thickness rather than fuel spray impingement. In order to pursue this conclusion further, a 2-D axisymmetric finite element analysis of a 3 mm wall thickness diffusion flame combustor operating under nominal conditions was performed. The 3 mm wall was selected based upon ceramic slip casting process limitations. As expected, the resulting maximum power steady-state corrected POS increased from 0.9544 for the 4 mm wall to 0.9925 for the 3 mm wall thickness. Maximum power steady-state temperatures and maximum principal stresses (no K_t effect) for the 3 mm wall thickness ceramic combustor are illustrated in Figures 21 and 22, respectively. Based upon these results, it was recommended that all future ceramic combustor designs incorporate a thinner 3 mm wall thickness.

---

[1] Stress Concentration Factors, R. E. Peterson, Copyright 1974, John Wiley & Sons, Inc.

[2] Roark's Formulas for Stress & Strain, Warren C. Young, 6th Edition, Copyright 1989, McGraw-Hill Book Company.

	F	C
A	2100.0	1148.89
B	2200.0	1204.44
C	2300.0	1260.00
D	2400.0	1315.56
E	2500.0	1371.11
F	2600.0	1426.67
G	2700.0	1482.22
*Max	2712.0	1488.89
*Min	2000.5	1093.61

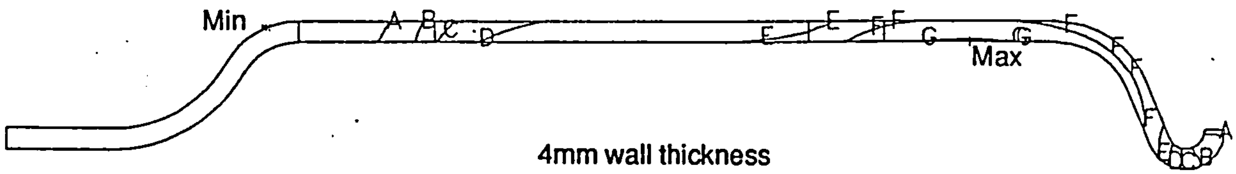

	F	C
A	2000.0	1093.33
B	2100.0	1148.89
C	2200.0	1204.44
D	2300.0	1260.00
E	2400.0	1315.56
F	2500.0	1371.11
G	2600.0	1426.67
H	2700.1	1482.22
*Max	2700.1	1482.28
*Min	1952.1	1066.72

*DENOTES HIDDEN

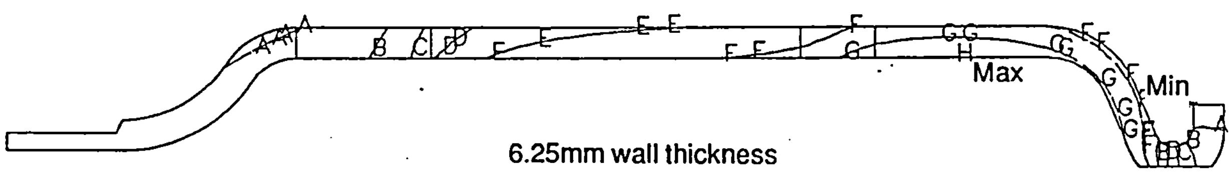

TE93-1529

Figure 15. Comparison of maximum power steady-state temperatures for the 4 mm and 6.25 mm wall thickness ceramic combustor bodies with nominal boundary conditions.

	F	C
A	1900.0	1037.78
B	2000.0	1093.33
C	2100.0	1148.89
D	2200.0	1204.44
E	2300.0	1260.00
F	2400.0	1315.56
G	2500.0	1371.11
H	2600.0	1426.67
Max	2633.3	1445.17
Min	1878.2	1025.67

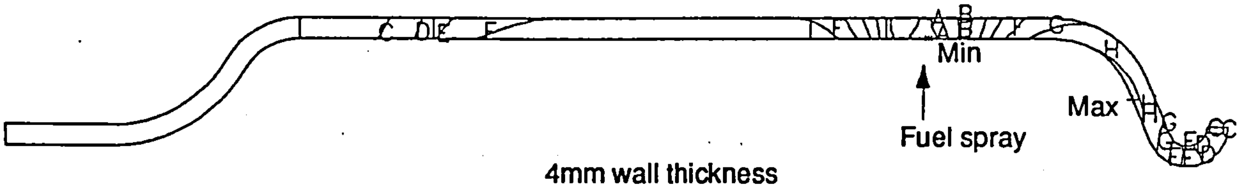

4mm wall thickness

	F	C
A	1980.0	1082.22
B	2070.0	1132.22
C	2160.0	1182.22
D	2250.0	1232.22
E	2340.0	1282.22
F	2430.0	1332.22
G	2520.0	1832.22
Max	2594.8	1423.78
Min	1947.4	1064.11

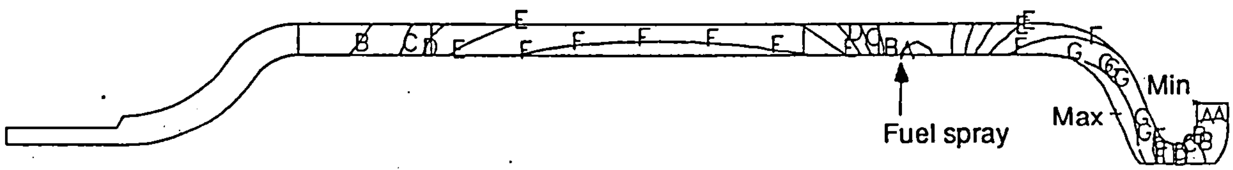

6.25mm wall thickness

TE93-1530

Figure 16. Comparison of maximum power steady-state temperatures for the 4 mm and 6.25 mm wall thickness ceramic combustor bodies with simulated fuel spray impingement.

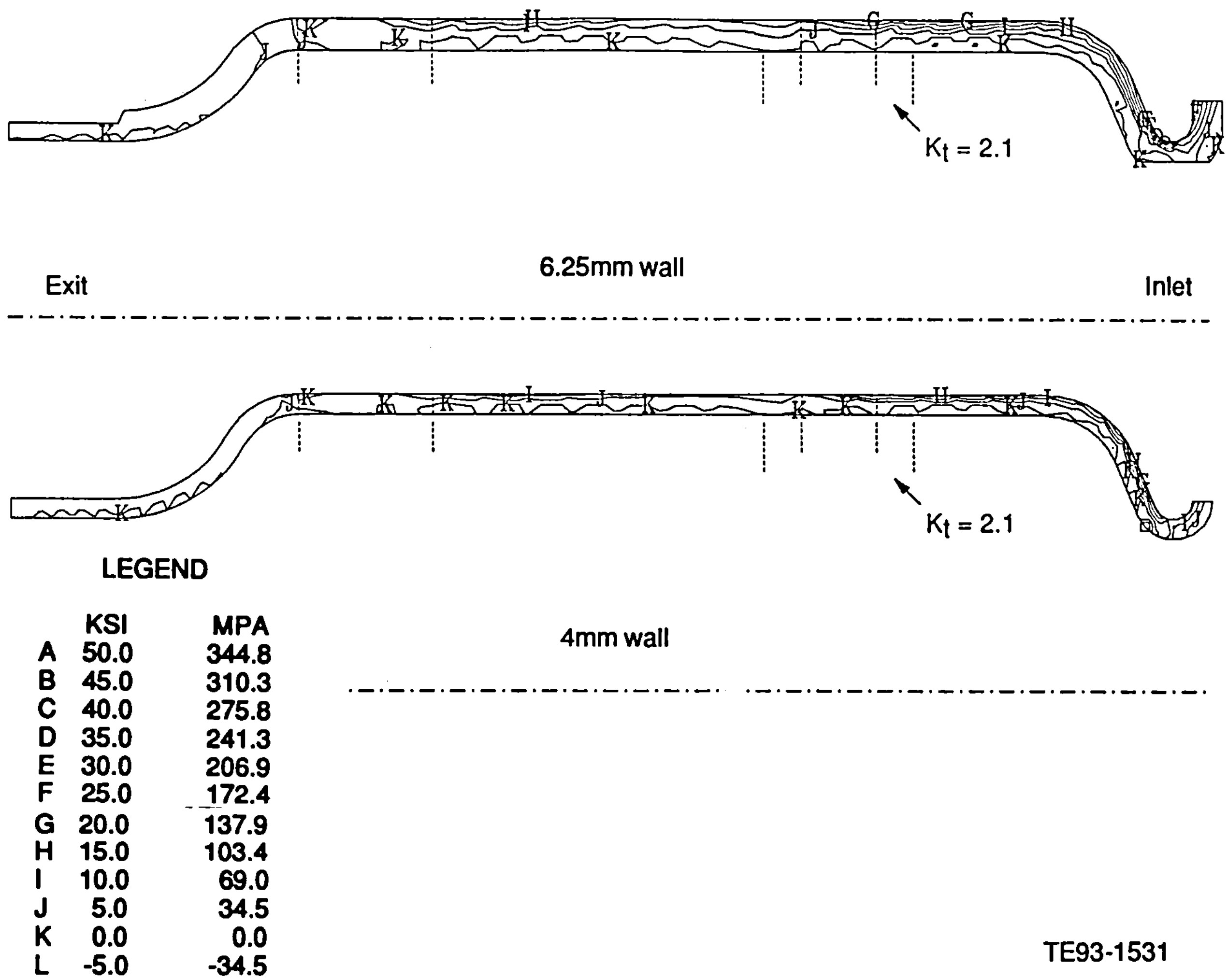

Figure 17. Comparison of maximum power steady-state maximum principal stresses for the 4 mm and 6.25 mm wall thickness ceramic combustor bodies (nominal boundary conditions).

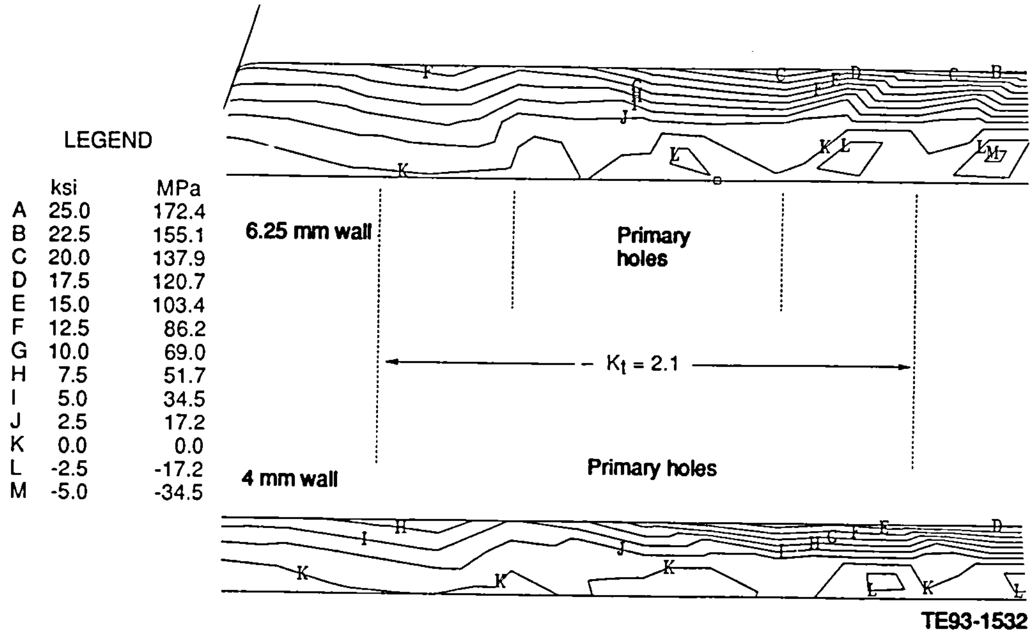

Figure 18. Comparison of maximum power steady-state maximum principal stresses for the 4 mm and 6.25 mm wall thickness ceramic combustor bodies (nominal boundary conditions).

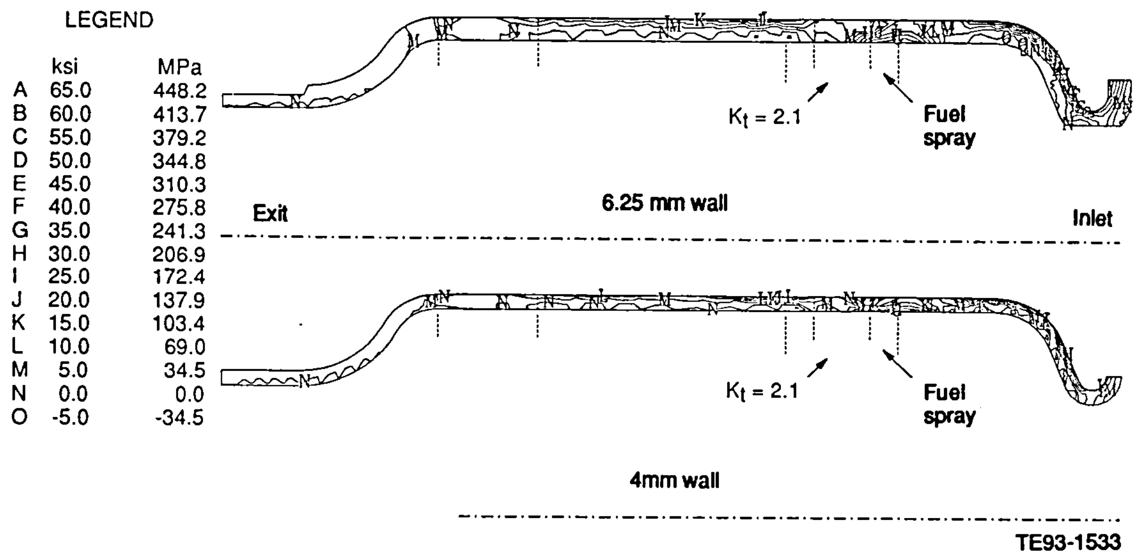

Figure 19. Comparison of maximum power steady-state maximum principal stresses for the 4 mm and 6.25 mm wall thickness ceramic combustor bodies (fuel spray impingement) .

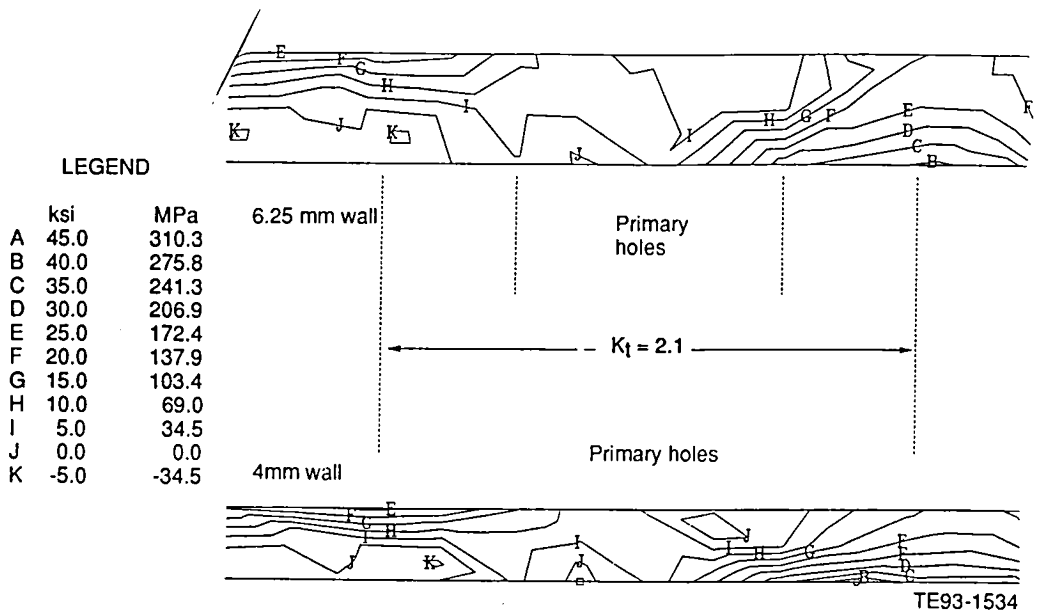

Figure 20. Comparison of maximum power steady-state maximum principal stresses for the 4 mm and 6.25 mm wall thickness ceramic combustor bodies (fuel spray impingement).

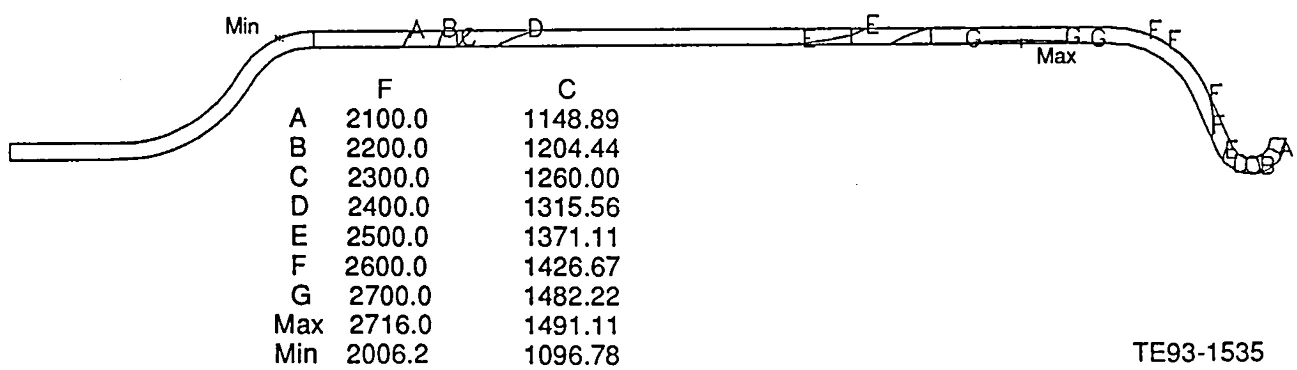

Figure 21. Maximum power steady-state temperatures for the 3 mm wall thickness ceramic combustor (nominal boundaries).

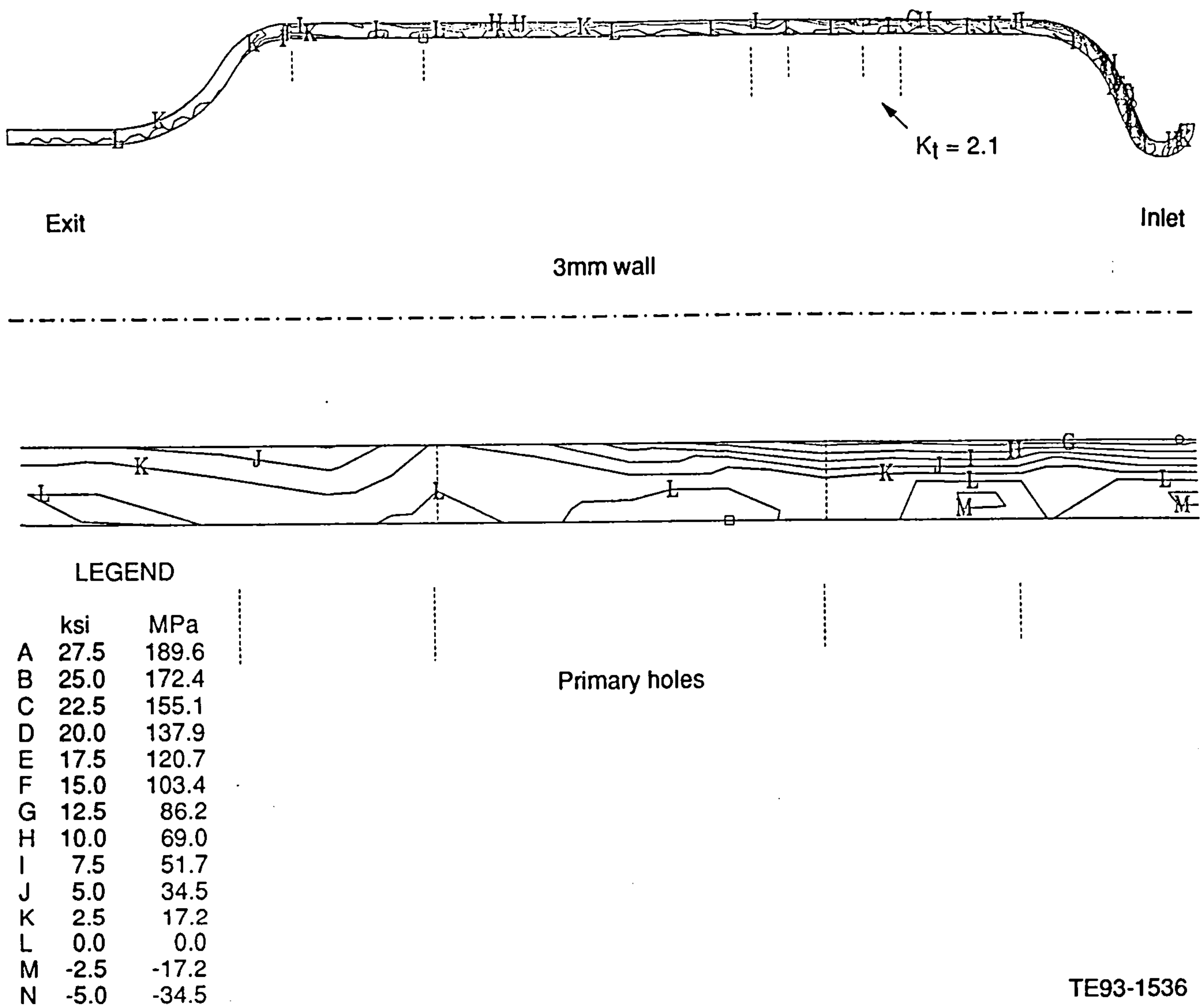

Figure 22. Maximum power steady-state maximum principal stresses for the 3 mm wall thickness ceramic combustor (nominal boundaries).

2.1.2 Gasifier Turbine Static Structure

Objective/Approach

The objective of this activity is to design ceramic components in the gasifier turbine static structure that operate satisfactorily at ATTAP RPD turbine inlet temperature conditions of 1371°C (2500°F) and achieve assigned POS criteria. Design concepts are prepared, finite element models created, heat transfer and stress analyses performed, and calculations of POS completed for each ceramic component of the gasifier turbine static structure. Efforts during 1991 concentrated on the design of a second generation advanced concept ceramic gasifier scroll, review of the gasifier scroll mount system preload, and generation of an advanced concept gasifier scroll rapid prototype.

Accomplishments/Results

- Completed the detailed design of a second generation advanced concept gasifier scroll which utilizes independent ceramic mount rings in order to eliminate high thermal stresses encountered with radial flange mounts.

- Completed a preliminary 2-D axisymmetric finite element structural analysis of the advanced concept scroll for the cold start transient. The analysis predicted an acceptable minimum POS of 0.9993 at twenty seconds into the acceleration.
- Completed detail drawings for the NT230 siliconized SiC scroll body and NT154 silicon nitride mount and seal rings.
- Initiated a detailed 2-D axisymmetric finite element structural analysis of the scroll and mount assembly.
- Generated full-scale polycarbonate prototypes of the advanced concept gasifier scroll.
- Designed a new ceramic piston ring to seal effectively across the operating range of the AGT-5 engine.
- Performed leakage tests on the design and compared results to the current ceramic and metal piston rings.
- The prototype models were utilized by the ceramic vendor in order to visualize the complex scroll geometry and to assist in pattern/mold development.

Discussion

The AGT-5 gasifier scroll (Figure 23) has proven to be one of the more difficult ceramic components to design, fabricate, and assemble. Difficulties in forming and machining have reduced scroll yields to unacceptable levels. In an effort to address these issues, an advanced concept ceramic gasifier scroll was designed and tested. The initial advanced concept scroll design is a silicon nitride (Kyocera SN252) component which has encountered limited success in terms of aerodynamic performance, survivability, and manufacturability. In order to pursue the advantages of this concept, a second generation advanced concept scroll design has been generated. The major objectives of this effort were to improve the ceramic component performance, survivability, and manufacturability via innovative design and strong vendor interaction. The design has been incorporated into the 1991-1992 N/TRW scroll fabrication effort. The attachment scheme is shown in Figure 24. The scroll body is mounted to the gasifier housing via a crosskeyed ceramic mount ring. Pertinent scroll assembly features are listed below:

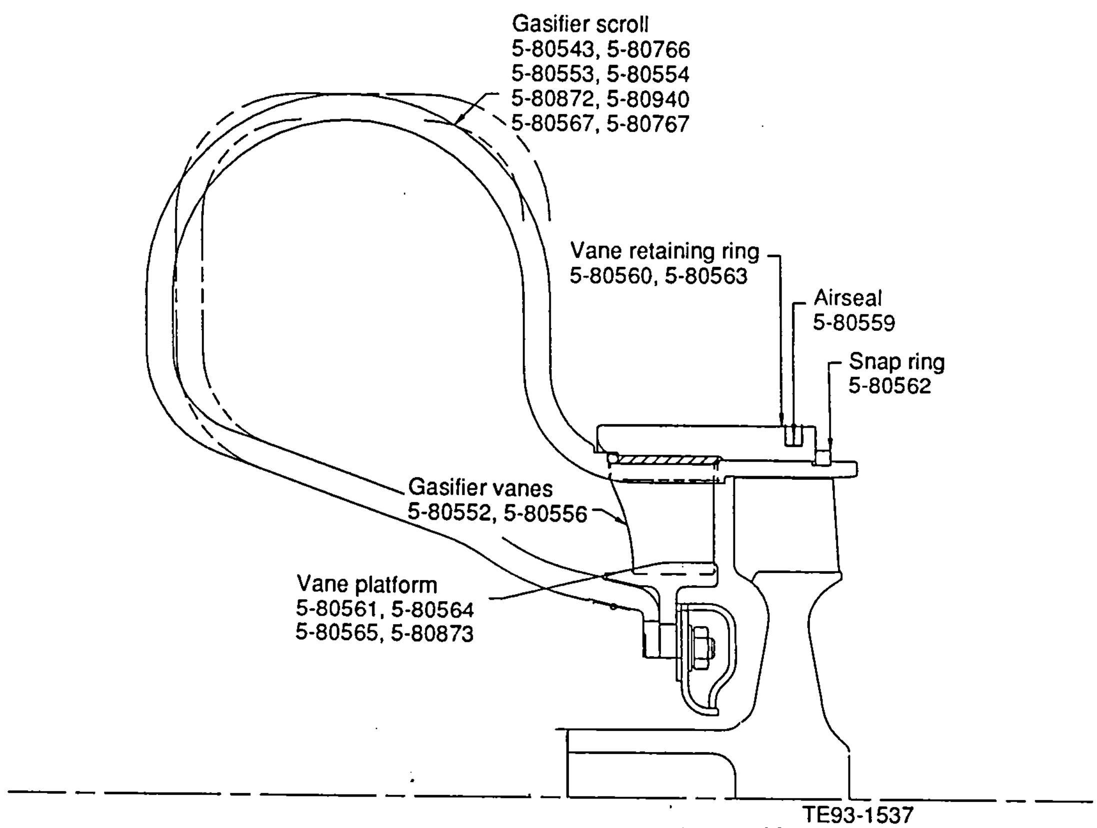

Figure 23. AGT-5 ceramic scroll assembly.

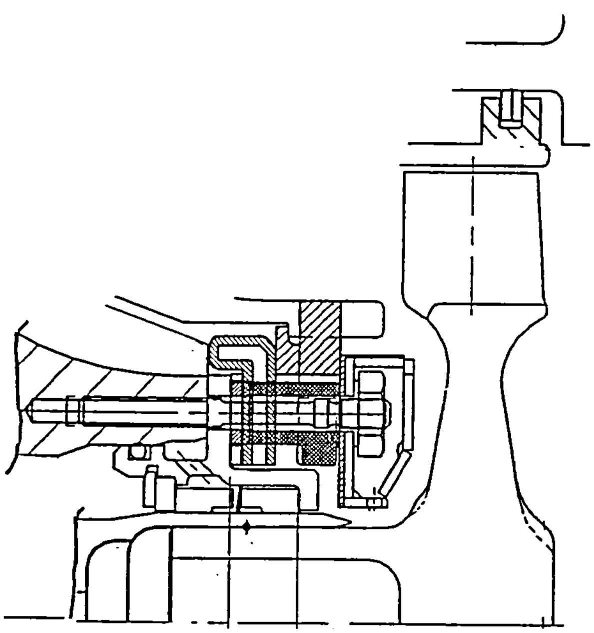

Figure 24. Advanced concept scroll assembly.

- NT230 siliconized silicon carbide scroll body
- NT154 silicon nitride mount and seal rings
- Improved scroll aerodynamics
- Enhanced manufacturability and inspectability
- Piston ring seal support integrated into scroll body
- Mount system detached from the scroll body
- Critical mount clearances minimum at assembly
- Mount geometry compatible with the existing hardware

Two separate reviews were held with N/TRW prior to design finalization in order to resolve issues of manufacturability and machinability. Recommendations/modifications resulting from these reviews were subsequently incorporated into the individual component designs. A preliminary 2-D axisymmetric finite element analysis of the scroll geometry was completed. The finite element analysis utilized the original scroll geometry which incorporated a divorced I.D. mount system and an independent piston ring air seal support. The structural analysis was performed for the standard cold start transient. The predicted minimum probability of survival occurred at twenty seconds into the transient. It is noted that the peak stress of 32.7 ksi at the piston ring groove O.D. is driven by the local thermal gradient in the seal support ring. This gradient and the associated thermal stresses should be significantly reduced in the final scroll configuration due to the integral piston ring seal support. Detail drawings of the SiC scroll body and Si_3N_4 mount rings have been generated. A 2-D axisymmetric finite element analysis of the finalized scroll assembly has also been initiated. This analysis will be completed in 1992.

A full size polycarbonate prototype of the finalized N/TRW advanced concept ceramic gasifier scroll was generated to provide verification of the complex geometry, to assist in vendor fabrication efforts, and to evaluate component aerodynamic performance prior to ceramic component production. The polycarbonate prototype was generated utilizing the DeskTop Manufacturing (DTM) Selective Laser Sintering (SLS) process.

Ceramic Piston Rings. The purpose of the piston rings is to provide an air seal between the gasifier and power turbine sections. The design must be able to tolerate radial and angular misalignment between the sections and provide sealing capability once all thermal growths are considered. If the piston ring material is different from the power turbine bore material, the differences in coefficients of expansion must also be taken into account.

A ceramic piston ring was designed to handle the maximum temperature (1371°C [2500°F]) condition of the engine. The gage diameter for this piston ring is equal to the cold power turbine bore diameter. When the components heat up during operation, the metal power turbine bore grows away from the ceramic piston ring. Consequently, the current ceramic piston ring design leaks excessively when hot.

A second way to design a piston ring is to machine it circular to the hot dimensions of the power turbine bore. When this is done, the piston ring will conform to the power turbine bore when hot but will not conform uniformly when cold. When cold, however, the piston ring will be compressed and will therefore have smaller end gap leakage. The new piston ring was designed using this approach.

To determine if the leakage of the new ceramic design was acceptable, a test rig was fabricated to pressurize the piston ring air seals. Four designs were tested: the current ceramic and metal piston ring designs as well as two versions of the new ceramic design. The two versions of the new ceramic design differ only in the type of end butt used. The ceramic designs were tested at two bore diameters, one to represent the cold dimensions and another to represent the hot dimensions. The ring material used for testing was metal with diameters adjusted to simulate the ceramic components.

The table below shows the non-dimensional leakage (percent) for each piston ring design. The numbers have been normalized based on the leakage from the metal piston ring. For all cases below, the test pressure ratio was based on the pressure ratio across the piston rings in the AGT-5 engine at 100% operating conditions.

	Leakage (percent) Cold bore diameter	Hot bore diameter
1. Metal piston ring	1	n/a
2. Current ceramic	7.79	>70.
3. New ceramic without overlapping end gap	1.46	4.01
4. New ceramic with overlapping end gap	0.52	1.16

The test results show the new ceramic piston ring with overlapping end gap to have a sealing capability comparable to the metal piston ring design. When cold, this ceramic design actually has less leakage due to the tighter end gap clearance. When hot, the ceramic design has expanded and, therefore, the leakage increases.

Comparing the new ceramic designs with and without an overlapping end gap shows the benefit of the overlap. For the cold conditions the overlap reduces the leakage by a factor of 2.8. When hot the overlap reduces the leakage by a factor of 3.5.

This ceramic piston ring design appears to be an acceptable replacement for the current metal design.

2.1.3 Gasifier Turbine Rotor

Objective/Approach

This activity is focused on designing structural ceramic rotors for the gasifier turbine which meet performance, mechanical strength, POS, and dimensional criteria for operating in the AGT-5 hot gasifier rig(s) and test bed engine(s) at Reference Powertrain Design conditions. Efforts include the analytic assessment of the structural reliability (statistical basis) of gasifier rotor designs considering various ceramic material systems. The rotor design reliability goal is 0.9797. Critical points in the engine operating cycle are analyzed, including 1371°C (2500°F) RIT maximum power steady-state and a cold start to maximum power transient. Twenty-six, twenty, and fifteen blade rotor designs utilizing silicon carbide and several grades of silicon nitride have been considered.

Accomplishments/Results

- Completed the design of a 26-bladed gasifier rotor to increase efficiency and further test foreign object damage (FOD) tolerance of axial turbines with thinner airfoils.
- Completed 2-D FEM thermal and stress analysis of the 26-bladed gasifier rotor designed for three different material systems: CPS's CM200, N/TRW's NT154, and Kyocera's SN252.
- Determined all three disks have acceptable POS under cold spin, transient, and steady-state maximum power conditions.
- Completed 3-D FEM dynamic analysis of each rotor design indicating that none of the rotor's natural frequencies will be excited during operation.
- Generated a 3-D CAD data base of the rotor for transmission to the vendors to expedite fabrication. Due to the complexity of the airfoil root fillet region at the leading edge, some difficulties were encountered and corrected in generating and translating the 3-D data.

- Reviewed the 3-D FEM cold proof spin test analysis. The analysis indicated that a larger blade root fillet was needed in the leading edge region. The larger fillet was incorporated into the N/TRW and Kyocera rotors. CPS's tool had already been fabricated with the smaller fillet.
- Generated a full size polycarbonate prototype of the 26-bladed rotor and a ten times size polycarbonate prototype of the rotor blade root fillet at the leading edge.
- The rotor prototypes were utilized by ATTAP designers and the ceramic vendors to visualize the geometric ramifications of a constant 1.5 mm blade root fillet.

Discussion

The 26-bladed gasifier rotor was designed to improve aerodynamics, to test foreign object damage resistance of thinner airfoils, and to enhance packaging of the gasifier. By using the same aerodynamic design, time was saved in the design process and interchangeability with the other turbines is ensured. Although the 26-bladed rotor has the same aerodynamic design as the other rotors, it will have increased efficiency due to the thinner trailing edge and improved height-to-cord ratio.

The original 15- and 20-bladed rotors were designed with extra thick trailing edges to resist foreign object damage. These rotors have proven to be very FOD tolerant, which suggests that thinner trailing edges may offer acceptable FOD tolerance as well.

Another advantage of the 26-bladed rotor is enhanced packaging of the gasifier. The 26-bladed rotor has a smaller cord than the 15- and 20-bladed rotors, which makes packaging the gasifier and power turbines easier.

2-D axisymmetric finite element transient thermal and stress analyses were performed for each material. To minimize stresses, 26-bladed rotors used the same airfoil fillet size as the 20-bladed rotor. During construction of a 3-D CAD data base, it was determined that the airfoil fillets intersected at the throat, so a slightly smaller fillet was specified all around the airfoil except at the leading edge. An even smaller fillet was specified in the leading edge region because a larger fillet would not fit.

CPS was the first vender to receive the 3-D data base for tool fabrication. Due to translation problems from one CAD system to another, CPS recreated some data with a smaller leading edge fillet. This was undetected until the tool had already been fabricated. The tool could not be reworked because it had already been final coated. The decision was made to utilize the tool for process development. A new tool could be made at a later date if the process development activities are successful.

A 3-D FEM analysis of the rotor under cold spin conditions was conducted. The analysis indicated unacceptably high stresses, 508 MPa (73.7 ksi), in the leading edge airfoil root fillet region. By reconstructing the 3-D data base, it was determined that the fillet size did not need to be reduced in the leading edge region. With the constant airfoil fillet, the stresses were reduced to an acceptable level of 435 MPa (63.1 ksi). Figure 25 shows both the initial and redesigned predicted stress distributions for the rotor under cold spin conditions. This design change was incorporated into the Kyocera and N/TRW rotors before fabrication began.

A rotor disk shape for each material was optimized for minimum volume and a goal POS of 0.9797. Figure 26 shows the relative size of the two final disk shapes. The CPS disk needed to be larger than the N/TRW and Kyocera disks due to the lower strength of CM200. The POS of the CM200 disk was volume driven due to its low volume strength. When the disk was made larger to reduce stress and increase POS, the POS remained the same or got worse due to the increased stressed volume. The final CM200 disk configuration was optimized to have the highest POS for the least volume using current material properties. The POS of the CM200 disk is 0.9506 during the transient. This is short of the design goal POS but acceptable for prototype testing. The Kyocera SN252 disk is also short of design goal POS because the disk was designed for a Kyocera material system, which later became unavailable. The POS of the SN252 disk is 0.9768, which is short of the goal POS but acceptable for prototype testing. Figures 27 through 29 show temperature and

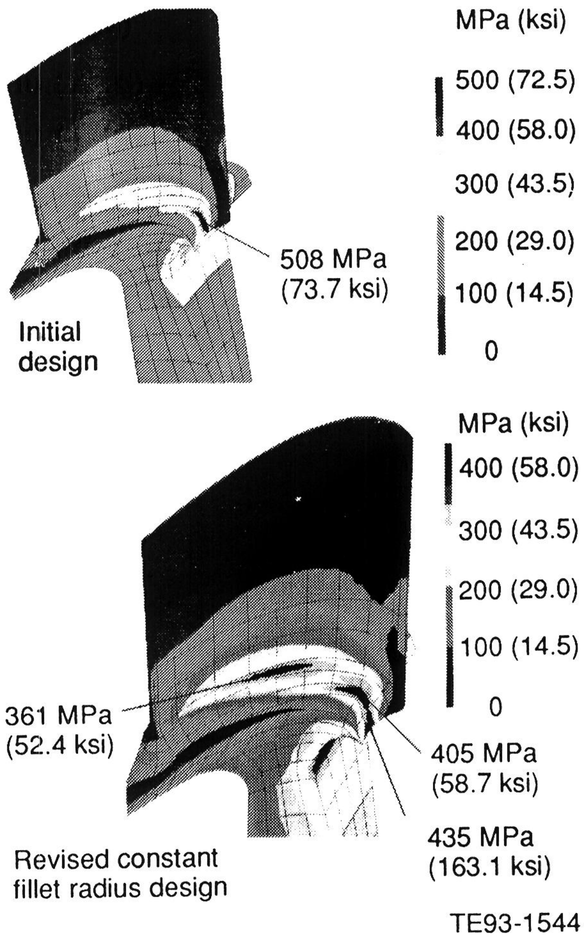

Figure 25. 3-D stress distributions of the SN252 26-bladed gasifier rotor under cold spin conditions.

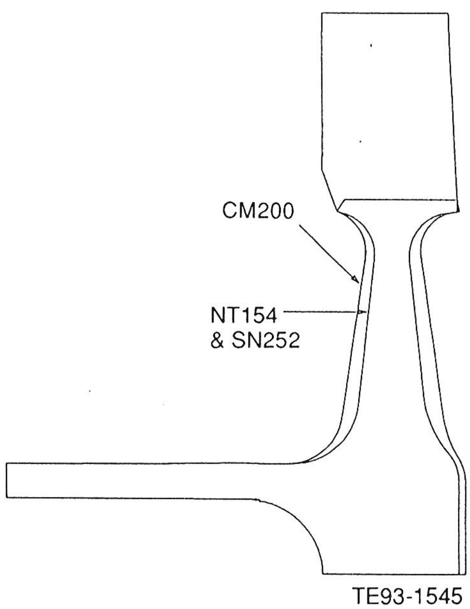

Figure 26. Comparison of optimized disk shapes for different materials.

stress plots for each material at the three design points: cold spin, cold start transient, and maximum power steady-state operation. Table IV summarizes the 2-D stress and POS results for each rotor under the three design conditions.

A 3-D FEM dynamic analysis was conducted to determine the natural frequencies of each rotor. Figure 30 shows the Campbell diagram for each of the three rotors. To pass Allison dynamic criteria:

- The 2nd diametral pattern frequencies must not coincide with the 2nd engine order within 10% of the engine operating range.
- The 14th diametral pattern frequencies must not coincide with the upstream vane passage excitation of 14th engine order within 10% of the engine operating range.
- The uncoupled first bend (1B) and first torsion (1T) blade modes must not coincide with 14th engine order excitation within 10% of the engine operating range. As shown in Figure 30, the Campbell diagrams of all three rotors pass the above criteria with at least a 13% margin from all excitations.

The N/TRW 26-bladed gasifier rotor design is a direct scale of the existing 20-bladed geometry. Since stress considerations do not allow for a direct ratio of blade root fillet radii, a compromise between stress and aerodynamic considerations was utilized resulting in the specification of a 1.5 mm constant blade root fillet radius for the 26-blade rotor. In order to clarify the geometric implications of this fillet radius, the DTM rapid prototype process was utilized to generate a full size polycarbonate model of the 26-bladed gasifier rotor and a ten times size polycarbonate blow-up of a single blade root fillet and leading edge rim (Figure 31).

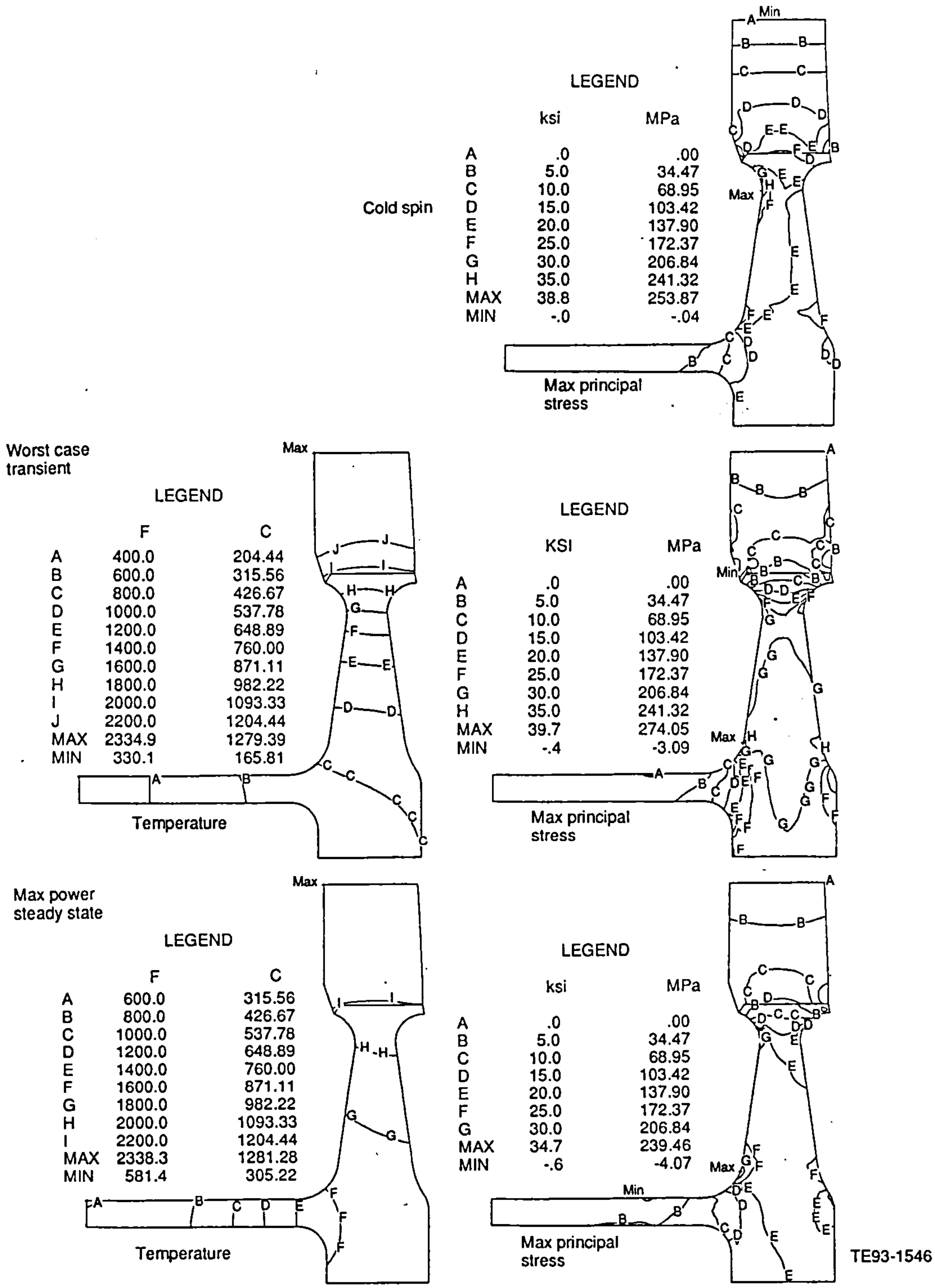

Figure 27. Twenty-six bladed gasifier rotor temperature and stress distributions for CM200 under the three design conditions.

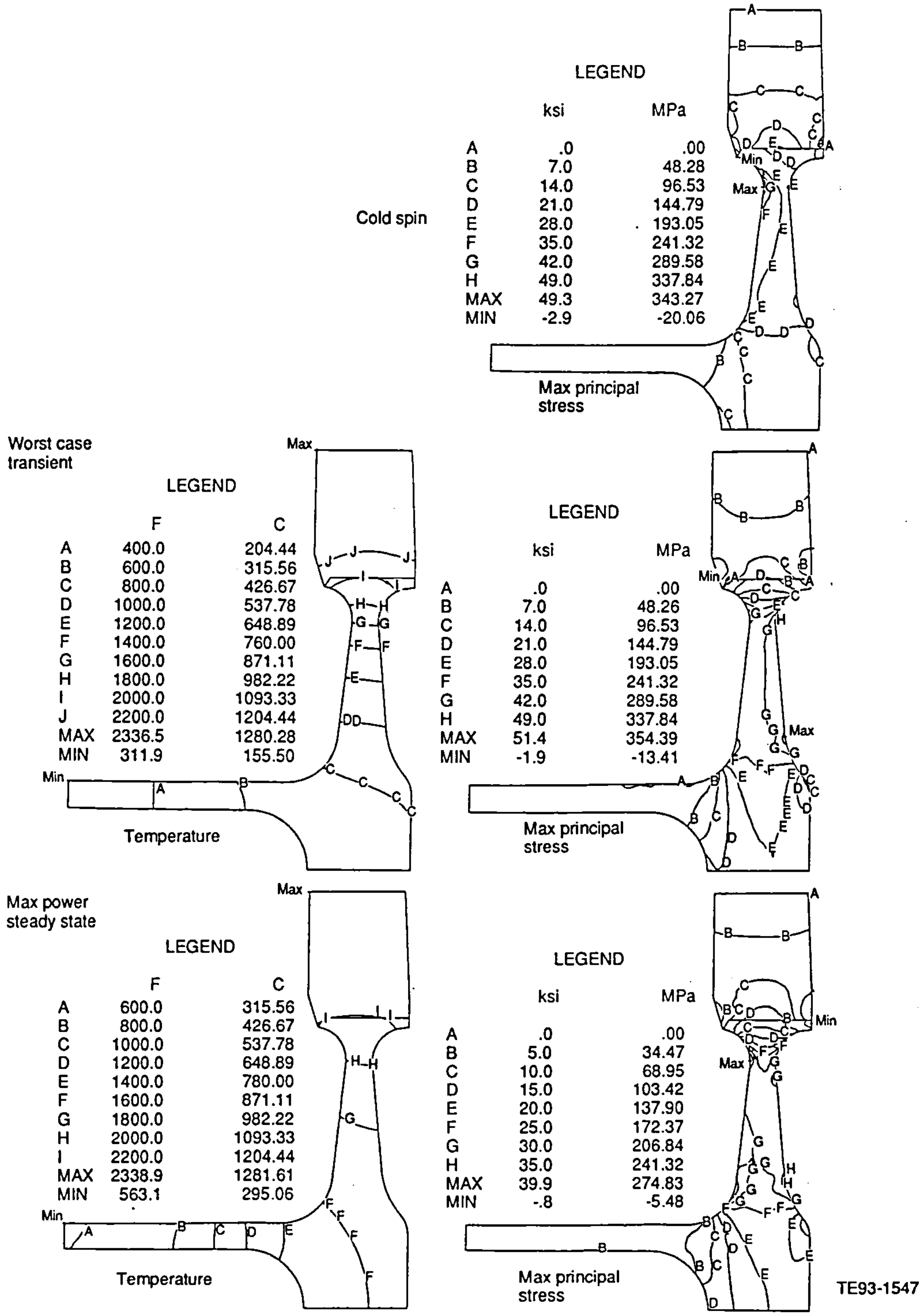

Figure 28. Twenty-six bladed gasifier rotor temperature and stress distributions for NT154 under the three design conditions.

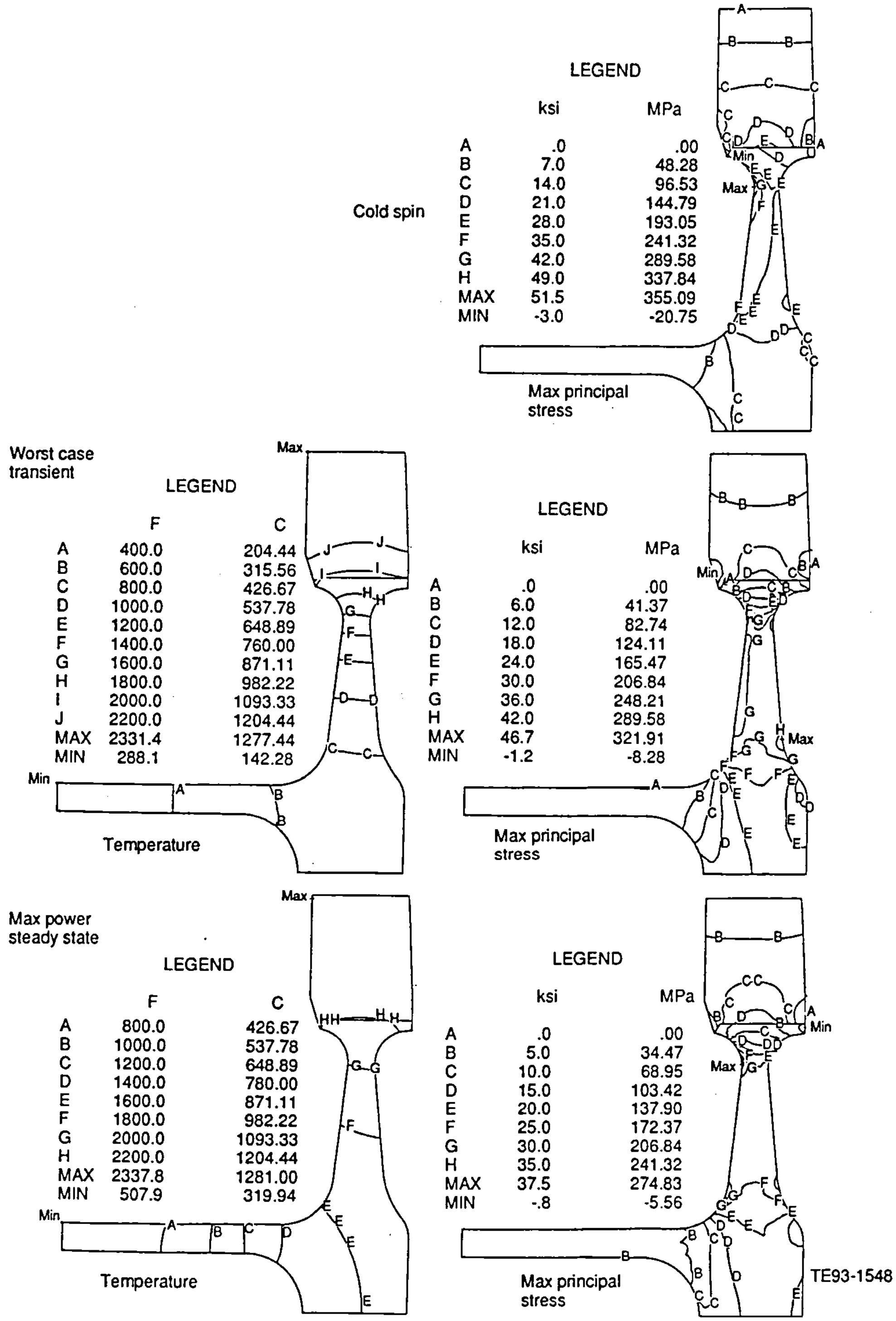

Figure 29. Twenty-six bladed gasifier rotor temperature and stress distributions for SN252 under the three design conditions.

Table IV.
Summary of results for 2-D stress and POS calculations of the 26-bladed gasifier rotors.

	Cold spin		Worst case trans.		Max power	
Material	MPa (Ksi)	POS	MPa (Ksi)	POS	MPa (Ksi)	POS
CM200	254 (36.8)	0.9961	274 (39.7)	0.9489	248 (35.9)	0.9844
NT154	343 (49.8)	0.9997	354 (51.4)	0.9966	275 (39.9)	0.9993
SN252	355 (51.5)	0.9958	322 (46.7)	0.9768	259 (37.5)	0.9970

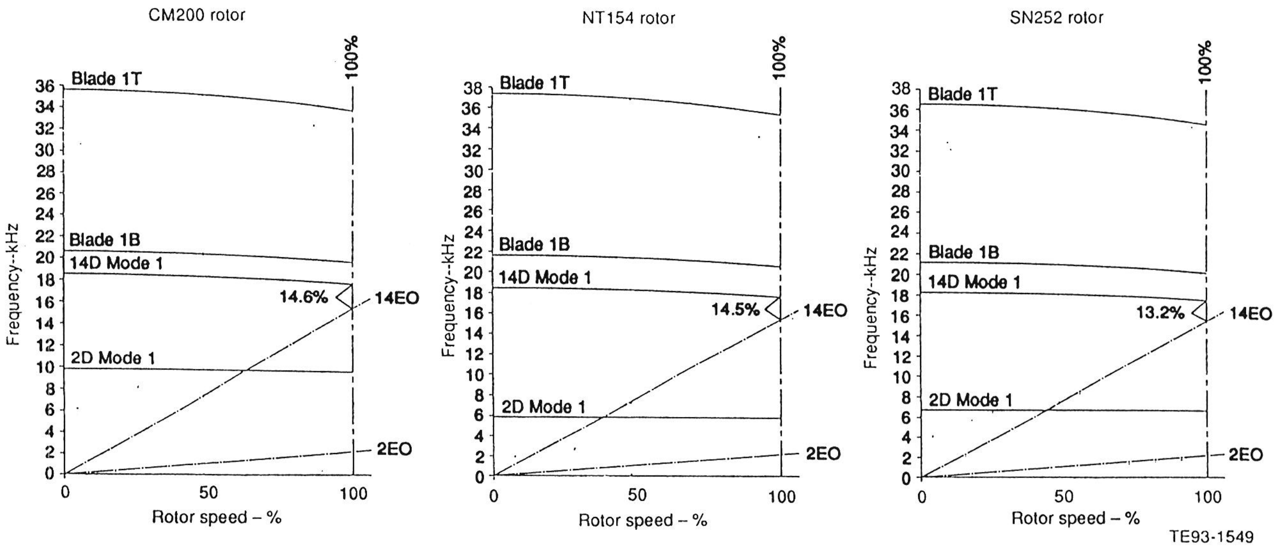

Figure 30. Campbell diagrams for each of the 26-bladed gasifier rotors.

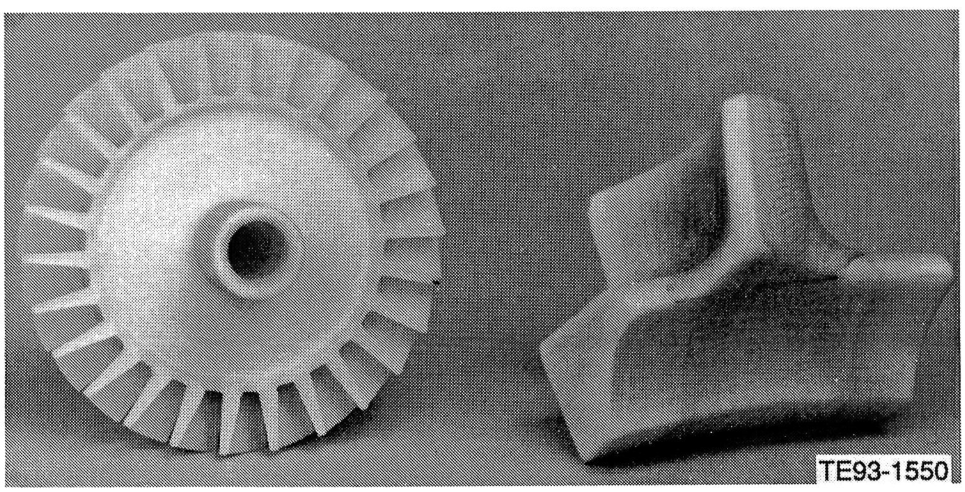

Figure 31. Polycarbonate models of 26-blade gasifier rotor and blade fillet/rim scallop region (10 x size).

III. MATERIALS CHARACTERIZATION AND CERAMIC COMPONENT FABRICATION

This section describes the ongoing ceramic material and component fabrication, characterization, and development activities, which are a key focus of ATTAP. The ceramic materials subsection documents the results of characterization and qualification of candidate ceramic materials and components being developed for gas turbine applications. This includes characterizations of material properties (microstructure, density, fracture strength, and fracture toughness), results of failure analyses of rig/engine tested components, and non-destructive evaluation development and results.

The ceramic component fabrication subsection describes the ongoing process development activities at the selected suppliers for ATTAP, including CBO, Manville, Corning, CPS, and N/TRW. Allison's approach to ceramic component technology development subcontracts process development to the domestic ceramic manufacturing community and works in an iterative development loop with those suppliers in areas of design, fabrication, characterization, and rig/engine data feedback. While basic ceramic materials development is not part of ATTAP, it does integrate material developments from DOE/Oak Ridge National Laboratory programs, supplier in-house activities, and other sources as they become available.

3.1 MATERIALS AND COMPONENT CHARACTERIZATION

3.1.1 Material Properties and Microstructure

Objective/Approach

Material and component characterization has focused on the testing and evaluation of candidate ceramic materials and components being developed for use in the AGT-5 gas turbine engine. The primary objective of this task is to establish a data base of appropriate material characteristics to support the design, analysis, development, and testing of hot section ceramic components. A secondary objective is to evaluate new candidate ceramic materials and suppliers and to assess which, if any, should be used in subsequent component development activities. The material characterization activities have focused on microstructural, density, flexural strength, and fracture toughness evaluations of various candidate ceramic materials. Fracture surface analysis is also used to determine the nature and location of the strength-controlling flaws. In addition, the tensile strength and time dependent strength characteristics are evaluated for select materials.

Accomplishments/Results

The ceramic materials and components that were characterized during this reporting period include the following:

- N/TRW NT230 SiC
- CBO sintered α-SiC
- GCC GN-10 Si_3N_4
- N/TRW NT154 Si_3N_4 gasifier turbine rotors
- Kyocera SN252 Si_3N_4 first-stage power turbine rotors
- Kyocera SN235 Si_3N_4 second-stage power turbine rotors

Discussion

N/TRW NT230 SiC. Evaluation of the material strength characteristics of N/TRW NT230 SiC material was conducted. The test specimens were sectioned from billets, which were fabricated by slip casting using process parameters similar to those established for fabrication of the turbine scrolls. The NT230 SiC material is a reaction sintered SiC with approximately 10-15% silicon. The microstructure, shown in Figure 32, consists of relatively fine SiC grains (compared to the prior NT235 [NC430] SiC) in a matrix of free silicon. N/TRW has concentrated on maximizing the purity of the NT230 SiC material, and routinely obtains a total impurity level of less than 100 ppm (parts per million). The average

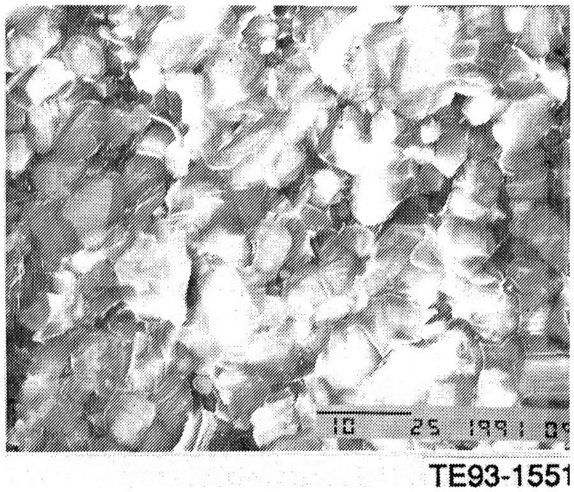

Figure 32. Microstructure of N/TRW NT230 SiC.

density of this material measured 3.121 g/cc (0.113 lbm/in^3).

All strengths reported in this document were obtained on specimens measuring 6.35 mm x 3.18 mm x 50.8 mm (0.25 in. x 0.125 in. x 2 in.) tested in four-point bending with an outer span of 38.1 mm (1.5 in.) and an inner span of 19.1 mm (0.75 in.) unless otherwise specified.

The strength characteristics of the NT230 SiC material are summarized in Table V and presented graphically in Figure 33 along with the strengths of prior Norton and N/TRW NC430 and NT235 SiC materials. All specimens were evaluated with a machined surface condition. The NT230 specimens had an average room temperature strength of 369.23 MPa (53.55 ksi) with an associated Weibull modulus of 8.85.

Table V.
Strength characteristics of N/TRW NT230 SiC material.

Temperature, °C (°F)	Strength, MPa (ksi)
25 (77)	369.23 (53.55)
1000 (1832)	440.73 (63.92)
1150 (2102)	411.84 (59.73)
1250 (2282)	422.46 (61.27)
1370 (2500)	468.52 (67.95)

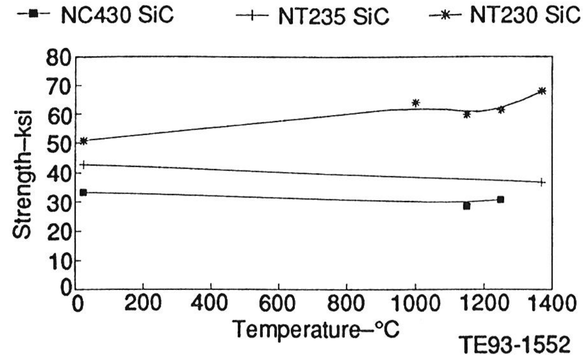

Figure 33. Strengths of N/TRW SiC materials.

The typical strength-controlling defects were observed to be surface flaws, as shown in Figure 34. The primary fracture origins observed in the specimens tested at elevated temperature were surface and internal pores, as shown in Figure 35.

CBO Sintered α-SiC. Characterization of CBO slip cast sintered α-SiC material was conducted this reporting period. While this material has been extensively evaluated in the past, both by Allison and others, recent improvements realized at CBO in the slip casting process through the use of powder beneficiation, particle size optimization, and high shear mixing have resulted in significant differences in the current generation of slip cast sintered α-SiC material relative to the previously evaluated material. The α-SiC material evaluated was sectioned

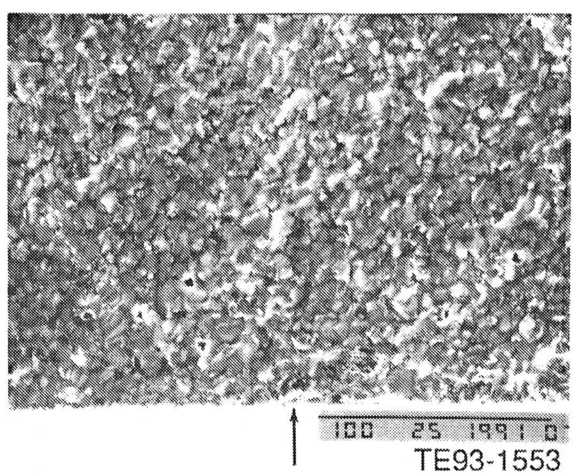

Figure 34. Typical strength-controlling defect (surface flaw) observed in N/TRW NT230 SiC tested at room temperature.

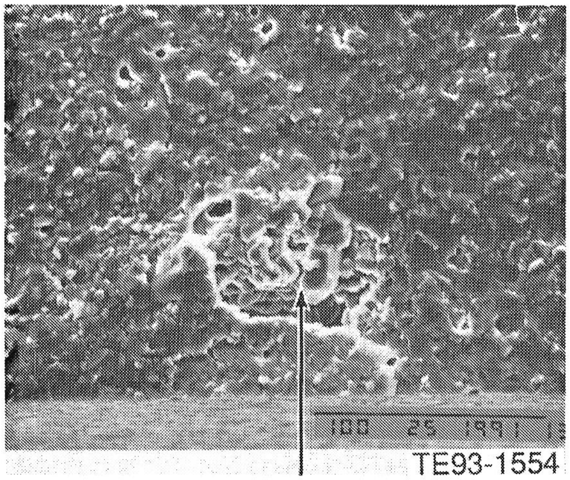

Figure 35. Typical strength-controlling defects (internal pore) observed in N/TRW NT230 SiC tested at 1370°C (2500°F).

from slip cast billets fabricated using the optimized process and densified by pressureless sintering. The average density of this material was 3.123 g/cc (0.113 lbm/in^3), which is 97.3% of theoretical density.

Material was tested with three distinct types of surface condition as the tensile surface: longitudinal ground, as-fired drain surface, and as-fired mold surface. The drain surface refers to the material which would be on the I.D. of the scroll during the slip casting process while the mold surface corresponds to material on the scroll O.D. which is in contact with the plaster mold during casting.

Material tested with the longitudinal surface in tension had an average room temperature fracture strength of 535.86 MPa (77.72 ksi) with an associated Weibull modulus of 7.1. This represents a 40% improvement in strength relative to similar CBO sintered α-SiC material fabricated in 1988. The primary strength-controlling features observed in the machined specimens were small surface and internal pores, as shown in Figure 36. Experience with CBO sintered α-SiC material has indicated no strength reduction occurs in this material as a function of temperature. To verify this assumption for the current SiC material, limited testing was conducted at a temperature of 1370°C (2500°F). The average strength of the CBO material at this temperature was 547.30 MPa (79.38 ksi).

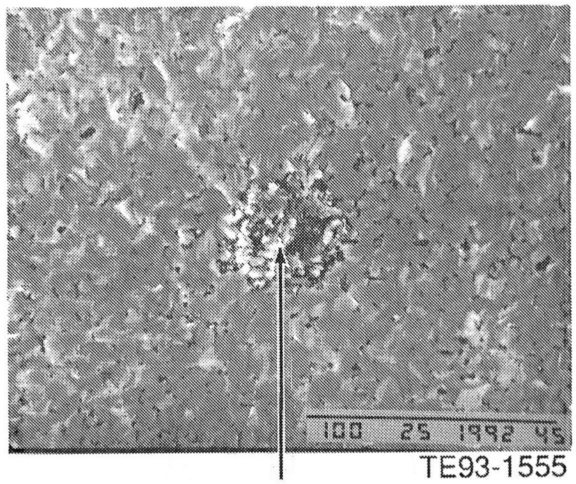

Figure 36. Typical fracture origin (internal pore) observed in CBO slip cast sintered α-SiC tested with a machined surface.

The difference between the room temperature and 1370°C (2500°F) strengths is not statistically significant. The primary fracture origins observed in the specimens evaluated at elevated temperature were similar to those found in the room temperature specimens, i.e., surface flaws and small pores.

Specimens tested with the as-fired mold surface in tension had an average room temperature strength of 455.53 MPa (66.07 ksi) with a Weibull modulus of 5.7. The typical strength-controlling features observed in these specimens were surface flaws, as shown in Figure 37.

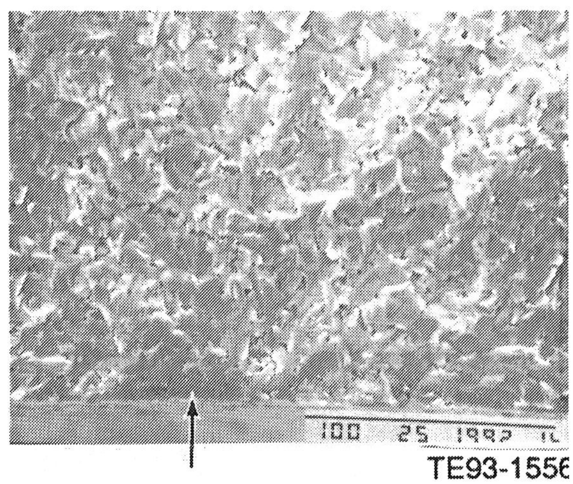

Figure 37. Typical fracture origin (surface flaw) observed in CBO sintered α-SiC with an as-processed mold surface.

Material evaluated with the as-fired drain surface in tension had an average room temperature fracture strength of 480.15 MPa (69.64 ksi). The typical primary fracture origins observed in the as-fired drain surface specimens were small pores on the surface and in the interior of the specimens, as shown in Figure 38.

GCC GN-10 Silicon Nitride. Characterization of the room temperature tensile strength of GCC GN-10 Si_3N_4 material was conducted. This activity was part of the International Energy Agency (IEA) Annex II agreement between the United States, the Federal Republic of Germany, Sweden, and Japan. The tensile testing was a round robin activity involving eleven companies, ORNL, and the NASA Lewis Research Center. A total of fifteen GN-10 Si_3N_4 tensile specimens of the ORNL configuration were provided to each participating organization for evaluation. The tensile specimens were fabricated by isostatic pressing and green machining, followed by hot isostatic pressing (HIPing). Ten specimens were supplied for testing with a straight collet configuration using the Instron equipment, with another five specimens configured for a tapered collet gripping arrangement. All of the tensile specimens were machined at Chand/Kare and dimensionally inspected at ORNL. Strain gages were attached to the gage section of the samples to determine the bending strain.

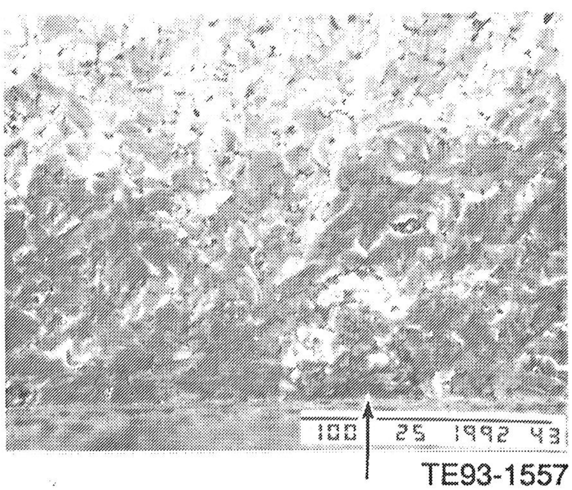

Figure 38. Typical fracture origin (surface pore) observed in CBO SiC tested with an as-processed drain surface.

The Allison evaluation of the GCC GN-10 material was conducted at the ORNL HTML using an Instron test frame and grips. The ten specimens with the straight collet configuration had an average room temperature tensile strength of 700.50 MPa (101.60 ksi) with a Weibull modulus of 13.2. The average bending strain at fracture was 2.6%. All but one of the specimens fractured in the gage section, with one specimen fracturing from the buttonhead grip feature. The primary fracture origins in the specimens were iron-containing inclusions in the 50 - 200 micron (0.002 - 0.008 inch) size range, as shown in Figure 39. The five specimens with the tapered collet configuration had an average room temperature tensile strength of 710.77 MPa (103.09 ksi) with a Weibull modulus of 11.5. The average bending strain at fracture was 2.1%. All of the tapered collet specimens fractured in the gage section. The primary fracture origins in the specimens were iron-containing inclusions similar to those observed in the straight collet specimens.

N/TRW Ceramics NT154 Silicon Nitride Gasifier Turbine Rotors. Evaluation of the material strength characteristics of N/TRW NT154 silicon nitride 20-bladed gasifier turbine rotors was conducted. Two rotors were sectioned into test bars for characterization: P/N 5-80598, S/N 3Z; and P/N 5-80598, S/N 4T. Both rotors were fabricated by pressure slip casting and hot isostatic pressing (HIPing).

Test specimens measuring 3.18 x 6.35 x 50.8 mm (0.125" x 0.25" x 2.0") were sectioned from each of the rotors. All the test bars were machined from the rotors with a radial orientation and tested with a longitudinally ground surface condition. Following machining, the test bars were heat treated at 1000°C (1832°F) for twenty hours in air. The average density was 3.229 g/cc (0.117 lbm/in^3), corresponding to 99.7% theoretical density, and 3.230 g/cc (0.117 lbm/in^3) for rotors 3Z and 4T, respectively. The results of the strength testing are summarized in Table VI.

The primary strength controlling flaws were similar in both rotors. The specimens tested at room temperature had small surface flaws as the primary fracture origins, as shown in Figure 40. The bars tested at elevated temperature

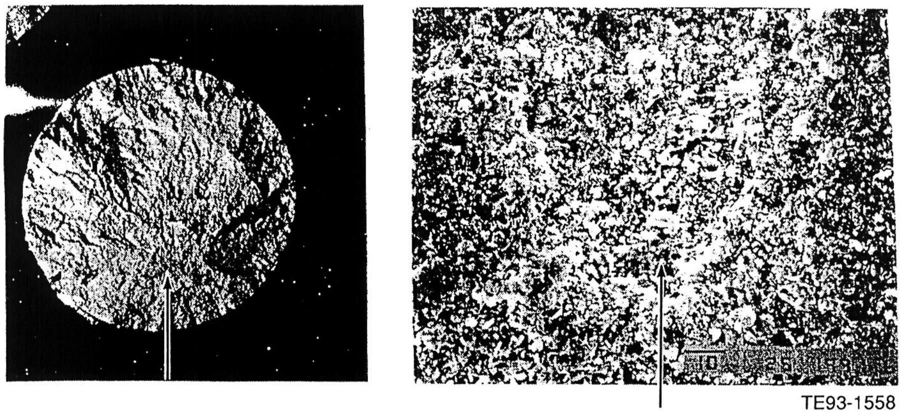

Figure 39. Typical fracture origin (iron-containing inclusion) observed in GCC GN-10 Si_3N_4 tensile specimens.

Table VI.
Strength characteristics of N/TRW NT154 silicon nitride gasifier turbine rotors.

Temperature, °C (°F)		Strength, MPa (ksi) Rotor 3Z		Rotor 4T		Test Bars	
25	(77)	893.76	(129.63)	1055.37	(153.07)	1070.33	(155.24)
1000	(1832)	527.24	(76.47)	621.63	(90.16)	700.02	(101.53)
1250	(2282)	525.17	(76.17)	585.08	(84.86)	729.25	(105.77)
1370	(2500)	462.57	(67.09)	480.15	(69.64)	631.83	(91.64)

Note: Test Bars are from billets

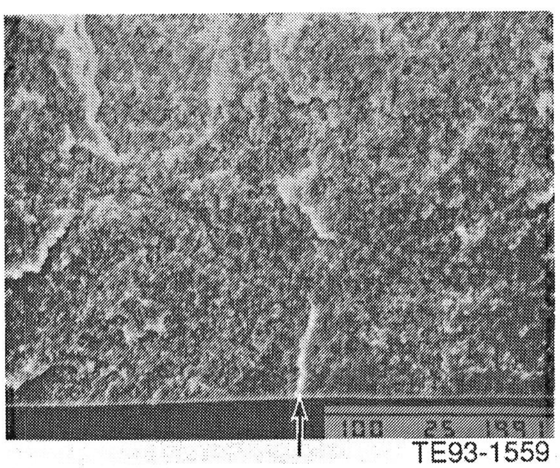

Figure 40. Typical fracture origin (surface flaw) observed in N/TRW NT154 Si_3N_4 rotor bars tested at room temperature.

also failed predominately from surface flaws, but had an increased incidence of failures from internal pores. An example of internal porosity at the failure site is shown in Figure 41.

Kyocera SN252 Silicon Nitride First-stage Power Turbine Rotors. Evaluation of the material strength characteristics of Kyocera SN252 silicon nitride first-stage power turbine rotors (P/N 5-80571) was conducted. The rotor was made of SN252 sintered reaction bonded Si_3N_4 material and fabricated by slip casting. The average density of the rotor was 3.398 g/cc (0.123 lbm/in^3).

To evaluate material strength characteristics, test specimens measuring 3.18 x 6.35 x 50.8 mm (0.125" x 0.25" x 2") were sectioned from the rotor hub. All specimens were subjected to

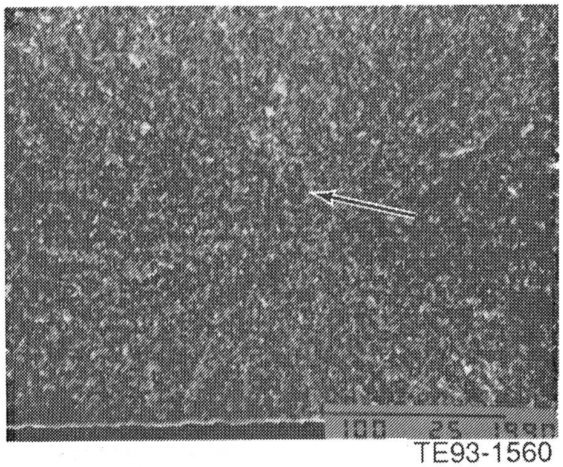

Figure 41. Primary fracture origin (internal flaw/pore) observed in N/TRW NT154 Si_3N_4 rotor bars tested at 1370°C (2500°F)

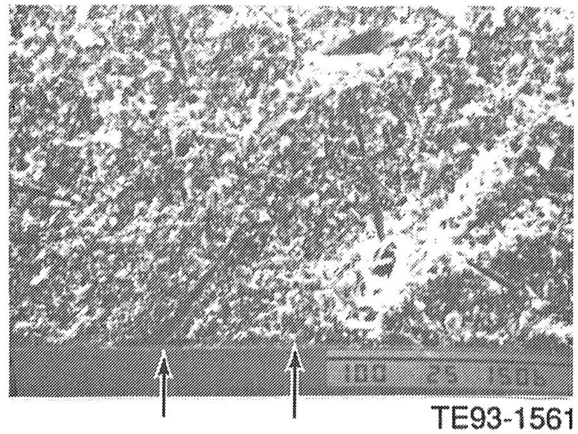

Figure 42. Typical fracture origin (surface flaw) observed in Kyocera SN252 Si_3N_4 first-stage power turbine rotor test bars.

Kyocera's recommended heat treatment and were tested with a longitudinally ground tensile surface condition. The results of the mechanical characterization are summarized in Table VII. Included in this table are properties obtained for Kyocera SN252 Si_3N_4 material in test bar form.

The test specimens from the rotor hub region compared quite favorably with the material properties supplied from Kyocera. The typical fracture origins in all specimens tested were small surface flaws, as shown in Figure 42. Occasional fractures were observed to initiate from the large tabular β-Si_3N_4 grains at the surface of the specimen. These fracture origins are shown in Figure 43.

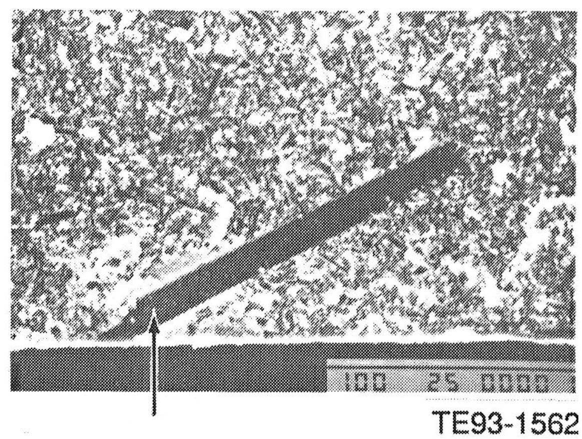

Figure 43. Fracture origin (large β—Si_3N_4 grain) observed in Kyocera SN252 Si_3N_4 first-stage power turbine rotor test bars.

Kyocera SN235 Silicon Nitride Power Turbine Rotors. Evaluation of the material strength characteristics of Kyocera SN235 silicon

Table VII.
Strength characteristics of Kyocera SN252 silicon nitride first-stage power turbine rotors.

Temperature, °C (°F)	Strength, MPa (ksi) Rotor Bars	Strength, MPa (ksi) Test Bars
25 (77)	713.01 (103.41)	634.13 (91.97)
1000 (1832)	560.15 (81.24)	538.50 (78.10)
1150 (2102)	538.84 (78.15)	533.12 (77.32)
1250 (2282)	495.68 (71.89)	518.30 (75.17)
1370 (2500)	495.34 (71.84)	507.96 (73.67)

nitride second-stage power turbine rotors (P/N 5-80544) was conducted. The rotor was fabricated of SN235 Si_3N_4 material using Kyocera's new forming process. Ongoing difficulties with dimensional distortions in the airfoils have resulted in a delay in component delivery of approximately ten months and necessitated fabrication of two new molding tools to achieve dimensionally correct components.

The microstructure of this material, shown in Figure 44, consists of tabular β-Si_3N_4 grains with an average grain size of approximately one micron. This material does not have the extremely large, high aspect ratio Si_3N_4 grains that the Kyocera SN252 Si_3N_4 material features. To evaluate material strength characteristics, test specimens were sectioned from the rotor as shown in Figure 45. The test specimen geometry and test methodology conformed to MIL-STD-1942, using 3 x 4 x 50 mm (0.12" x 0.16" x 2") test bars broken in four-point bending with quarter-point loading with an outer span of 40 mm (1.575 inches) and an inner span of 20 mm (0.788 inches). A total of twelve bars were obtained with an axial orientation from the rotor shaft, while an additional six bars from the hub region were evaluated. All of the test specimens were evaluated with a longitudinally ground tensile surface condition and were heat treated at 1000°C (1832°F) for three hours in air per Kyocera's recommendation. Characterization of the specimens revealed a significant difference in mechanical properties in the different sections of the rotor. The results of the mechanical characterization are summarized in Table VIII. Included in this table are properties furnished for the SN235 Si_3N_4 material from Kyocera.

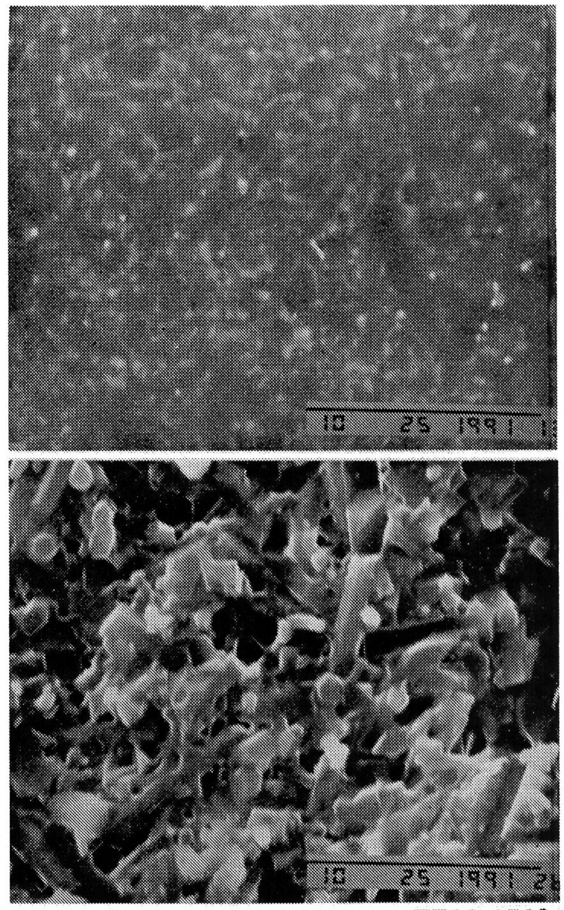
TE93-1563

Figure 44. Microstructure of Kyocera SN235 Si_3N_4 second-stage power turbine rotor test bars.

Test specimens from the rotor hub region compared quite favorably with the material properties supplied from Kyocera. The average density of material from the hub section of the rotor was 3.244 g/cc (0.117 lbm/in^3). The

Table VIII.
Strength characteristics of Kyocera SN235 silicon nitride second-stage power turbine rotors.

Temperature, °C (°F)		Strength, MPa (ksi) Kyocera Data		Rotor Hub		Rotor Shaft	
25	(77)	924.0	(134.0)	1112.32	(161.33)	780.07	(113.14)
1000	(1832)	738.0	(107.0)	856.94	(124.29)	567.92	(82.37)
1150	(2102)	517.0	(75.0)	516.55	(74.92)	383.97	(55.69)
1250	(2282)	345.0	(50.0)	365.83	(53.06)	167.68	(24.32)

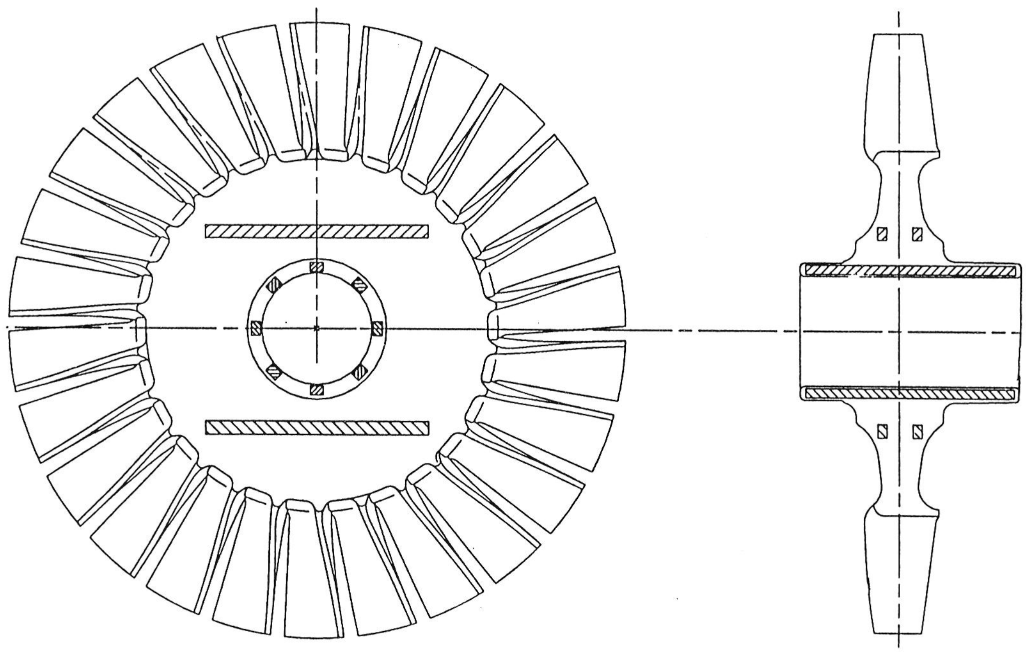

Figure 45. Schematic of test bars sectioned from second-stage Kyocera power turbine rotor.

typical fracture origins in the specimens from the hub region were small surface flaws, as shown in Figure 46.

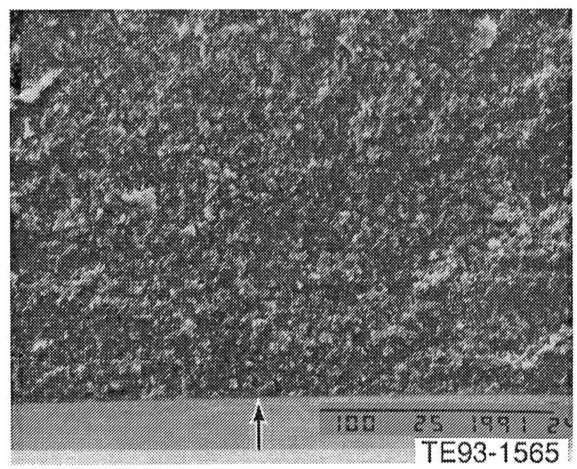

Figure 46. Typical fracture origin (surface flaw) observed in second-stage Kyocera power turbine rotor test bars.

Test specimens sectioned from the rotor shaft had strengths much lower than either the specimens from the rotor hub region or the test bar data from Kyocera. The average density of the bars from the rotor shaft was 3.241 g/cc (0.117 lbm/in^3). The typical fracture origins for the shaft bars tested at both room and elevated temperature were observed to be surface flaws. Small surface and internal pores, as shown in Figure 47, were occasionally observed as the strength-controlling features in the specimens tested at elevated temperature. In spite of the strength differential observed between the hub and shaft bars, no discernible difference in microstructure or failure origins were observed. Kyocera informed Allison that the reason for the strength decrease in the shaft bars was related to the flow characteristics of the SN235 Si_3N_4 material in the molding tool. Kyocera is currently modifying the tool to improve the flow pattern to provide a more uniform structure in the rotor.

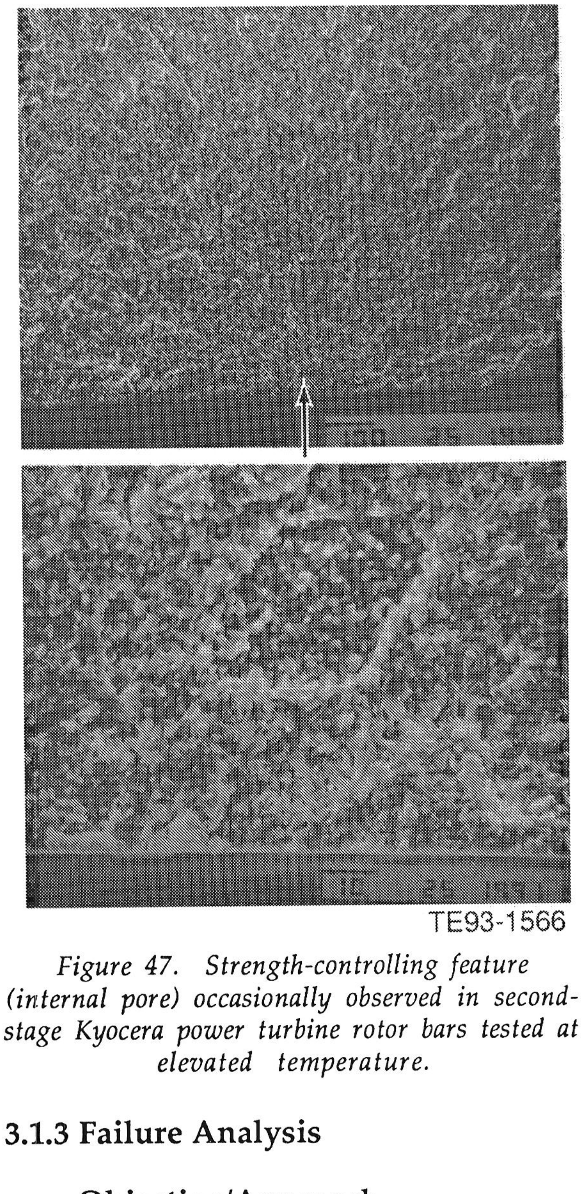

TE93-1566

Figure 47. Strength-controlling feature (internal pore) occasionally observed in second-stage Kyocera power turbine rotor bars tested at elevated temperature.

3.1.3 Failure Analysis

Objective/Approach

Fractographic analyses of ceramic components that experienced damage during rig/engine testing are the basis of understanding and correcting the sources of failures. Fractographic analysis is one of the most powerful tools used in the failure analysis of an engine or rig tested component. A careful study of the general and detailed features of the topography of a fracture by visual assessment and scanning electron microscopy provides a wealth of information concerning the failure origin and the failure mode(s). Analysis of hardware failures allows the separation of design features from material deficiencies, defects, or nonoptimum fabrication procedures and can suggest appropriate corrective measures.

Accomplishments/Results

- Conducted fractographic analysis of a CBO SiC 15-blade rotor (P/N 5-80501, S/N FX78527) which had been run in the hot gasifier rig S/N 12, BU3. The rotor failure originated at a deep cut created during the balance stock removal.
- Conducted fractographic analysis of a CBO SiC combustor (P/N 5-80583, S/N FX79402) which had been run in the hot rig S/N 12, BU28. The combustor failed by thermal stress originated at the outside corner of a small dilution air hole.
- Conducted fractographic analysis of a Kyocera scroll (P/N 5-80554, S/N S-1) which had been run in the hot rig S/N 12, BU23. The scroll developed long circumferential cracks originated at the gap of the scroll-flange joint.
- Conducted failure analyses of ceramic and metallic components tested in hot rig S/N 13, BU2. The C/C seals rubbed and overheated the rotor shaft, which then released the rotor.
- Conducted failure analyses of a ceramic gasifier containing a Kyocera 20-blade rotor (P/N 5-67200, S/N 5K26) and a Kyocera scroll (P/N 5-81111, S/N KX55599).

Discussion

Hot Rig S/N 10, BU 3. A CBO fifteen-bladed silicon carbide gasifier rotor was tested in the hot rig. The test lasted only ten seconds. Post test inspection revealed the rotor burst. Figure 48 shows the reconstructed rotor. The failure origin was located at the trailing edge side surface. The cracking pattern demonstrated the fracture spread from the origin to both sides and branched into equal size pie shaped pieces as the fracture progressed.

Inspection of the origin area showed that the fracture originated at the edge of the balance stock removal area where abnormally deep cuts from the abrasive wheel existed, Figure 49. The origin consisted of several pre-existing 50-

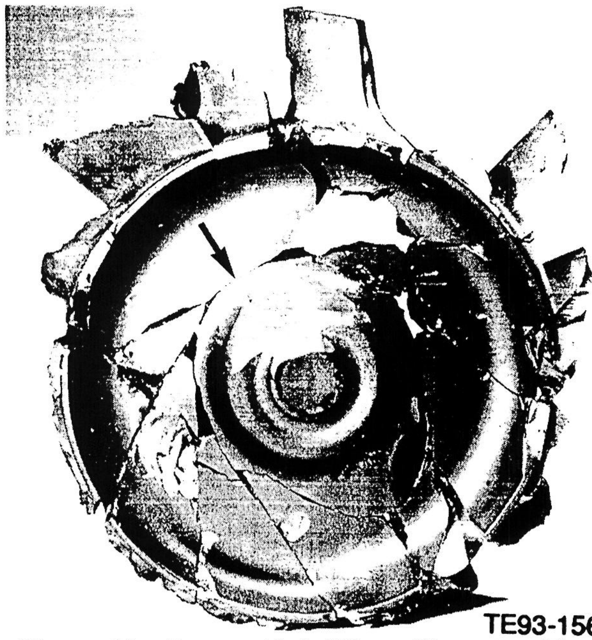

TE93-1567

Figure 48. Reassembled SiC gasifier rotor (the arrow points to the location of the failure origin).

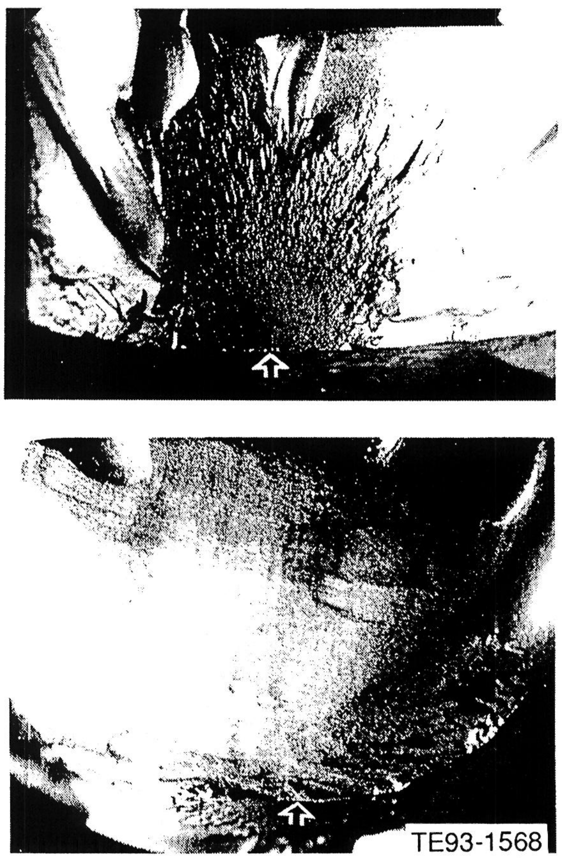

TE93-1568

Figure 49. Fractograph (top) of the gasifier rotor at origin area (hollow arrow) and the hub surface adjacent to the origin (bottom) (magn 5X).

100 micron diameter semi-circular cracks created by the deep cuts, Figure 50. According to the fracture mirror size analysis, the fracture strength was 18.3 ksi.

Hot Rig S/N 12, BU 28. A CBO silicon carbide combustor was tested and failed in 0.6 hour in the hot rig. The maximum turbine inlet temperature was 922°C (1692°F). Inspection revealed the combustor cracked into three large pieces, Figure 51.

The crack originated at the outside corner of one small dilution air hole as indicated in Figure 52. No defect or damage at the origin was observed. The fracture was initiated by thermal stress. Certain areas of the fracture had been discolored (dark gray or blue) indicating the fracture occurred at the start up or during testing but before shutting down the test. Applying the fracture mirror size analysis to the combustor indicated the fracture strength was 42.6 ksi.

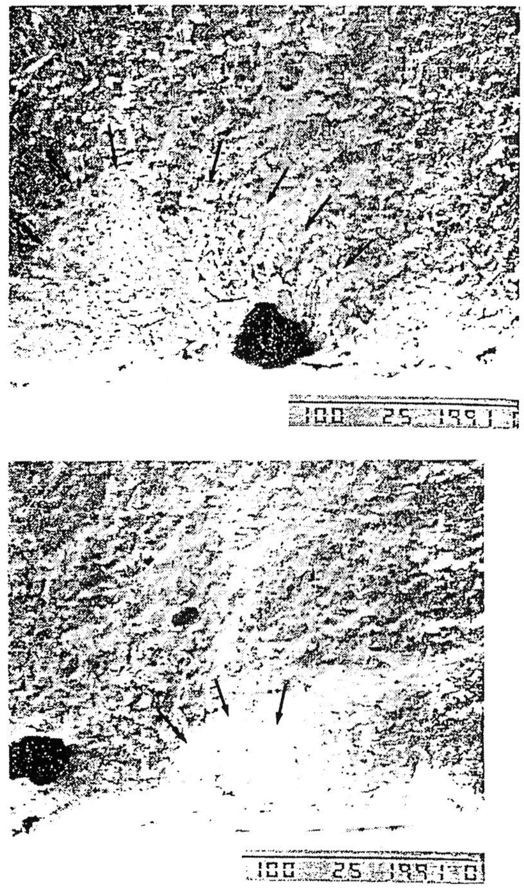

TE93-1569

Figure 50. SEM fractographs of the origin area. Small arrows outline the preexisting small cracks.

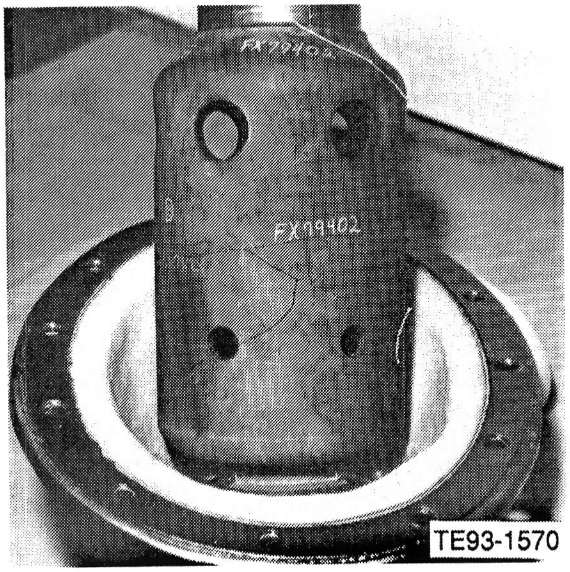

Figure 51. As-disassembled condition of the combustor, P/N 5-80583, S/N FX79402. The combustor was still attached to the dome.

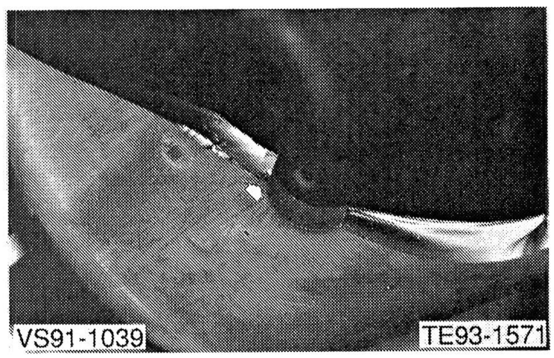

Figure 52. Fractography of the primary fracture origin area.

Hot Rig S/N 12, BU 23. A Kyocera SN252 scroll was rig tested. The peak test temperature was 1401°C (2554°F). The test was terminated after detecting cracks. Total test time was 7.2 hours.

Fluorescent penetrant inspection of the scroll revealed cracks at four key slots and at the scroll-flange joint. The radial key slot cracks were short and ended within the flange. One crack extended into the scroll body. There were several circumferential cracks which almost completely covered the scroll-flange joint. The cracks were opened in the laboratory for inspection.

Circumferential Cracks. Figure 53 shows the opened long circumferential crack connected to key slot crack No. 1. This crack originated at the corner of a 0.85 inch section of the scroll-flange joint where barely any bonding material existed.

Radial Key Slot Cracks. Figure 54 shows the optical fractographs of the four radial key slot cracks. No. 1 and No. 2 originated at the aft side slot corner. No. 3 originated at the middle of the key slot and No. 4 originated at the forward side slot corner. No witness marks of contacting with the key or other object were observed. All key slots had sharp corners and chipping on the corners. According to fracture mirror size analysis, the fracture strength for Nos. 1, 2, 3 and 4 cracks were 87.86, 82.19, 67.12 and 82.19 ksi, respectively. The fractures are considered normal in comparison to the flexural strength of this material test bars which are 91.97, 78.10, 75.17 and 73.67 ksi respectively for room temperature, 1000°C (1832°F), 1250°C (2282°F), and 1371°C (2500°F).

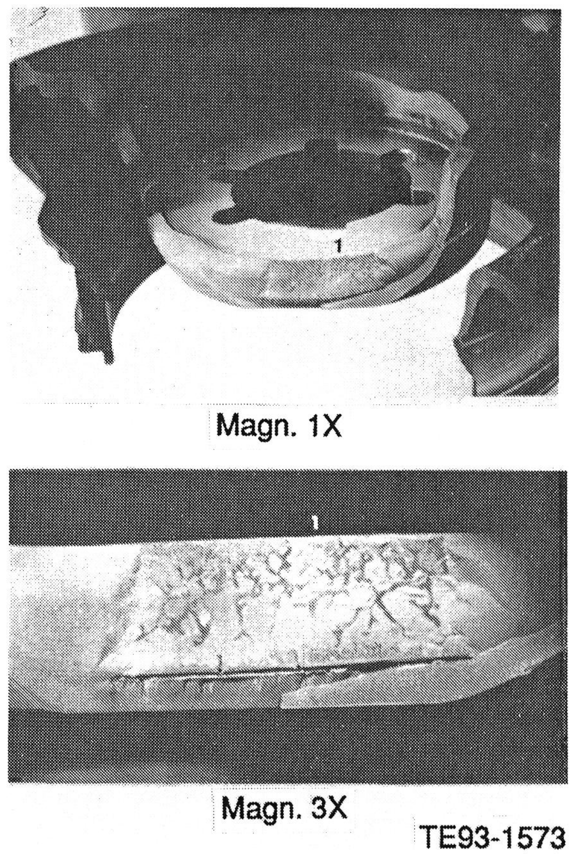

Figure 53. Large unbonded area which meets the key slot crack No. 1.

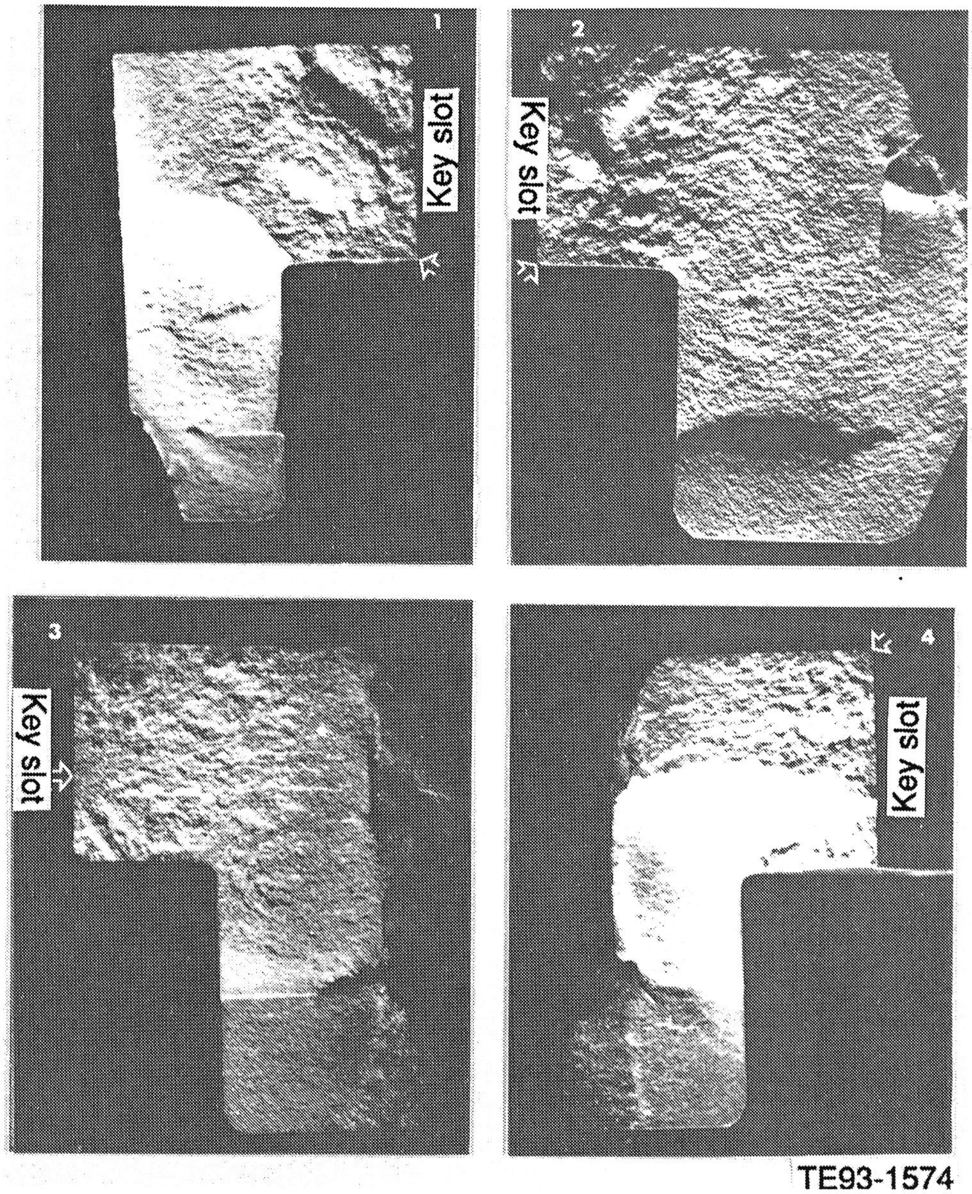

Figure 54. Fractographs of the key slot cracks. Hollow arrows point to origins (magn. 8X).

Hot Rig S/N 12, BU 2. Testing of a 15-bladed gasifier turbine rotor and a scroll was terminated when the rotor burst at 90.5% speed at rotor inlet temperature = 1270°C (2318°F). Total part time was 0.8 hour.

Inspection revealed that the scroll suffered minor chipping at the aft end while the rotor came out of the metal shaft and broke into two large and many small pieces, Figure 55. Long metallic marks exhibited on the rotor stub shaft outside diameter were caused by rubbing against the inside diameter of the heat shield base when the rotor was spinning out of the metal shaft. Those marks were heavier at one side of the stub shaft. There was a light, and almost continuous, rub mark on the back face of the rotor which was also caused by rubbing the outside diameter of the heat shield base.

The rotor's main fracture was at the radius of the back face, Figure 56. No apparent flaw was found. The fracture stress calculated from the fracture mirror size was 13 ksi. The low fracture stress was due to impact on the rig wall.

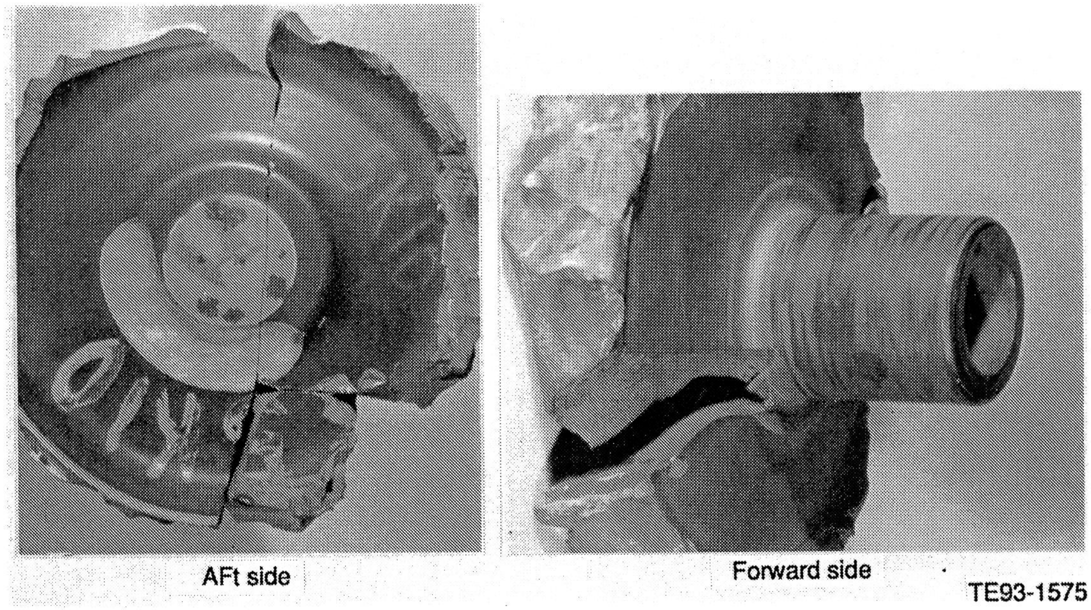

Figure 55. The condition of the 15-blade gasifier rotor, P/N 5-66946, S/N 5K10.

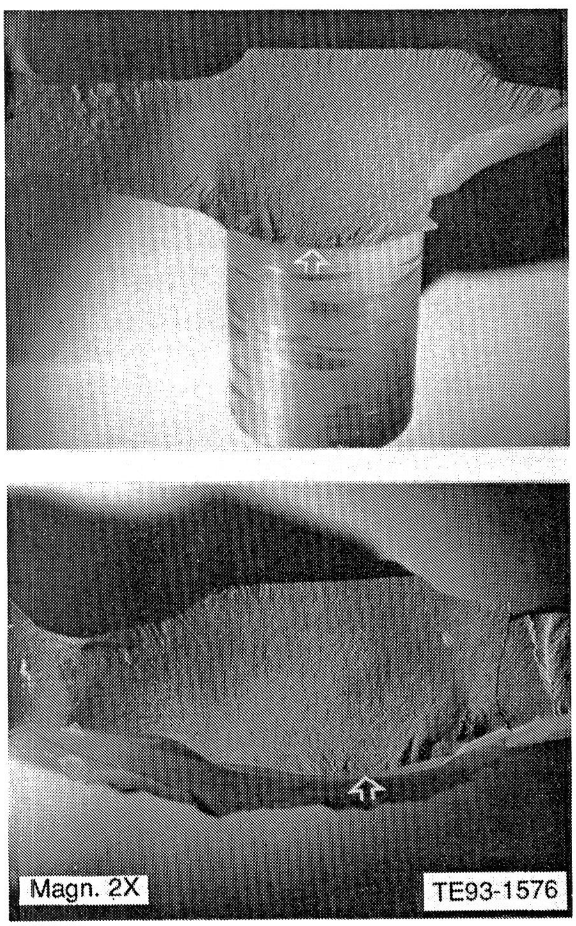

Figure 56. The mating fracture surfaces of the rotor. Hollow arrows point to the origin.

Figure 57 shows the inside and outside condition of the metal shaft. There were heavy and light rub bands located at the outer diameter where the two carbon seals seated in the gasifier. Broken carbon fibers were buried in the shaft surface, Figure 58. The area adjacent to the heavy rub band was overheated as is illustrated in the etched cross section in Figure 59. In this area, the grain boundaries became less distinct due to partial solutioning, an indication of a surface temperature close to 1950°C (3542°F).

A metallic substance was smeared on part of the I.D. of the forward seal is shown in Figure 60. Semi-quantitative XEDA indicated the smeared metal was the rotor shaft material.

Apparently, heavy rubbing between the carbon seal and the shaft raised the shaft temperature above the shrink fit temperature and released the rotor which then failed upon impact.

Hot Rig S/N 13, BU 3. The scroll (P/N 5-81111, S/N KX55599) which survived from BU 2 was tested in this buildup with a Kyocera SN252 20-bladed rotor. In order to use the Kyocera rotor, which had a smaller diameter, a shroud needed to be braised to the scroll for proper tip clearance. The rig ran for 0.3 hours up to a

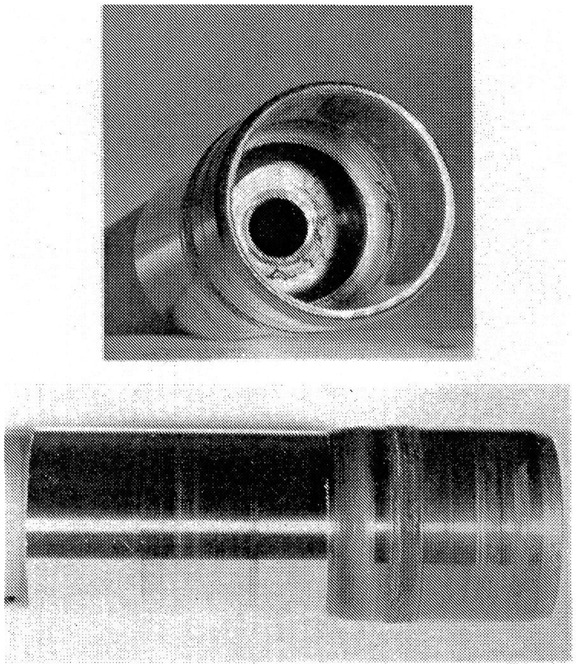

TE93-1577

Figure 57. Condition of the metal rotor shaft.

maximum condition of rotor inlet temperature = 904°C (1659°F) at 80% N_1 and failed.

Inspection revealed that the rotor lost all blades from impact. Almost half of the shroud on the scroll was missing and the whole sleeve lined at the shroud I.D. was lost. Separation of the sleeve from the shroud occurred at the bond. No fracture of the sleeve or the shroud was observed. Figure 61 shows a representative large piece of the sleeve. There were heavy rubbing marks on the I.D. of the sleeve in the circumferential direction. On the O.D. of the sleeve the dark regions had no bonding material. The light regions had been wetted by the bonding material but no bonding occurred. Figure 62 shows the surface of the bonding material exhibited an as-sintered surface which indicated there was no bonding between the sleeve and the shroud.

In conclusion, evidence showed that the rotor rubbed the poorly bonded shroud sleeve but the exact origin of the gasifier failure could not be determined.

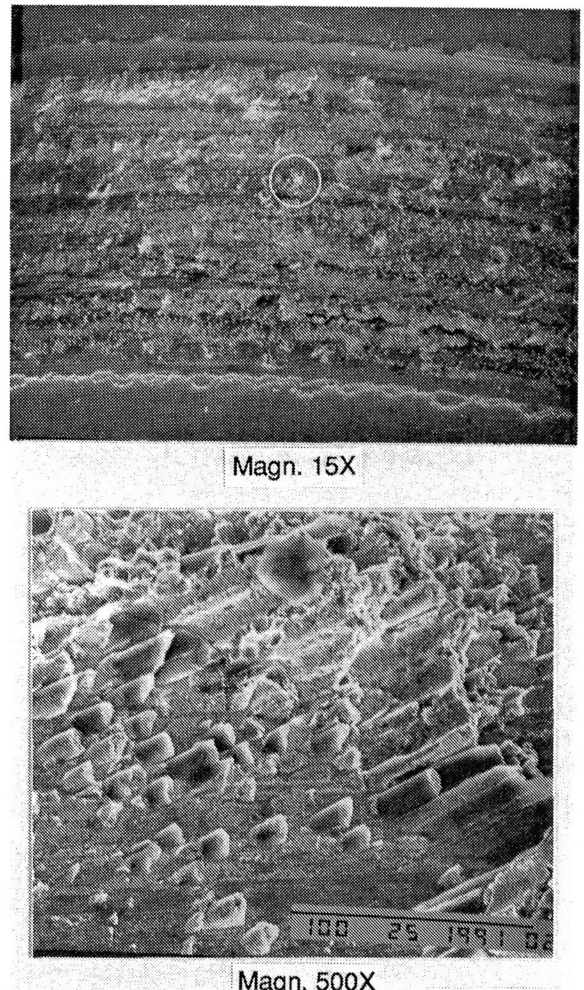

TE93-1578

Figure 58. SEM photographs of the rub band on the rotor shaft seen in Figure 57.

3.2 CERAMIC COMPONENT PROCESS DEVELOPMENT AND FABRICATION

This subsection details the ceramic process development and fabrication at the component developers (CBO, Manville, Corning, CPS, and N/TRW). Allison continues to subcontract process development to the domestic ceramic manufacturing community and works in an iterative development loop with those suppliers in component design, characterization, and rig/engine test data feedback.

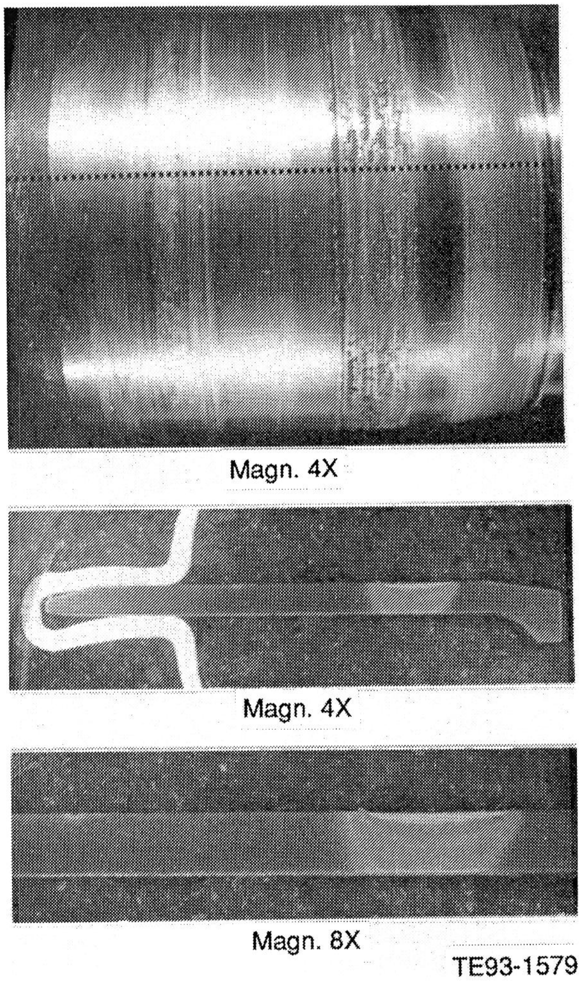

Figure 59. The axial cross-section profile of the rotor shaft. Etching revealed the heat affected areas by rubbing.

Component development activities at CBO included slip cast SiC combustors and scrolls. Manville concentrated on development and fabrication of ceramic thermal insulation for test rigs and engines. Corning continued the development of one-piece extruded regenerator disks utilizing four material systems: alumino-silicate (AS), magnesium alumino-silicate (MAS), aluminum titanate (MAT), and zirconium phosphate (NZP). CPS addressed fabrication of CM200 sialon gasifier turbine rotors using their Quickset injection molding process. N/TRW Ceramics' efforts were directed towards development of both gasifier turbine rotors fabricated by pressure slip casting NT154 and NT164 Si_3N_4, and turbine scrolls fabricated of slip cast NT230 SiC. A cooperative effort between N/TRW and CPS focused on codeveloping NT154 Si_3N_4 vane platforms utilizing the Quickset injection molding process.

3.2.1 Carborundum Company (CBO)

Objective/Approach

The ceramic component development during 1991 with CBO consisted of two major tasks: slip optimization and process development. Slip optimization focused on the effects of powder beneficiation and particle size distribution on slip properties, while process development focused on optimizing the slip casting methodology to fabricate combustors and scrolls.

Accomplishments/Results

- Beneficiation and aging of α-SiC carbide powder and slip, respectively, decreased the shrinkage of cast and sintered material without adversely affecting the density and strength of the material.
- Optimized envelope for milling time and grit concentration, resulting in α–SiC slip rheology to yield reproducible component castings.
- Scrolls were successfully drain cast and low pressure slip cast, and sintered using a new five piece mold. Voids were observed on the inside drain surface of the scrolls.

Discussion

Slip Optimization. The slip optimization included evaluation of the effects of (1) beneficiated SiC powder on the slip casting behavior and (2) particle-size distribution of the SiC grains on the sintered density and shrinkage.

Beneficiated silicon carbide powder was used to prepare three experimental slips by varying the solids content between 77.5% and 81.3%, and by varying the amount of each of the three dispersants required to properly deflocculate the slip. The slips were both drain and low pressure cast at about 20 psi for five minutes to fabricate rectangular crucibles. The results of

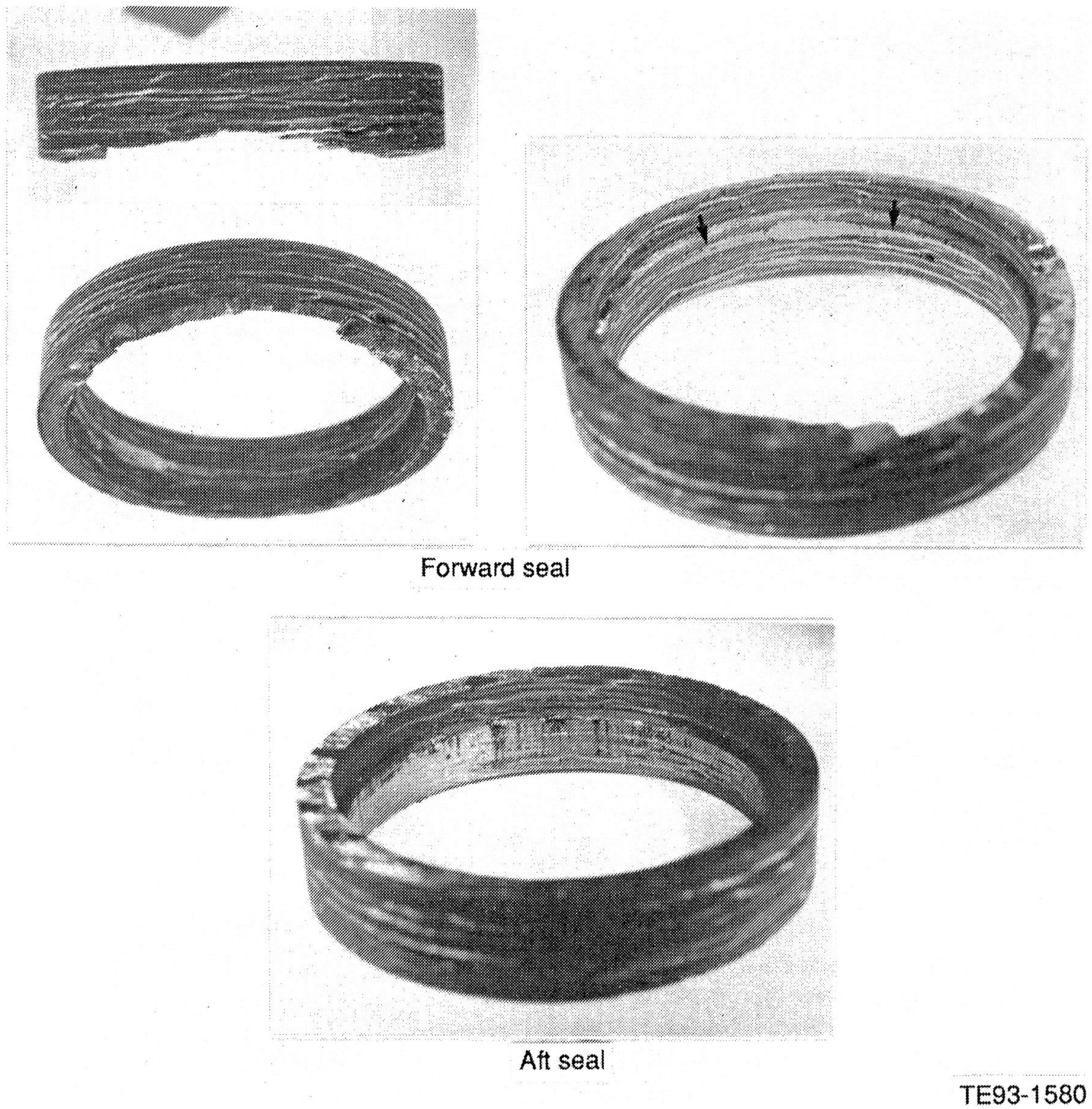

Figure 60. The condition of the C/C seals. Arrows outlined the metallic smear on the seal I.D.

the cast and sintered crucibles indicated that the slip with 79.1% solid content and normal level of additives provided material with an optimum sintered density of 3.10 gm/cc, shrinkage of 6.21%, and optimum cast wall thickness. It did not stick to the mold, and had insignificant skimming/settling.

Based on these encouraging results, a 75 kg batch of scaled-up slip with a similar composition was subsequently formulated to ascertain the repeatability of the results. The density and shrinkage of the test crucibles cast and sintered from this slip were 3.16 gm/cc and 9.01%, respectively. The slight improvement in the density and a large increase in the shrinkage compared to the batch slip are attributed to the variation in the particle size distribution of the two slips caused by the different size of the ball mills used in the two independent experiments. The 9.01% shrinkage is still about 10% lower than that of the normal slip, and should allow better dimensional control of complex shape components.

The average 4-point MOR strength of this material was found to be 467.8 MPa (67.85 ksi) compared to 481.7 MPa (69.86 ksi) for the

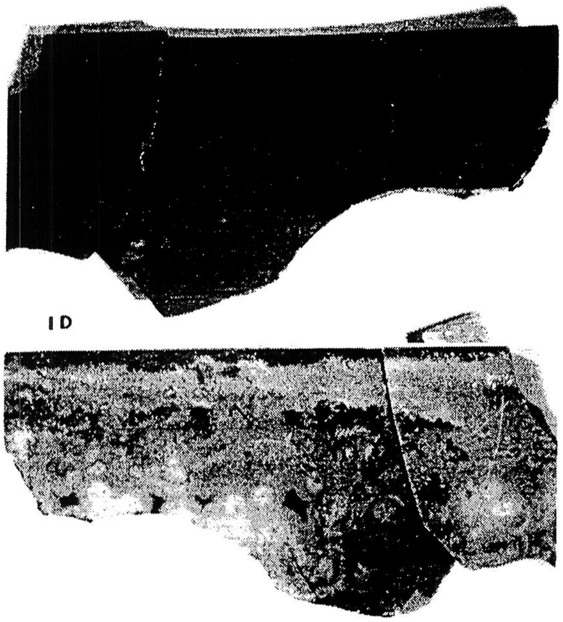

ID

OD TE93-1582

Figure 61. Large broken pieces of the sleeve.

TE93-1583

Figure 62. SEM photographs of the bonding material (top) and bonding material wetted sleeve O.D. surface (bottom).

normal slip material. Aging of the beneficiated slip for a month did not show any effect on the cast and sintered properties of the material. It is concluded that beneficiated slip offers improved density and decreased shrinkage over the normal slip without any statistical loss in the strength of the material, and should result in a more consistent starting material leading to more reproducible processing and finished component properties.

Particle size distribution of the solids in the slip has a major impact on the casting behavior, skrinkage and the density of the material. A three-factor interactive designed experiment was conducted during 1991 to optimize the milling time of the submicron powder and the grit (coarse SiC), and the grit concentration. Table IX summarizes the experiments which required ten different slips.

Contour plots were generated for each of the five most important experimental responses: slip plastic index, casting rate, green density, percent shrinkage, and sintered density. The contour plots depict how each response varied with changes in Mill 1, Mill 2, and grit. Mill 1 was the length of time required for milling the submicron fraction of the powder alone, Mill 2 was the additional milling time required after the coarse grit that was added to the milled submicron powder, and the grit was the coarse SiC powder as a weight percent of the total solids. The contour plots were then used to identify regions of operation in which each response was optimized.

The overall operating conditions were experimentally optimized, and isolated by weighing the importance and variability of each of the response factors as depicted by the shaded region in Figure 63. The shaded area shows that (i) Mill 1 should be between -0.5 to 1 (ii) Mill 2 should be between 0.5 to 1 and (iii) grit concentration should be contained between -0.5 to 0.5. Any slip made within the shaded region should yield good reproducible casting.

Optimization of the grit size and concentration was also experimentally assessed. Powder blending studies were conducted to ascertain the optimum amount of Grit 1 (coarse), Grit 2 (fine), and submicron powder required to obtain the slip rheology for casting components with optimum material properties. Thirteen different slurry blends were prepared, characterized, and used to cast ten crucibles each. The results indicated that coarse to fine ratio of the grit had minimum effect on the cast material properties.

Table IX.
Designed experiment to optimize particle size distribution and milling time.

Factors	Level (-, 0, +)	Responses
X_1 = mill time (submicron)	6 hr, 24 hr, 72 hr	y_1 = density
X_2 = mill time (grit)	4 hr, 10 hr, 16 hr	y_2 = % shrinkage
X_3 = grit concentration	N, 1.25 N, 1.5 N	y_3 = distribution modulus
		y_4 = calculated porosity
		y_5 = part quality

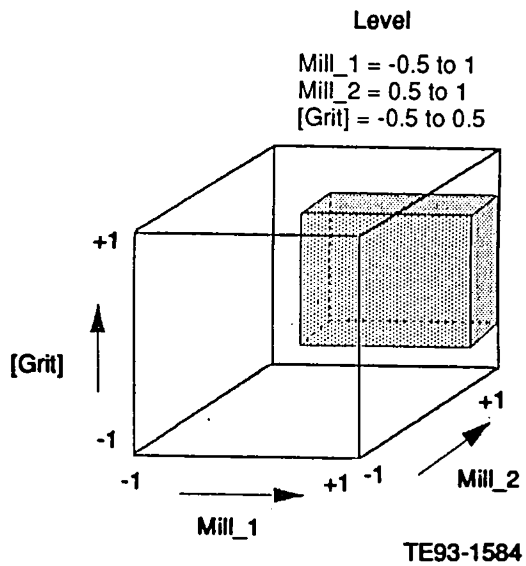

Figure 63. Optimization of Carborundum SiC processing.

Process Development. The objective of the process development task is improvement in the mold material and iterative development of scroll mold design and pressure casting methodology. The goal is to accelerate casting rates for fabricating engine quality scrolls free of defects.

Several pressure cast multi-piece molds were designed, fabricated, and evaluated. A standard procedure for filling, pressurizing, and draining of the mold was established and casting trials were conducted. Feed rate, casting pressure and time, feed line location, and mold tilting procedures were modified to optimize the parameters to obtain the best quality scrolls. Cast scrolls had the desired wall thicknesses, were free of cracks, and demolded readily; however, the majority of the scrolls had excessive air voids on both the mold and drain surfaces. Experiments were then conducted to identify the cause of the air voids by varying slip viscosity, manual deairing, fill method, tank stirring speed, cast pressure, fill/drain port, and fill rate. After eight scrolls were cast under varying conditions, it was revealed that voids were formed due to poor slip deairing. In addition, small cracks were also observed under the scroll inlet.

The scroll mold design was modified to fabricate a multi-piece low pressure casting mold, Figure 64, in which (i) the number of seams were reduced to eliminate the source of defects and (ii) a seam from the base of the throat was removed which had caused cracking problems in earlier designs. This mold consisted of two halves with a single core that could be pulled from the top. The throat section was comprised of pieces that bolted into place instead of the previously used disposable insert. The mold also had a fill/drain in the bottom of the shroud and a vent line at the inlet end. A similarly designed drain casting mold was also fabricated. The mold model was also adjusted to add a downward angle to the underside of the scroll and to tilt the inlet neck upward with a less abrupt ledge leading to a smoother inside drain surface. Two other modifications in the mold were three rubber pads which formed alignment holes/tabs (Figure 64(b)) to facilitate alignment for finish machining, and elongation of the neck to provide extra cutoff stock to eliminate air pockets observed in the neck.

Casting trials for both drain and low pressure casting methods were conducted in the multi-piece piece mold design. The center core of some

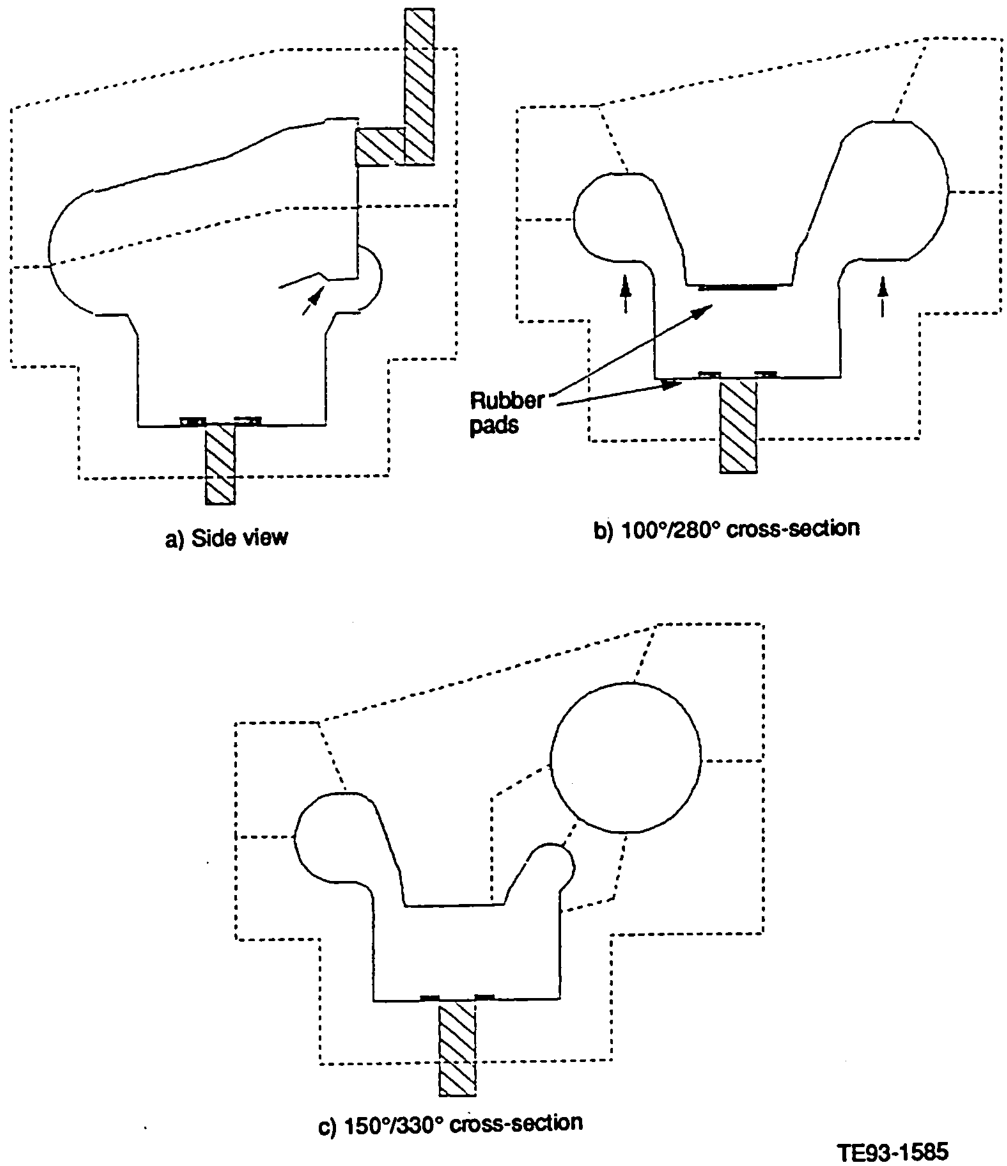

Figure 64. Vortex pressure casting mold.

of the drain and low pressure cast scrolls collapsed. However, the drain cast method resulted in a yield of 72% whereas the low pressure casting yield was only 53%. The collapsing of the scrolls was found to be related to the draining and air pressure (3-4 psi) drying operations. Four low pressure scroll castings were fabricated during which the top vent cap was removed prior to draining, and both vent/drain lines were left open for natural drying. None of the scrolls collapsed.

The second major problem with the scroll castings was the presence of excessive air voids on both the mold and drain surfaces. Various remedies including a new feed tank, mold filling method, tank and feed pressure, new procedures for mold tilt, fill rate, and fill pressure were systematically varied and modified to ascertain the underlying root cause of the defects. Round crucibles formed by the same slip casting protocol as the scrolls also had large number of air voids. It was concluded that the voids were not caused by the complex shape of the scroll but rather by the mold filling process step. Additional crucible castings were fabricated in which piping and valves between the slip delivery system and the mold were removed to eliminate the source of air bubbles. No air defects were observed. Four scrolls were slip cast by this arrangement. None of them showed external defects. Large air voids were still present on the inside drain surface. The origin of the voids remains unknown and continues to be under investigation.

The objective of the mold material development task was to formulate a plaster blend with desirable properties (mold strength, permeability, and microstructural uniformity) suitable for producing consistent low pressure casting. Twenty different plaster blends of Hydrocal and No. 1 Pottery plaster were mixed and evaluated. Responses to experimental factors such as plaster blend ratio, mixing time, percent water added, and deairing were measured. A permeability rig was assembled. Permeability is defined as the amount of water flow per unit time under 20 psi differential pressure assuming viscosity, pressure differential, puck thickness, and flow area are constant. Results to date are mixed with no trend. This work will continue during 1992 with a goal to identify a plaster blend which exhibits the best characteristics with respect to high water permeability, strength, and fast casting rate.

3.2.2 Manville Corp

Objective/Approach

Manville tasks are aimed at developing an injection moldable insulation capable of low-cost, high-volume production for automotive gas turbines. The approach is to modify the insulation material system for improved injection molding properties while developing the injection molding process for both simple and complex engine components. In addition to the development of the molding process, several other developmental items are being addressed including: insulation/metal hardware bondability, erosion resistance, and non-hazardous non-respirable materials.

Accomplishments/Results

- Completed mixing experiments to identify the cause of drying shrinkage.
- Confirmed the elimination of drying shrinkage by use of deshotted fiber produced on pilot mat machine.
- Determined level of fiber cleaning necessary to produce insulation with low drying shrinkage.
- Tested drying shrinkage at various fiber contents and mechanical processing of the cleaned fiber to improve moldability while maintaining acceptable drying shrinkage.
- Set up laboratory injection molding equipment at Manville using a hydraulic drive unit.
- Conducted an injection molding trial of a gasifier housing with the cleaned, processed fiber.
- Conducted an injection molding trial of the complex engine housing with the latest designed metal mold inserts using the cleaned, processed fiber.
- Measured thermal conductivity of smooth surface finished and rough finished insulation.

Discussion

Investigations into the drying shrinkage problem indicated that the primary cause was related to the quantity of fiber in the drying insulation structure. Insulation batches prepared with very clean, deshotted fiber exhibited satisfactory drying shrinkage. Insulation formulations with variations of the other components resulted in minor changes in drying shrinkage. The fiber was deshotted in limited quantities by dispersing the raw fiber in a thirty gallon bucket, allowing the shot to settle and then withdrawing the fiber from the top of the water. This deshotting technique was very time consuming and yielded only enough clean fiber for small-scale experiments. A wet-process pilot machine at the Manville Technical Center has been adapted to produce larger quantities of deshotted fiber. The pilot machine produced adequate quality fiber in quantities useful for pilot scale injection molding. Additional refinements of the pilot machine production of cleaned fiber have resulted in no further change in the low drying shrinkage. The drying shrinkages of the hand deshotted and the pilot machine deshotted fiber based insulation are compared below in Table X.

Larger quantities of the pilot deshotted fiber, prepared and shipped to the GM Technical

Table X.
Drying shrinkages of hand deshotted and pilot machine deshotted fiber based insulation.

Fiber preparation	length mm (inch)	Drying length mm (inch)	Shrinkage thickness (%)	Dry density PCF kg/m^3 (lbm/ft^3)
Raw (not deshotted)	23 (0.9)	124 (4.9)	9.8	434 (27.1)
Hand deshotted	3 (0.1)	13 (0.5)	1.0	333 (20.8)
Pilot deshotted	3 (0.1)	8 (0.3)	1.4	330 (20.6)

Center, have been used in development engine insulation test pieces and trial injection moldings. The injection molding trials showed evidence of liquid separation during the injection molding of different pieces. The molding showed voids and insufficient mold fill-out, probably as a result of the liquid separation. Additional molding trials have been conducted with insulation that does not show the liquid separation.

Twenty-eight small scale batches of insulation were prepared following various fiber cleaning operations of increasing levels of fiber cleaning. The drying shrinkage results are presented in Table XI and plotted in Figure 65. The fiber cleaning levels ranged from raw fiber (no cleaning) to very long time (intense cleaning) indicated by Level 4. The shrinkage results for length, width, and thickness have been normalized by comparing to the desired maximum levels. The raw and washed fibers resulted in unacceptably high shrinkages. Cleaning Levels 1 through 4 resulted in acceptable drying shrinkages. Further testing of the fibers prepared by Levels 3 & 4 at various insulation fiber contents ranging from 50% to 57% showed a minimum acceptable fiber level of 55%. The results are plotted in the Figure 66.

Table XI.
Drying shrinkage results.

Fiber preparation	Normalized shrinkage (%)
Raw fiber	3.05
Washed fiber	2.86
Level 1 (hand deshotted)	0.45
Level 2 (hand deshotted)	0.38
Level 3 (pilot deshotted)	0.17
Level 4 (pilot deshotted)	0.12

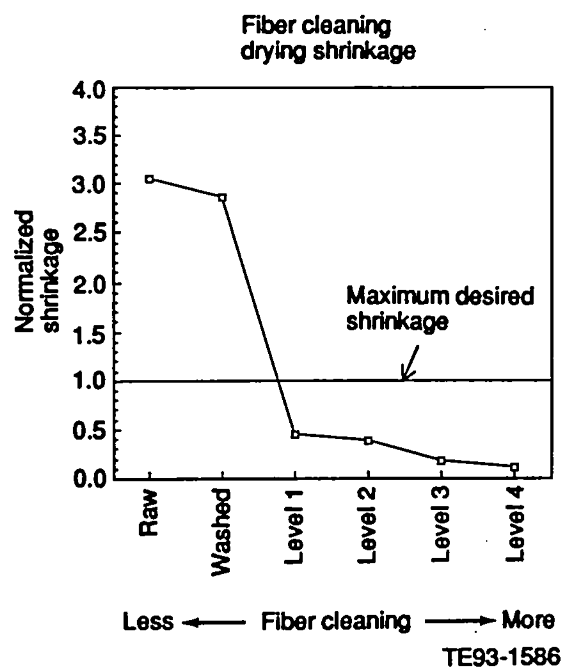

Figure 65. Fiber cleaning, drying shrinkage.

Thirty-seven small scale batches of insulation were prepared using Level 3 fiber cleaning, followed by increasing levels of mechanical processing. The mechanical processing was intended to improve the moldability of the wet insulation. The drying shrinkage results are plotted in Figure 67. The fiber processing levels ranged from Level 3 cleaned fiber with no further processing to increased levels of fiber treatment indicated by 300, 500, and 700 settings. The various fiber processing levels were evaluated at increasing fiber contents, so that

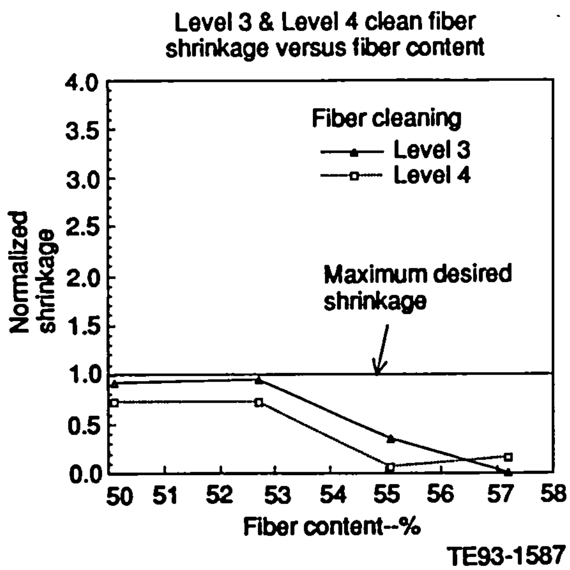

Figure 66. Level 3 and level 4 clean fiber shrinkage versus fiber content.

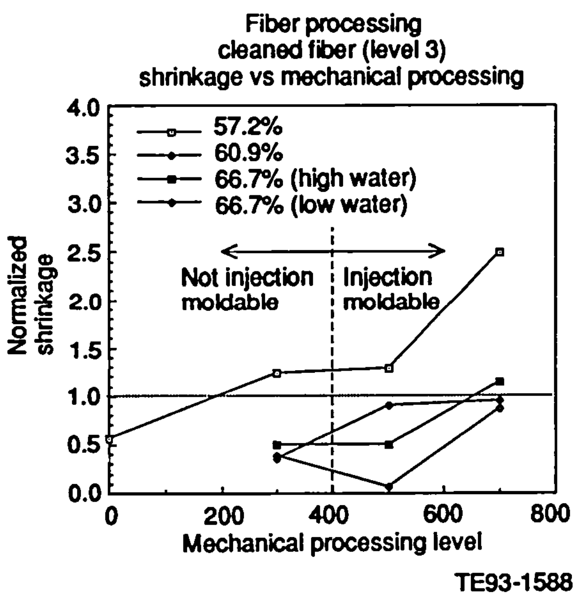

Figure 67. Fiber processing, cleaned fiber (level 3), shrinkage versus mechanical processing.

the moldability could be improved while maintaining acceptable drying shrinkage. The shrinkage results for length, width, and thickness have been normalized by comparing to the desired maximum levels. The lower fiber contents resulted in unacceptable, or marginally high shrinkages. Higher fiber contents at a mechanical processing level of 500 appears to have produced an insulation with acceptable drying shrinkage and desirable molding characteristics.

The best molding and lowest drying shrinkage material of the experimental series described above, 66.7% fiber (low water) at 500 mechanical processing level, was prepared for injection molding trials. An engine structure was successfully injection molded with complete fill-out of the mold but with a few holes in the molded surface. An engine housing with metal core inserts was injection molded with almost complete mold fill-out. After drying, the metal core inserts were removed with some difficulty. The resulting insulation was intact with some small holes in the surface. Further development work on mold core removal techniques and core insert design is anticipated.

Thermal conductivity test results comparing smooth and rough surface finishes are plotted in Figure 68. The rough surface sample simulates the characteristics of the present quality of the simple piece injection molding. Over the range of mean temperatures that represent the normal engine operating temperatures, the rough surface thermal conductivity appears to be only slightly higher, (10% to 15%), than the smooth surface thermal conductivity. At higher mean temperatures, the difference in thermal conductivity of the rough surface insulation approaches 30% higher than the smooth surface insulation. Thermal modeling of the turbine engine comparing the rough and smooth surface insulations should determine whether or not the difference in thermal conductivity has a significant impact on the design of the insulated engine.

3.2.4 Corning, Inc.

Objective/Approach

The objective of the Corning program is to develop a reliable, low cost, extruded ceramic regenerator disk capable of operating for full life at required conditions.

Accomplishments/Results

In late 1991, Corning initiated a major ATTAP ceramic regenerator program. The principal goal of the program is to develop a low cost

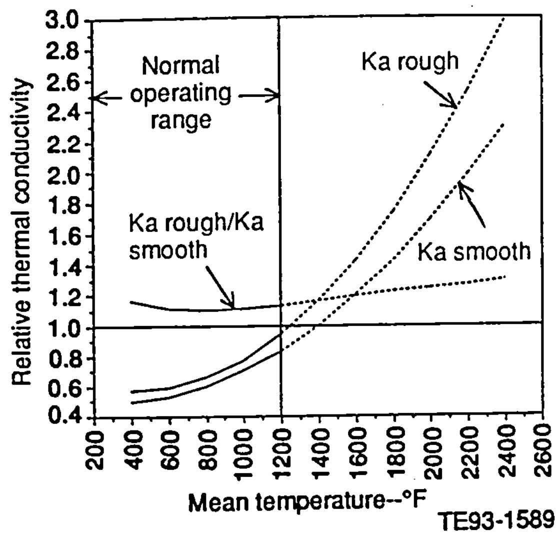

Figure 68. Moldable high temperature insulation thermal conductivity.

ceramic regenerator which meets the RPD engine durability requirements. The ceramic development program is a three phase program. The initial phase, preliminary evaluation, is broken down into two major areas of work: material technology and extrusion technology.

Four material systems will be investigated under the material technology section of the program:

Alumino-silicate (AS)
Magnesium alumino-silicate (MAS)
Mullite aluminum titanate (MAT)
Zirconium phosphate (NZP).

For the selected material systems, four principal areas of material development have initially been identified:

Temperature Durability
Chemical Durability
Strength
Cost

The primary issues relative to AS materials are chemical durability and cost. Under the AS material family, lithium alumino-silicate (LAS) will be investigated as a lower cost alternative to AS. The chemical durability of LAS is poor and material development will be required.

For MAS, temperature durability and strength require development. Initial investigations indicate that the matrix strength of MAS will not meet the RPD engine requirements. Cost and chemical durability are not an issue with MAS. Less is known about the MAT and NZP materials. Initial work for these material will focus on material property evaluations.

The goal of the extrusion technology portion of the program is to produce a one piece extruded regenerator core. The core matrix will have 171 cells/cm^2 (1100 cells/$in.^2$). The technology required to meet this goal will be developed through the manufacturing of a series of regenerator dies. The die size and matrix cell density will be increased with each die until the program goal is achieved.

The second and third phases of the regenerator development program will be prototype development and process proof demonstration, respectively.

Discussion

Corning will develop ceramic materials and an extrusion process for regenerators capable of withstanding cyclic thermal stresses and other requirements. Four materials will be explored through a series of six extrusion dies of increasing size and cell density. The four materials and their development emphasis are as follows (listed in order of probability of success):

	Material	Development emphasis
1.	Alumino-silicate (AS)	Cost and higher thermal stability
2.	Magnesium alumino-silicate (MAS)	Lower porosity and expansion plus cyclic stability
3.	Mullite aluminum titanate (MAT)	Thermal stability, shock, and cyclic stability
4.	Zirconium phosphate (NZP)	Thermal stability, shock, and cyclic stability

Laboratory tests will evaluate development success. Extrusion die sizes and cell densities to be evaluated are as follows:

	Extrusion die size diam. cm	(in.)	Cell density cells/cm2	(cells/in.)
1.	2.5-7.6	(1-3)	171	(1100)
2.	>15.2	(>6)	62.2	(400)
3.	12.7-15.2	(5-6)	124.4	(800)
4.	>15.2	(>6)	124.4	(800)
5.	12.7-15.2	(5-6)	171	(1100)
6.	>15.2	(>6)	171	(1100)

The schedule should allow demonstration of a segmented, cost-effective, durable, 800 cells/in.^{2} AS disk early in the program. Three inch diameter, 171 cells/cm^2 (1100 cells/in.^{2}) samples of fully capable AS and MAS for evaluation of properties and thermal cyclic stability tests will be available in about a year. The start of MAT development will be deferred until the second year. At that time, success with AS or MAS could preclude the need for MAT. Available NZP materials will be evaluated in the first year.

Phase II, lasting one year, will start at the end of the second year of activity. Material selection will be made and larger batches used to establish raw material property limits to ensure consistent product. Full size segmented 171 cells/cm^2 (1100 cells/in.^{2}) disks will be evaluated. Process development will be completed and firing cycles for large kilns established. A one-piece 171 cells/cm^2 (1100 cells/in.^{2}) extrusion >15.2 cm (>6 in.) diameter could be achieved by the end of the third year.

Phase III, lasting one year, and ending after four years would prove consistency, identify production equipment, and provide a basis for manufacturing cost estimates.

Delivery of parts for Allison test of fully developed materials

7.6 cm (3 in.) diameter:

171 cells/cm^2 (1100 cells/in.^{2})	AS samples
171 cells/cm^2 (1100 cells/in.^{2})	MAS samples

35.6 cm (14 in.) diameter:

124.4 cells/cm^2 (800 cells/in.^{2})	AS segment disk
124.4 cells/cm^2 (800 cells/in.^{2})	MAS segment disk
171 cells/cm^2 (1100 cells/in.^{2})	AS segment disk
171 cells/cm^2 (1100 cells/in.^{2})	MAS segment disk

The program will consider new and revised materials, extrusion technology, cementing, and performance evaluation. A need for this development program stems from Corning's determination that the previously favored aluminosilicate (AS) material would be too expensive for automotive use, and from excessive loss in strength of the latest magnesium alumino-silicates (MAS) due to thermal cyclic crack growth. Corning believes that the required properties probably can be achieved in revised AS or MAS, or in new materials.

3.2.6 Ceramics Process Systems (CPS)

Objective/Approach

A development program with CPS is being conducted to address fabrication of gasifier turbine rotors utilizing CM200 sialon material. Quickset injection molding was selected as the fabrication process. The initial program plan, directed towards a 20-blade rotor configuration, was redirected to address a 26-blade rotor design. The overall program consists of three phases: injection molding tool fabrication, rotor processing development, and deliverable rotor fabrication.

Accomplishments/Results

- Initial process development and fabrication of prototype rotors conducted.
- Design and fabrication of 26-blade rotor tool for Quickset injection molding completed.
- Material development and optimization of duophase sialon materials initiated.

Discussion

Initial efforts addressing rotor development were directed towards fabrication and processing of a prototype four-bladed rotor. The prototype rotors, shown in Figure 69, had a hub geometry similar to the 26-blade rotor, but with only four equally spaced straight airfoils. The prototype rotor was used to evaluate gating and demolding concepts, to determine the process shrinkage factor from the mold cavity to the fired part, and to conduct process development work with respect to the hub section prior to receipt of the production 26-blade rotor tool. The prototype rotor mold was designed and delivered to CPS in May 1991. Some initial components Quickset injection molded exhibited surface defects where the slip flow changed direction. These flow textures originated when the slip folds over itself when radically changing direction rather than exhibiting smooth flow characteristics. The rheological properties to this type of slip are characterized to be pseudoplastic.

A study was conducted to improve the processability of CM200 slip with respect to complex geometry components. The pseudoplasticity of CM200 slip was decreased by reducing the surface area of the sialon powder and by modifying the slip additives and the additive levels. The flow textures observed in the prototype rotors were significantly reduced with this modified CM200 slip formulation with no change in density or microstructure relative to the original CM200 formulation.

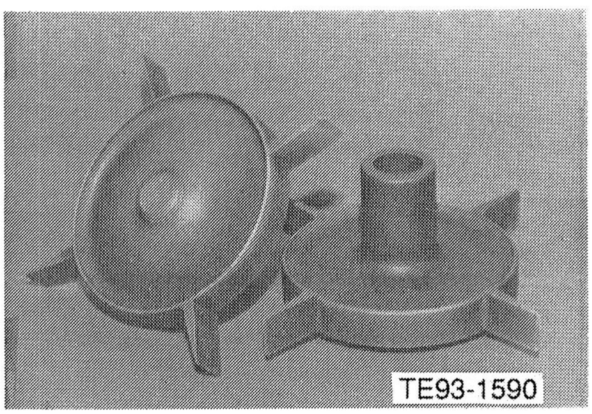

Figure 69. CPS CM200 sialon 4-blade prototype rotors.

The CM200 prototype rotors fabricated with the modified slip formulation had good external quality, with minimal flow textures and no surface cracks. The internal structure was also high quality, with components routinely achieving full sintered density (3.24 - 3/25 g/cc [99.4 - 99.7% theoretical density]) with no density gradients. SEM photos illustrating the microstructures in the blade and hub regions are shown in Figure 70.

The design and fabrication of the 26-bladed rotor injection molding tooling was conducted concurrently with the prototype rotor development efforts. The rotor tool was produced directly from the 3-dimensional part database, including data for the hub section, blade profiles, and blade-to-hub fillets. During part/tooling design work, the fillet radius specification was modified to avoid producing a negative draft

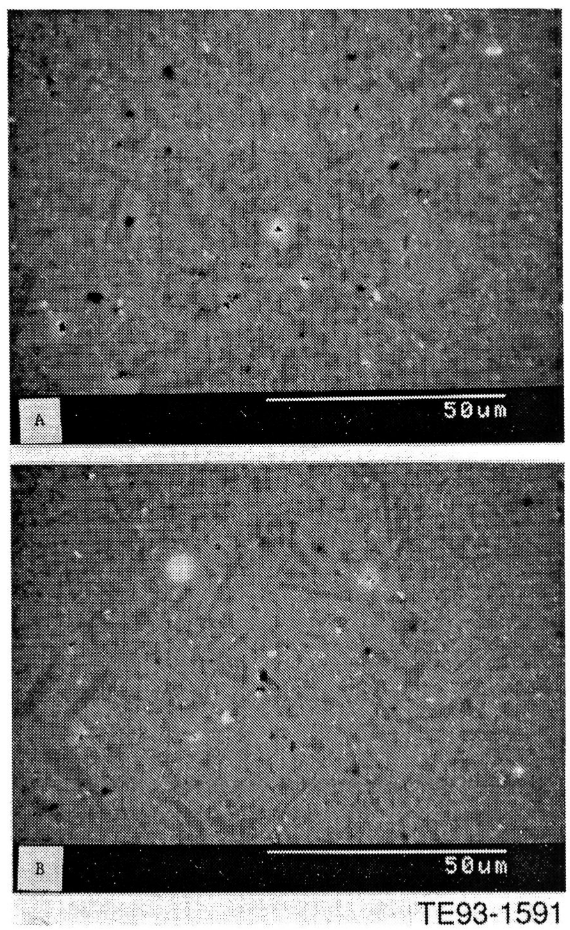

Figure 70. Microstructures of 4-blade prototype rotors at 1000 X magnification in (a) hub center and (b) hub outer diameter.

angle on the tooling blade inserts. Rotors fabricated on a tool with a negative draft angle cannot be demolded without damaging the molded part. The original specification had required that the fillet radius transition smoothly from 0.4 mm (0.016") to 1.5 mm (0.060"). However, the specification was modified so that the fillet radius transitioned smoothly from 0.05 mm (0.002") to 1.5 mm (0.060") so that the basic part geometry definition could be maintained without generating a negative draft angle on the blade inserts.

Preliminary finite element stress analysis conducted on the rotors indicated a high localized stress in the fillet region due to the small radius. In spite of this deviation, a decision was made to use the existing tool to conduct rotor process development and mechanical strength characterization of the rotors. This was due to the high cost and significant time delay which would result from remachining the blade inserts. A new mold will be fabricated only if the rotors do not survive room temperature proof spin testing.

The rotor injection molding tool was received by CPS in late November and functioned as designed. Only minor mold modifications were required to ensure that the mold surfaces mated properly at the molding temperature. Initial molding work with the tool was successful. Processing of the hub section of the 26-blade rotors was similar to that of the prototype rotors, with the same surface quality and internal macrostructure and microstructure observed for both rotors. However, each blade of the 26-blade rotors had a 1 - 2 mm (0.04 - 0.08 inch) flow texture on the trailing edge due to incomplete filling of the mold. Modifying the injection parameters improved blade fill and decreased the size of the blade flow texture.

The dimensions of the sintered rotors were typically within the print tolerances. Both the outer hub ring diameter and the hub profiles satisfied the print specifications. The blade profiles did not appear to droop during firing under their own weight. However, the blades do appear to slightly twist. The extent of the blade twisting increased as the size of the texture on the trailing edge of the blade increased. Elimination of the flow texture on the blade trailing edge should eliminate the blade twisting.

The mechanical strength properties of the CM200 sialon material used for the rotor processing activities have decreased relative to the prior CM200 material properties used in the vane platform fabrication. The flexural strength properties of the 1991 material, Batch 16, was lower than the strength properties of the 1990 material, Batch 13. The average room temperature strength was 590 MPa (86 ksi) for CM200 Batch 16 and 700 MPa (102 ksi) for billets and vane seat platforms fabricated using Batch 13 powder. The 1300°C (2372°F) strength was approximately 390 MPa (57 ksi) for CM200 Batch 16 material and 490 MPa (71 ksi) for the CM200 Batch 13 material.

A single type of fracture origin was dominant in the CM200 test specimens. Approximately 71% of all bars tested at room temperature had fractures originating from 20 - 50 micron iron-containing defects. The high values of Weibull modulus observed in these specimens, ranging from 13 to 23, indicate the dominance of this single fracture origin. Only 16% of the test specimens from CM200 Batch 13 failed from this type of inclusion. These iron-containing inclusions have been established to have originated in the CM200 powder provided by Vesuvius Zyalons.

Similar mechanical property and fracture origins were observed in the next lot of CM200 powder, Batch 18. The average room temperature fracture strength was 609 MPa (89 ksi) with 80% of the specimens failing from the same iron-containing inclusions. This batch of powder was produced by Vesuvius Zyalons before the inclusion problem was well understood, so the material and processing conditions were similar to those used in the production of CM200 Batch 16. The CM200 Batch 18 material was rejected by CPS for rotor fabrication efforts.

Vesuvius Zyalons has conducted tests to determine the source of the iron-containing defects. Based on the results of these tests, Vesuvius Zyalons is producing Batch 19 of the CM200 powder, which will be available for qualification testing at CPS in February 1992.

In conjunction with the activities pursuing the source and remedy for the iron-containing inclusions in CM200 sialon, CPS is also working on the development of a pressureless sintered duophase sialon material. The rheological properties of this material, designated SRS201, are less pseudoplastic than slip made with CM200 at the same solids loading levels. Initial evaluations of material strength are promising, with room and elevated temperature fracture strengths equivalent or higher than CM200 sialon material. Only 15% of the SRS201 specimens tested had fractures originating from inclusions. Additional optimization of this material system are proceeding, with 100 test specimens of the SRS201 to be delivered in early 1992 for mechanical property evaluation.

3.2.9 Norton/TRW Ceramics (N/TRW)

Objective/Approach

The ceramic component development efforts being conducted with N/TRW are directed towards three AGT-5 components: the gasifier turbine rotor, turbine scroll, and vane platform. The turbine rotor activity is being directed towards fabrication of both 20- and 26-bladed configuration parts. Pressure slip casting is being used for component production for both NT154 and NT164 silicon nitrides. The turbine scroll efforts are focused on pressure slip casting of reaction sintered NT230 SiC. Extensive development and optimization of the automated high pressure casting process, including slip optimization, plastic mold formulation, and casting trials are being conducted. The vane platform work is a cooperative effort with CPS to codevelop Quickset injection molded NT154 Si_3N_4 vane platforms for the AGT-5 engine.

Accomplishments/Results

- Process parameters were established for fabrication of NT154 Si_3N_4 turbine rotors.
- 26-blade configuration rotor pattern designed and fabrication initiated.
- NT230 SiC slip and plastic mold formulation optimized for automated pressure slip casting.
- Three NT230 SiC scrolls delivered for rig/engine test activities.
- Four batches of Quickset injection molded NT154 Si_3N_4 vane platforms processed for evaluation.

Discussion

Gasifier Turbine Rotors. In 1989-90, NTC developed and produced a number of 20-blade NT154 silicon nitride gasifier turbine rotors. Four of these components met the dimensional and structural requirements and were qualified for rig and engine testing by passing the proof spin test. One of these rotors, S/N 5S, successfully completed in excess of 200 hours of cyclic durability rig testing. However, the rotors required extensive machining on the hub surfaces and had several linear indications on the airfoils. As a follow-on effort to the initial rotor program, a subsequent rotor development effort was initiated with N/TRW in March 1991. This program involved development and fabrication of both 20- and 26-blade rotor configurations, with rotors produced using both NT154 and NT164 silicon nitride materials.

Under the prior rotor development program, N/TRW developed pressure slip casting as the forming method for fabrication of AGT-5 axial turbine rotors. A detailed flow chart for this fabrication process is shown in Figure 71. N/TRW's pressure slip casting techniques involve several additional steps beyond the casting operation to optimize the process for axial turbine rotors, the most notable being the use of freezing to provide additional strength in the green rotors. N/TRW utilized this process under the prior program to prepare rotors which met the dimensional, mechanical, and spin test requirements. However, the as-cast components contained excessive stock in certain areas, particularly the shaft and hub regions. This was allowed in the initial rotor castings to reduce the complexity of the tooling and to minimize problems during the pressure casting operation. Because of this additional stock, the casting times for rotors were long (approximately 15 hours). The first generation rotor casting mold, shown in Figure 72, utilized

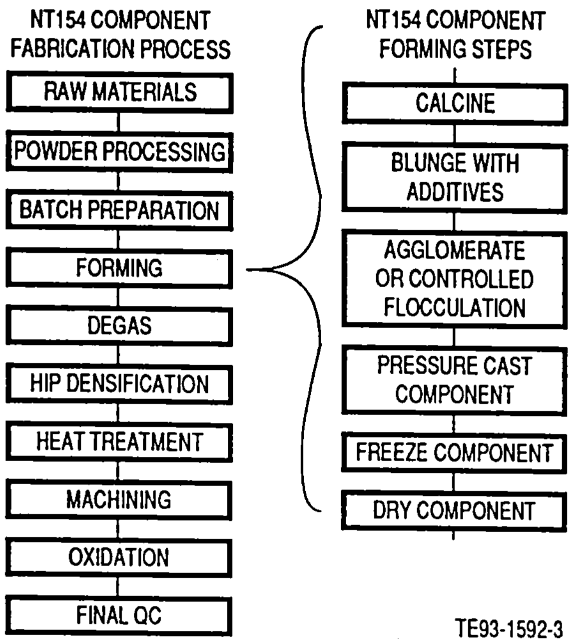

Figure 71. N/TRW NT154 Si_3N_4 rotor process flow chart.

a single gate for slurry supply and bidirectional casting. For this component geometry and mold configuration a number of defects were observed at the intersection of the blade and the hub on the shaft side. At this location, the hub section of the rotor was cast-off early in the process and closed the slip supply to the blade, resulting in a slip-starved region where voids or linear defects occurred.

To correct these problems, N/TRW conducted casting trials on several iterative mold designs. To minimize casting time and machining stock, it was decided to cast both the hub and shaft regions of the rotor to near-net-shape. In this second generation mold design, shown in Figure 73, the axial direction was reversed from the original design. One gate was placed at the center of the hub opposite the shaft. From this gate a reservoir fed a small auxiliary ring gate placed at the intersection of the hub and blades. By providing multiple gates to the mold, it was hoped that the void defects found in this prior design would be eliminated. All hub and shaft surfaces and the blade tips were designed with 1.27 mm (0.050") machining stock. The inside diameter of the shaft was designed to be cast to near-net-shape through the use of a non-porous rubber insert. The blade surfaces were cast to net-shape. Analysis of the casting design, optimized using 2-D computer casting models, predicted that the casting time should be reduced by at least a factor of four.

Several modifications of this design, involving mold dimensions, materials, configurations, and de-molding procedures were required to obtain test hardware. Most of these changes proved beneficial, with casting times reduced to approximately 1.5 hours. Despite the attainment of near-net-shape configuration rotors, voids

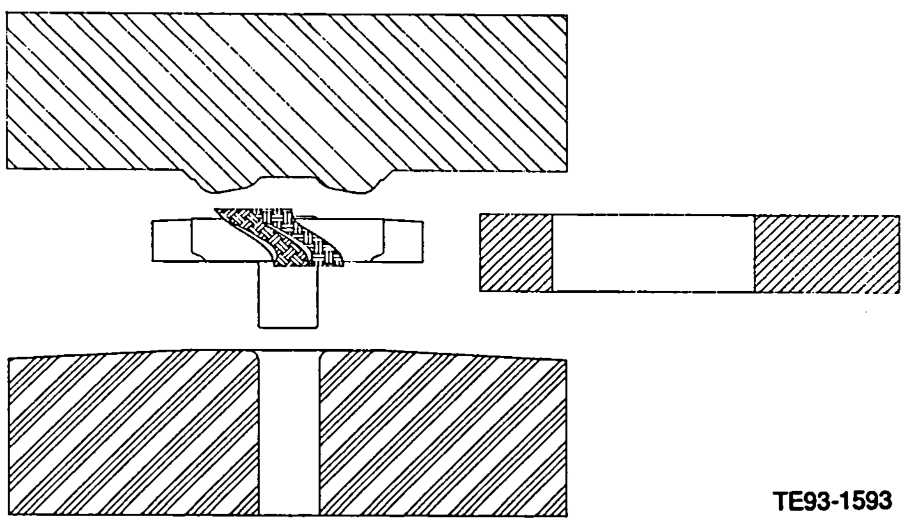

Figure 72. N/TRW first generation rotor casting mold.

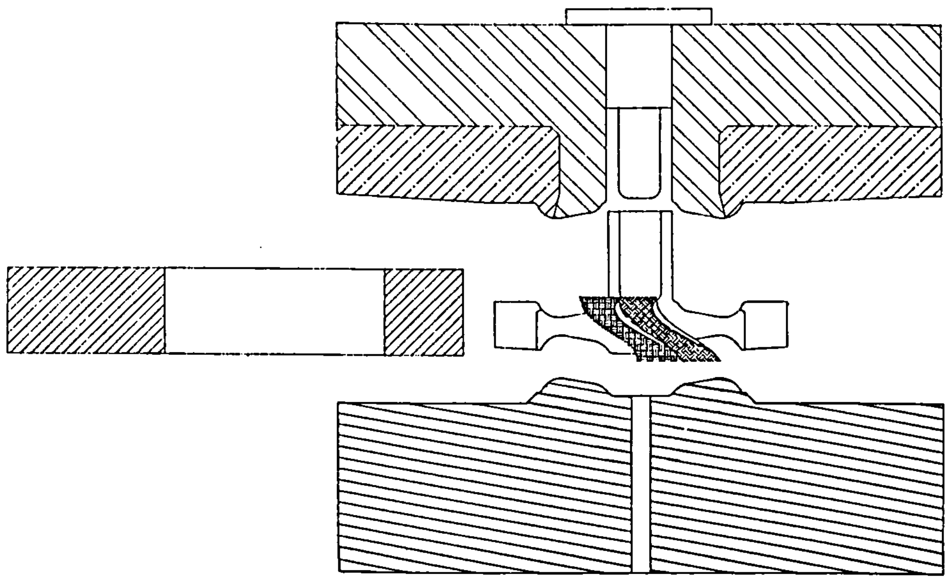

Figure 73. N/TRW second generation rotor casting mold.

were still observed in the trailing edge of the blades. These voids were the result of intersection of the two casting fronts, which caused a slip-starved condition and incomplete casting of the blade. Since the trailing edge is thinner than other sections of the blade, this portion casts much faster than the remaining areas. All attempts to correct this problem by modifying the active plaster dewatering surfaces were unsuccessful.

A third generation mold configuration was designed to prevent slip starvation in the airfoils. To test and optimize this new design, N/TRW conducted eight casting trials. All rotors cast using this design exhibited no visual signs of blade voids. Additional inspections of the rotors using microfocus X-radiography revealed only a few randomly distributed voids, all of which were well below N/TRW's quality acceptance limit of 500 microns (0.020"). In addition, the X-ray inspections revealed no cracks or high density indications within the components.

Following the mold optimization activities, a total of four rotors were fabricated using process conditions selected to yield dimensions that would bracket the requirements of the finished component. All four rotors were cast with minimal difficulty. The rotors also passed N/TRW's internal criteria for voids, cracks, and high density indications. The parts were then densified and subsequently evaluated using fluorescent penetrant inspection (FPI). No significant surface defects were identified by FPI examination. Metrology was performed on each of the four rotors. Two of the rotors met the dimensional specifications for hub diameter and blade tip diameter. Both rotors had as-cast shaft O.D.s with adequate machining stock but had shaft I.D.s which were too large. Correction of this problem was easily accomplished by reducing the diameter of the plug which defines the shape during casting. From this study, the casting conditions for the two rotors were selected as the outer processing limits for fabrication of engine quality hardware.

With the successful completion of the mold and dimensional determination activities, efforts were initiated on production documentation and casting mold fabrication for production of the engine quality 20-blade NT154 rotors. Component casting activities are expected to be initiated in early 1992, with deliverable hardware completed by the end of April.

Processing of NT164 silicon nitride powder was initiated late in 1991 in preparation for optimization casting trials using the 20-blade AGT-5 rotor mold. After a casting optimization experiment on this material, scheduled for completion in early 1992, production of rotors will begin. Delivery of hardware is expected by the end of June 1992. Concurrent with the rotor deliverables, 200 test specimens of NT164 silicon nitride will be supplied for material characterization activities. One hundred of the test bars will have a machined surface condition and 100 will have an as-cast surface condition.

N/TRW completed reviews of the 26-blade rotor design with Allison during the latter half of 1991. Finalized prints were received in December. Based on the prints, N/TRW initiated the design of a stainless steel pattern for mold fabrication. Completion of the design, ordering, and delivery of the pattern is anticipated in February 1992.

Turbine Scrolls. A program for development and fabrication of AGT-5 scrolls is also being conducted at N/TRW. The material selected for this effort is NT230 SiC, a reaction-sintered SiC with a bimodal distribution of silicon carbide grains in a matrix of metallic silicon. Compositionally, NT230 SiC contains approximately 10% silicon, along with extremely low levels of trace impurities. By modification of the grain size distribution and selective changes to the fabrication process, N/TRW was able to essentially double the strength of existing siliconized SiC compositions. The material is also ideally suited for scroll fabrication due to the minimal shrinkage (1-2%) upon densification. Four major tasks are being conducted on the scroll development program, including: automated pressure slip casting development, scroll component production, process proof demonstration, and component cost analysis.

The automated pressure slip casting task is directed at developing semi-automated forming procedures for scroll components. N/TRW selected pressure slip casting as the preferred forming method for scrolls. To facilitate performance of this work, N/TRW acquired a semi-automated pressure casting machine and porous mold technology. The activity in this area has been focused on development of the automated pressure casting process for advanced ceramics, involving slip system development, porous plastic mold development, and automated pressure slip casting development.

Initial work with the porous plastic mold technology suggested that slip characteristics were a critical element to successful casting. It was found that a slip formulation which cast readily at low pressure (<0.550 MPa [80 psi]) in plaster molds did not necessarily produce good castings at high pressures in plastic molds. Therefore, a study of appropriate parameters contributing to successful high pressure casting of siliconized SiC was planned and conducted. Screening tests were performed first in an effort to isolate appropriate factors. Solids concentration, pH, and various additives were tested. Of these factors, both solids content and pH had beneficial effects on castings. Of the additives, a number of flocculents, binders, and other casting agents were tested. Slips containing a flocculent exhibited high viscosities and cast bodies with unacceptable water contents. Certain binders were found to improve viscosity and resulted in enhanced green strength and release behavior.

Based on these trials, a factorial experiment, shown in Figure 74, was designed and conducted. Binder and casting additive amounts were evaluated at three levels, while solids content, pH, and slip temperature were conducted at two levels. In addition, two plastic mold materials were selected as trial casting surfaces. For each condition of the experiment, two discs weighing approximately 100 grams (0.22 pound) each were cast at a pressure of 0.414 MPa (60 psi). Viscosity, cast weight, mold release, and shape retention were selected as the four critical response variables. One of the mold materials was superior in mold release characteristics.

Run No.	Binder Content	pH	Solids Content	Slip Temp.	Casting Additive Content
1	1	2	1	1	0
2	0	1	2	1	1
3	2	2	1	2	1
4	0	2	1	2	2
5	1	1	2	2	2
6	1	2	2	2	0
7	2	1	2	2	0
8	0	1	1	1	0
9	2	2	2	1	2
10	1	1	1	2	1
11	1	1	1	1	1
12	0	2	2	1	1
13	0	1	1	2	0
14	2	1	1	1	2

TE93-1595-3

Figure 74. N/TRW NT230 SiC slip system development experiment.

The effects of the various treatment factors on the response variables are shown for this mold material in Figure 75.

Using this factorial design, the treatment factors were prioritized and optimized, and specification limits set for each variable. Within the graphs, broken horizontal lines indicate limits for response variables, while broken vertical lines indicate the value to which the treatment factor was adjusted under optimized conditions. In reviewing the data, it was found that the addition of one particular casting additive had a negative effect on shape retention and mold release. There were no significant effects on viscosity or cast weight.

Because of this, N/TRW elected to discontinue further efforts on casting additives. pH was found to have a moderate effect on all response variables. The pH level was selected to produce components of low cast weight. Cast weight indicates the degree of water retention. Low water content castings have better shape retention and are less prone to crack during drying. The binder was effective in aiding mold release and shape retention. For this particular binder, viscosity decreased with increasing binder content. The binder level was optimized at conditions which gave the lowest cast weight. Solids content had the most pronounced effect on all of the response variables. As expected, a lower solids content resulted in lower viscosities and cast weights.

Conditions for this factor were selected to give low viscosity and minimal cast weight. Increasing the slip temperature decreased the slip viscosity, but also increased the cast weight, resulting in poor mold and shape retention. Because of this, ambient temperatures were selected as optimal for the slip formulation. In summary, a low solids content, high binder content, casting additive-free formulation was selected as the optimal NT230 slip for use with porous plastic molds.

The effects of various porous plastic mold materials and fabrication techniques were also investigated. Initial screening tests were conducted with two different porous plastic products, the standard formulation from Dorst/ Laufen and a similar Japanese material. Water flow rate and casting tests were performed and compared with conventional plaster. Both plastic mold materials had slower casting

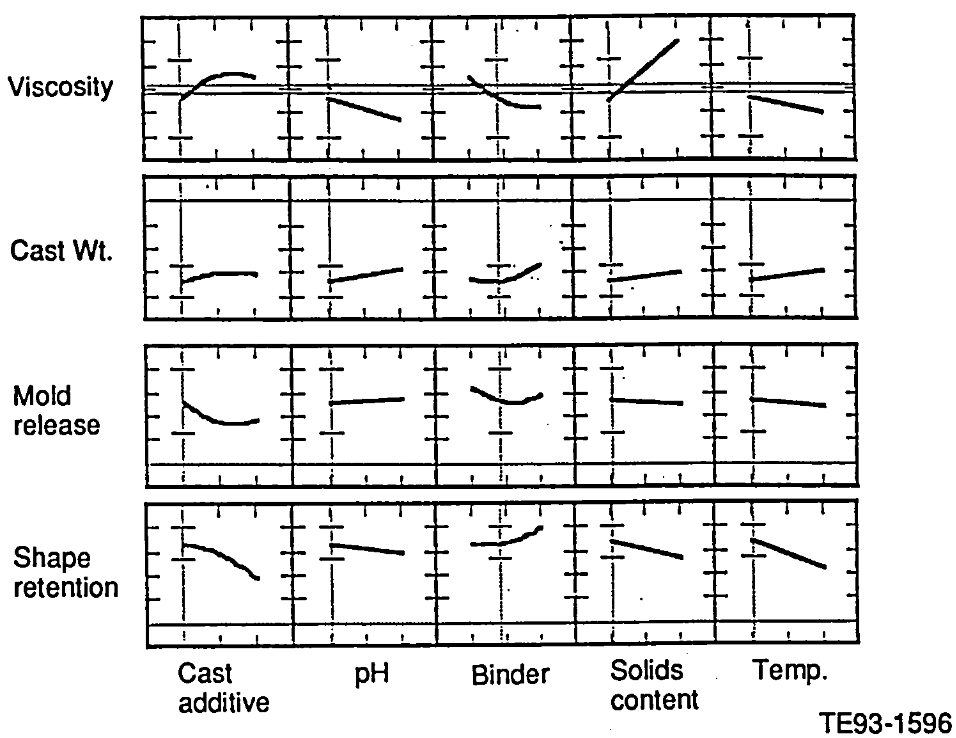

Figure 75. Response curves for N/TRW NT230 slip system development experiment.

characteristics than plaster; however, these were judged to be adequate for casting with either mold material. N/TRW therefore selected the Dorst/Laufen material for additional development and testing.

The microstructure of the standard Dorst/Laufen composition was examined to determine whether changes in raw materials or fabrication methods might affect casting behavior. From SEM analyses, the microstructure was found to be quite uniform. Quantitative measurements taken in three different regions of the mold showed nearly identical pore shape and size distributions, with the pores ranging in size from 5 to 90 microns (0.0002 to 0.0036"). It was noted that changes in mold composition, particularly the size fraction of the plastic constituents or the reactive monomer, might alter pore size and shape. It was reasoned that a smaller size distribution might provide improved casting and release characteristics.

Based on this postulate, a factorial experiment was designed and conducted. The matrix consisted of 12 experimental trials encompassing three formulation variables believed to be of importance in altering mold performance. Conditions for each of the 12 experimental trials, a summary of the data, and observations collected as part of the experiment are shown in Table XII. For each plastic mold formulation trial, at least one 7.62 mm (0.3") diameter disk was single directionally cast at a pressure of 0.414 MPa (60 psi) using the optimized NT230 slip formulation. Critical evaluations for each experiment included: measuring the volumetric flow rate of water through a standard geometry of mold material, quantifying the release of the cast disks from the molds, and quantifying the shape retention of castings. A rating of 1 to 5 was determined for each trial with 5 being the best mold release and shape retention. As shown in Table XII, a number of the mold formulations did not yield a cast piece. None of the twelve trials produced a casting with acceptable mold release and shape retention.

Observations from the L12 experiment led to additional screening tests of the porous plastic mold variables. As part of these subsequent trials, two factors were found to dominate casting behavior. These factors involved the mold formulation and the casting pressure characteristics. By incorporation of these two factors into the fabrication and use of plastic molds, excellent quality components were cast.

Using the optimum NT230 slip system and plastic mold formulation, simple geometry tile, tube, and elbow shaped molds were produced for use on the Dorst equipment. Casting tests

Table XII.
Design and results of N/TRW L12 porous plastic mold optimization experiment.

Trial No.	Filler ratio	Percent monomer	Percent initiator	Flow rate (L/min)	Cast time (min)	Surface quality	Mold release (1-5 rating)	Shape retention (1-5 rating)
1	2	1	0	5	70	--	3	3
2	2	0	2	4	N/A	--	N/A	N/A
3	2	1	1	6	N/A	--	N/A	N/A
4	0	2	0	14	30	Rough	4	3
5	1	0	0	6	N/A	--	N/A	N/A
6	0	0	2	8	N/A	--	N/A	N/A
7	2	0	0	2	N/A	--	N/A	N/A
8	2	2	2	10	36	Rough	3	3
9	0	0	1	9	N/A	--	N/A	N/A
10	1	2	1	12	38	--	5	3
11	1	1	2	12	80	--	2	2
12	0	1	2	14	25	--	3	3

N/A = did not cast

were conducted at pressures ranging from 1.03 to 4.14 MPa (150 to 600 psi). Thicknesses of approximately 10 mm (0.4") were cast in three to eight minutes depending on the pressure. It was observed that shape retention and mold release were independent of pressure, and paralleled results obtained in bench-top casting tests. Mold release was improved by modifying the design of the mold, similar to features which resulted in enhanced release characteristics in plaster molds.

Subsequent tests were performed with a two-piece modified formulation porous plastic mold. A total of forty tubes were cast at various conditions to explore the operational ranges of the casting cycle and machine parameters. Casting pressures were varied from 1.72 to 2.76 MPa (250 to 400 psi). NT230 tubes with wall thicknesses ranging from 2.5 to 15 mm (0.1 to 0.6 inch) were successfully cast by varying pressure and casting time. Following this activity, the casting parameters and machine settings were held constant for ten consecutive cycles to get an initial indication of casting consistency. Cross-sections of these tubes appeared to have improved wall thickness uniformity compared to equivalent test pieces cast in plaster molds.

Concurrent with the automated pressure slip casting activities, efforts were also conducted on fabrication of AGT-5 scrolls. In the prior scroll program, technical difficulties were encountered in finish machining. The main goal of this task was therefore to resolve these problems and deliver engine quality hardware to Allison. After completion of appropriate engineering documentation, N/TRW initiated preproduction of scrolls by casting three components. Pressure casting proceeded with minimal difficulties; however, one part was lost due to a crack on the radius between the scroll inlet and body. An investigation revealed that this crack occurred during the drying cycle. Corrective action was taken to reduce stress during drying. A significant problem was encountered during the silicon infiltration step. Both components were rejected due to incomplete siliconization. The cause of this was judged to be insufficient silicon in the local furnace environment. This resulted in a reengineering of the silicon impregnation step. To improve the furnace environment, future scrolls will be placed inside separate closed crucibles to ensure that the localized silicon content is maintained.

Machining development was initiated on an additional scroll assembly produced through the firing operations. All aspects of the machining operation were reviewed during this effort. Tooling and fixtures were modified to minimize stress on the component. This part was successfully machined and passed all inspection criteria and delivered in April 1991.

Using information from the preproduction task, production of engine quality scrolls was completed. A total of nine scrolls were cast, from which three components were eventually delivered. One scroll was rejected after casting for variations in wall thickness. Another part was rejected due to a crack in the shroud region. Two additional parts were damaged in handling during the carbon impregnation step. The remaining five parts were successfully siliconized and passed all inspection criteria. Of these, three parts were selected for finish machining. Two were fully machined, including ultrasonic machining of the vane pockets, and delivered in June and November, 1991. The remaining part without finish machined vane pockets was also delivered in November.

Vane Platforms. N/TRW initiated a cooperative developmental program in 1990 with CPS to codevelop NT154 Si_3N_4 vane platforms for the AGT-5 engine. The program included three major tasks: CPS Quickset injection molding development for NT154 Si_3N_4, N/TRW vane platform processing, and N/TRW/CPS vane platform machining, inspection, and qualification.

N/TRW supplied prequalified NT154 Si_3N_4 powder to CPS for the Quickset injection molding process development. CPS then formed components and returned them to N/TRW for an evaluation of green and dense quality. To date, N/TRW and CPS have collectively produced four batches of vane platforms. The first lot of parts, fabricated in 1990, were processed through HIPing and assessed to determine the mechanical properties and dimensional conformance of the components.

To address the dimensional problems, CPS produced a second batch of components at a higher solids loading in an effort to reduce overall shrinkage. These increases in the solids loading resulted in the formation of knit line defects and large (>500 micron [0.002"]) voids within the green components. This second batch also possessed a high percentage of foreign contaminants in the platforms. Because of these problems, all components were rejected in the green state. N/TRW proceeded to densify several parts to determine if the difficulties related to shrinkage had been resolved. These components were HIPed to full density and achieved correct dimensions.

CPS designed and conducted a processing test matrix to resolve the void and knit line problems. Experimental trials were conducted in mid-1991 and a third batch of components was Quickset molded and delivered to N/TRW. Under microfocus X-ray examination, all of the green hardware from these trials was observed to contain high density defects (primarily metallic inclusions) and unacceptably large voids. Subsequent to these trials, N/TRW worked closely with CPS to aid them in upgrading their microfocus X-ray inspection capability. In turn, CPS identified areas of their process requiring modifications in order to eliminate the inclusion and void defects. CPS also worked on optimization of the slip batch conditions using their own CM200 sialon powder as a model.

Upon completion of these tasks, CPS produced a fourth batch of seventeen components. Significant improvement was noted for the metallic inclusions. While high density indications were still present, they were minimal compared with the prior batches. However, a substantial number of large voids were still present in the green hardware. In addition, most parts possessed severe flow texture problems, particularly in the cone area of the component opposite the sprue. From this group of seventeen parts, N/TRW inspected and selected five platforms as potential engine components. An additional five parts were processed for sectioning into test specimens for mechanical property evaluation. Delivery of the five finished machined vane platforms is anticipated in early 1992.

IV. COMPONENT RIG DEVELOPMENT AND TEST

4.1 COMPONENT RIG DEVELOPMENT

The objective of this activity is the design, fabrication, and development of rigs required to test ATTAP ceramic components and assemblies. In addition, these rigs are utilized to develop nonceramic hardware/systems necessary to evolve the AGT-5 to a high temperature test-bed. Currently, two hot gasifier rigs are being developed.

4.1.3.3 Hot Gasifier Rig Development

Objective/Approach

The objective of this section is to develop the hot gasifier rig to the point of being ready for full steady-state and cyclic operation with ceramic gasifier rotors up to RPD conditions.

Accomplishments/Results

- Test results validated the quartz window mounting system redesigned for improved high temperature retention.
- Fabricated, installed, and completed shakedown of second hot gasifier rig.
- Designed a regenerator bypass exhaust system to reduce regenerator inlet temperature.
- Obtained, installed and tested a remote exhaust cooling air valve controller.

Discussion

In the previous year, the quartz window mounting system was re-designed in order to provide increased clamping force on the window. Increased clamping force was required to prevent gas leakage around the gasket interface previously observed during high temperature rig operation. The system was installed on two hot rigs this year. Over 700 hours of hot rig operation were accumulated over the year with no noticeable gas leakage at the gasket interface.

The engine block of the first hot gasifier rig was replaced after developing cracks. Keeping two rigs operational will allow for the anticipated increased amount of testing as ceramic components are delivered from the ceramic suppliers.

Test experience with makeup air has shown that as the air flow rate to the regenerator disk inlet is increased at high gasifier speeds, the rise in turbine back pressure causes higher turbine inlet temperatures. This rise in temperature results in excessive regenerator surface temperature. A regenerator bypass exhaust system was designed to reduce the back pressure on the gasifier turbine and allow the additional cooling air to reduce the regenerator surface temperature during high turbine inlet temperature testing. Parts have been ordered for both hot gasifier rigs.

In order to control regenerator inlet temperatures to acceptable levels for the ceramic regenerator cores, the amount of makeup air must be varied while running the rig. A linear controller was obtained, installed, and tested on one of the rigs. The controller allows the cell operator to vary the amount of makeup air without having to enter the test cell or shut the rig down to vary the valve opening, thus improving productivity.

4.2 COMPONENT RIG TESTING

The objective of this activity is to develop the necessary test procedures and to conduct rig testing of the ATTAP ceramic components and assemblies. A secondary objective is to conduct tests of nonceramic hardware/systems related to the evolution of the AGT-5 engine into a high-temperature test-bed. All ceramic components are rig proof tested prior to AGT-5 test-bed engine testing. Rig tests of the ceramic components are generally conducted with more instrumentation than normally available within a test-bed engine. Critical data provided by rig testing are used in the development and verification of the ceramic design methodology. Currently, two hot gasifier rigs and a regenerator cyclic sample rig are being utilized.

4.2.3.3 Hot Gasifier Rig Test

Objective/Approach

Hot gasifier rig testing is utilized to screen/ proof test and evaluate structural ceramic components (namely combustors, gasifier turbine components and regenerators) prior to introduction into the AGT-5 test-bed engine(s). Develop-mental rig evaluation is continuing while domestic ceramic components are being fabricated for test.

Accomplishments/Results

- Completed 100 hour durability test, with peak conditions of 1371°C (2500°F) at 100% speed, of an all-ceramic gasifier.
- Completed 1000 hour durability test of a 20-bladed Si_3N_4 gasifier rotor.
- Accumulated 224 hours on a N/TRW Si_3N_4 20-bladed gasifier rotor.
- Achieved 1350°C (2460°F) at 100% speed with an all-ceramic gasifier and a 15-bladed Si_3N_4 ceramic gasifier rotor.
- Achieved 1365°C (2489°F) at 100% speed and 1406°C (2563°F) at 96% speed with an advanced ceramic gasifier scroll and a 20-bladed Si_3N_4 ceramic rotor.
- Achieved 1270°C (2320°F) at 90% speed with a second advanced ceramic gasifier scroll and a 20-bladed Si_3N_4 ceramic rotor.
- Successfully proof tested a 15-bladed Si_3N_4 ceramic rotor.
- Proof tested a 15-bladed SiC ceramic gasifier rotor and a SiC ceramic combustor.

Discussion

Two significant test milestones were reached in 1991. High temperature capability of ceramic static and rotating components was demonstrated with an all-ceramic gasifier assembly that successfully completed a 100 hour durability test. The majority of the test time was on the ATTAP Durability Schedule with peak conditions of TIT = 1371°C (2500°F) at 100% speed. Long term rotor durability was established with a ceramic gasifier rotor that reached a total of 1000.7 test hours under severe test operating conditions. Additional proof tests were run on three other ceramic scroll assemblies and four gasifier rotors. Over 699 hours of ceramic gasifier rotor test time, and over 114 hours of ceramic scroll test time were accumulated in 1991 as outlined in Tables XIII and XIV.

Ceramic Component Durability Testing. The all-ceramic gasifier containing the components listed in Table XV initially ran with a ceramic combustor (CBO, α-SiC, S/N FX79402). The combustor was fabricated with 6.25 mm thick walls, although the print specified 4 mm thick walls. After starting the rig twice and running for 0.6 hours up to a peak condition of TIT = 920°C (1688°F) at 100% speed, an inspection revealed that the burner had cracked into three segments. (See section 3.1.3 for the burner failure analysis.) A complete inspection revealed no damage to the other ceramic components. The assembly was reinstalled into the hot gasifier rig with a Lamilloy burner assembly. The assembly was taken to 1385°C (2525°F) TIT at 101% speed. A complete inspection following the test revealed no damage to the ceramic components.

A second metal burner was then fabricated from Haynes 188 material, which has better high temperature capability than the original metal combustor. The combustor was instrumented with two platinum-rhodium thermocouples in order to measure burner outlet temperature. After running to full RPD conditions, the rig began operation on the ATTAP durability schedule. The durability schedule was limited to three accelerations to full speed and temperature per each one hour cycle because of concerns about the metal burner durability under high temperature operation. An inspection at 41 hours revealed no damage to the ceramic components, however, the burner was replaced because the platinum rod containing the burner thermocouples had yielded. Testing then continued on the ATTAP durability schedule until 100 hours total test time (95.8 hours on the durability schedule) were accumulated. Inspection following the test revealed that two vanes had developed cracks at the trailing edge and that the scroll had developed four cracks; three small cracks around the scroll vane pockets and one small surface crack in the

Table XIII.
Ceramic rotor accumulated test time.

Subcontractor	Rotor S/N	No. of blades	Material	Hours on test 1991	Total	Peak speed (%)/ peak temperature (°C)
N/TRW	5S	20	NT154	224.3	224.3	100/1350
CBO	FX78527	15	α-SiC	0.002	0.002	N/A
Kyocera	5K10	15	SN252	0.8	0.8	90/1270
Kyocera	5K12	15	SN252	106.1	132.5	101/1385
Kyocera	5K13	15	SN252	8.9	8.9	93/1150
Kyocera	5K22	20	SN252	340.2	1000.7	100/1395
Kyocera	5K26	20	SN252	18.8	22.7	100/1365

Table XIV.
Ceramic scroll accumulated test time.

Subcontractor	Scroll type	Scroll S/N	Material	1991	Total	Peak speed (%)/ peak temperature (°C)
N/TRW	Standard	KX56721	NT230	8.5	8.5	100/1350
Kyocera	Standard	0001-1	α-SiC	100.0	100.0	101/1385
Kyocera	Advanced concept	KX55836	SN252	5.2	5.2	100/1365 96/1406
Kyocera	Advanced concept	KX55599	SN252	1.1	1.1	90/1270

Table XV.
Ceramic components in 100-hr durability all-ceramic gasifier build.

Component	Supplier	Material
Scroll, P/N 5-80553, S/N 0001-1	Kyocera	SN252, Si_3N_4
Vane platform, P/N 5-80561, S/N 0002-1	Kyocera	SN252, Si_3N_4
Vanes (14), P/N 5-80552	GTE	PY6, Si_3N_4
Vane retaining ring, P/N 5-80560, S/N 0001-1	Kyocera	SN252, Si_3N_4
Rotor (15Nb), P/N 5-66946, S/N 5K12	Kyocera	SN252, Si_3N_4

scroll shroud area. Testing of this gasifier assembly will continue in the next calendar year for crack propagation evaluation.

Long-term rotor durability continued to be evaluated in 1991 with a 20-bladed Si_3N_4 ceramic (Kyocera, SN252, S/N 5K22) rotor in the hot gasifier rig. The rotor accumulated 340.2 hours in 1991 for a total of 1000.7 hours, at which point the rotor was successfully retired in engine-ready condition. The vast majority of the 340.2 hours were run on the ATTAP Durability Schedule. Peak conditions on the durability cycle were limited to TIT = 1150°C (2100°F) at 100% speed due to metal components in the gasifier build. At 874 hours in the rotor test history new chipping on the blade trailing edges and on the rotor rim were noticed. Rotor testing continued after blending the blade chips and rebalancing. A significant amount of testing was carried out unattended using computer control which allowed around-the-clock operation. Figure 76 shows the rotor at 874 hours. No new chipping occurred during the last 126 hours of testing.

Additional long-term rotor durability evaluation was carried out with a 20-bladed Si_3N_4 ceramic gasifier rotor (N/TRW, NT154, S/N 5S). After running an initial proof test up to TIT = 1200°C (2190°F) at 100% speed in a metal gasifier assembly, the rotor began running on the ATTAP durability schedule with peak conditions of TIT = 1150°C (2100°F) at 100% due to metal component temperature limitations. After accumulating 222 hours run time, an oil seal set screw came loose during low speed operation and lodged between the impeller and static structure causing the rig to automatically shut down due to a TIT over-temperature condition. The rotor had rubbed during the failure and inspection revealed that two blades had chipped at the trailing edge and three other blades had chipped at the leading edge tip. A crack on the leading edge tip of a blade was discovered with FPI analysis. After blending the blade crack and chips, the rotor was balanced and utilized in testing with an all-ceramic gasifier containing a N/TRW scroll.

Ceramic Gasifier Assembly Proof Testing. In addition to the all-ceramic gasifier which completed the 100 hour durability test, three other all-ceramic gasifiers were proof tested in 1991.

The all-ceramic gasifier containing the components listed in Table XVI was initially assembled with a 15-bladed Si_3N_4 ceramic rotor (Kyocera, SN252, S/N 5K12). The gasifier ran for 5.1 hours up to a peak condition of TIT = 1385°C (2525°F) at 99% speed. A complete post-test inspection revealed no damage to the ceramic components.

The 20-bladed Si_3N_4 ceramic rotor (N/TRW, NT154, S/N 5S) that had originally accumulated 222 run hours in a metal gasifier assembly (see discussion above) was then installed into

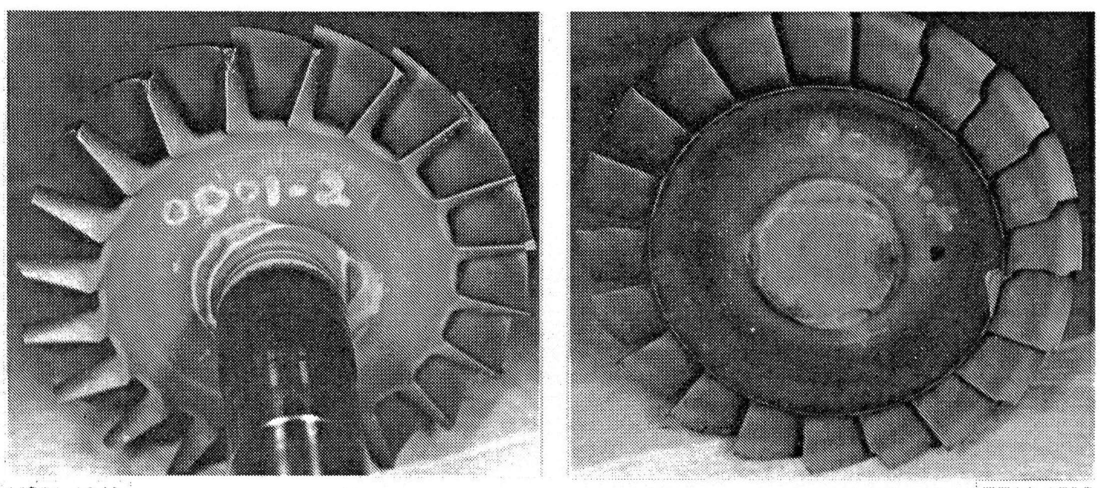

VS91-1046 TE93-1598

Figure 76. AGT-5 Kyocera gasifier rotor.

Table XVI.
Ceramic components in second all-ceramic gasifier build.

Component	Supplier	Material
Scroll, P/N 5-80567, S/N KX56721	N/TRW	NT230, SiC
Vane platform, P/N 5-80561, S/N 0002-2	Kyocera	SN252, Si_3N_4
Vanes (14), P/N 5-80552	GTE	PY6, Si_3N_4
Vane retaining ring, P/N 5-80563, S/N KX79352	CBO	α-SiC
Rotor (15Nb) (initial build), P/N 5-66946, S/N 5K12	Kyocera	SN252, Si_3N_4
Rotor (20Nb) (second build), P/N 5-80598, S/N 5S	N/TRW	NT154, Si_3N_4

the ceramic gasifier. The gasifier was then taken to TIT = 1350°C (2460°F) at 100%. A number of turbine and compressor impeller tip rubs occurred while proof testing this gasifier. The cause of these rubs was traced to a bad high speed bearing bore which led to bearing failures. Testing with this assembly was discontinued to repair the static structure.

An advanced concept Si_3N_4 ceramic scroll (Kyocera, SN252, S/N KX55836) was built and installed into the gasifier rig for the purpose of evaluating the new flow path geometry, the scroll mounting system, and the ceramic rotor at high temperature. The first advanced concept scroll had developed cracks around the mounting flange after running in 1990. As a result, the second scroll was fabricated with a new mount geometry. The gasifier housing was instrumented with three thermocouples to record scroll mount temperatures during rig operation to 1371°C (2500°F). A 20-bladed Si_3N_4 ceramic rotor (Kyocera, SN252, S/N 5K26) was used for this test. Compressor air bypass valves were installed on the rig in order to obtain peak required turbine inlet temperatures without inducing compressor surge. The gasifier ran up to a peak TIT = 1406°C (2563°F) at 96% speed; at 100% speed the peak TIT was 1345°C (2453°F). The ceramic components were in excellent condition following the test.

Because the scroll mount temperatures were lower than expected, the hardware was reassembled with no cooling air supply to the attachment bolts. The rig ran to a peak TIT = 1365°C (2489°F) at 100% speed. Carbon from the burner had passed through the gasifier rotor during this test but did not cause any damage to the rotor or scroll. A post-test inspection revealed that the scroll had developed cracks around the attachment flange.

The third advanced concept Si_3N_4 ceramic scroll (Kyocera, SN252, S/N KX55599) had additional modifications made to the mounting flange. The gasifier was assembled with a 15-bladed Si_3N_4 ceramic rotor (Kyocera, SN252, S/N 5K10) that had not previously been run. The rig ran to TIT = 1200°C (2192°F) at 89% speed, was visually inspected, and then ran to TIT = 1270°C (2320°F) at 90% speed when the rig was shut down by the safety system. Upon inspection, the rotor had come out of the shaft and was destroyed, but the scroll was not damaged. (See section 3.1.3 for a complete failure analysis.) The module was rebuilt with a modified seal system and a 20-bladed Si_3N_4 ceramic rotor (Kyocera, SN252, S/N 5K26). This module ran to TIT = 900°C (1650F) at 80% speed when the rig safety system shut down due to a gasifier speed less than 25% condition. The blades had broken off the rotor and the scroll was severely damaged. (See section 3.1.3 for a complete failure analysis.)

Ceramic Gasifier Rotor Proof Testing. Four ceramic gasifier rotors were proof tested in hot gasifier rigs in 1991. A 20-bladed Si_3N_4 ceramic rotor (N/TRW, NT154, S/N 5S) successfully completed 224 hours of hot gasifier rig testing as discussed above. A 15-bladed Si_3N_4 ceramic rotor (Kyocera, SN252, S/N 5K10) ran for the first time with the third advanced concept scroll and was destroyed after running for 0.8 hours when the rotor/shaft shrink fit came loose during testing (see discussion above). A 15-bladed Si_3N_4 ceramic rotor (Kyocera, SN252, S/N 5K13) was proof tested in an all-metal gasifier assembly. The rotor ran to a peak condition of TIT = 1150°C (2100°F) at 93% speed and accumulated 8.9 total test hours. This rotor will be used in future all-ceramic gasifier tests. A 15-bladed SiC ceramic rotor (CBO, α-SiC, S/N FX78527) failed during the initial start attempt. The rotor failed at 38% speed shortly after the start was initiated. (See section 3.1.3 for a complete failure analysis.)

4.2.4 Regenerator Rig Tests

Objective/Approach

The objective of this activity is to evaluate the suitability of ceramic and metal candidate regenerator materials with pressure tests and cyclic thermal durability tests.

Accomplishments/Results

- Utilized data from Inco Alloys to rank metal regenerator material candidates.
- Inco Alloys' thermal cyclic oxidation tests have ranked IN6262 conventional nickel alloy nearly as good as much more expensive, and difficult forming, MA956.
- Inco will supply IN6262 foil for Allison cyclic oxidation tests.
- Plansee provided a sample of PM2000 ferritic, mechanical alloyed, oxide dispersion strengthened material similar to MA956.
- Allison was unable to corrugate PM2000 foil to the full required height.
- Began effort to determine cause of drooping temperature on regenerator cyclic durability rig.
- Allison cyclic rig troubleshooting and repair continues.

Discussion

Inco Alloys had started a thermal cyclic test for a new metal regenerator candidate material to compare with the best previous candidates tested (Haynes 214 and 230). Allison will not conduct preliminary screening tests on bars but will use Inco results to decide which materials merit the rolling, forming, and diffusion bonding of foil for actual matrix thermal cyclic tests.

Based on their initial trials, the excellent performance of Inco 6262 in their comparative cyclic oxidation tests shows that a much more realistic and demanding Allison cyclic test would be worthwhile. Inco will supply foil for Allison to corrugate.

Allison was unable to corrugate Plansee PM2000 foil to a height greater than 0.022 in. without cracking. A height of 0.029 in. is required. Plansee will provide foil that is in a more fully annealed condition for corrugation.

Allison started a thermal cyclic test on a Corning extruded aluminum silicate sample with negative expansion up to 982°C (1800°F) and probably to 1204°C (2200°F). The test stopped when it was noted that the temperature was dropping during the five seconds full throttle dwell period for the cycle where a constant 982°C (1800°F) should be maintained. An investigation of the control system is in progress to determine the cause. A slow drop in temperature precludes the punishing down shock to idle which should occur at the end of the full throttle dwell. This is not acceptable as a valid test.

Instrumentation of the Allison cyclic rig has suggested valve deterioration to be the cause of droop in the full power dwell temperature. The valves will be replaced, and proper duplication of the engine cycle will be demonstrated. A burner blowout problem, when quench air is introduced to control the cycle, is also being evaluated.

5.2 DURABILITY TESTING

The objective of this activity is to conduct test-bed engine fabrication and testing to verify those advancements in ceramic components that address program performance and durability goals. Ceramic component designs and integrity are to be ultimately verified at maximum engine steady-state and cyclic durability conditions. As the ceramic component technology improves, the test-bed engines are being modified to allow operation up to RPD conditions. Test efforts continue to demonstrate the durability and reliability of the test-bed engines, as well as the ceramic components and designs. Both long-term cyclic and steady-state tests are being performed. Cyclic tests simulate the GM automotive gas turbine driving cycle while steady-state tests are being performed at idle, cruise, and full-power conditions.

5.2.3 Test-Bed Engine Fabrication and Test

5.2.3.1 Test-Bed Engine Fabrication

Objective/Approach

Test-bed engine fabrication supports all engine test activities through instrumentation, build, and repair where necessary (see Section 5.2.3.2). New engine component fabrication supports the design/development efforts to evolve the AGT-5 to a high temperature durability test-bed engine.

Accomplishments/Results

- Supported more than 40 gasifier rig and engine builds.

Discussion

During 1991, all phases of test-bed engine fabrication were supported for both test stand and vehicular engine testing. Over forty engine and gasifier builds were completed including teardown for inspection and reassembly. Other fabrication efforts supported numerous other goals such as high temperature combustion components, instrumentation, and simple brackets.

5.2.3.2 Test-bed Engine Testing

Objective/Approach

Test-bed engine testing is conducted on the dynamometer stand and in vehicles. Dynamometer stand operation is performed for high temperature durability verification of the test-bed and evaluation of ceramic hot flow path components and engine insulation. This testing also supports the ceramic redesign process and evaluates new engine hardware as it becomes available. Test-bed engine testing is performed in a vehicle to evaluate ceramic hot-flow path components in a real-world automotive environment. This ensures that ceramic components' performance and/or durability design criteria, unique to vehicular gas turbine operation, are not overlooked.

Accomplishments/Results

- Supported engine emission test work in the dynamometer cell and in a test-bed vehicle.
- Completed gasifier transient behavior tests.
- Tested the effect of two different ceramic regenerator cores on engine performance.
- Ran a baseline test of a test-bed engine prior to operation in a test-bed vehicle.

Discussion

Emissions Test Work. A test-bed engine ran in the test cell to study the effects of various burner hardware configurations on exhaust emissions. Five different burner configurations (changes to the burner, burner dome, and fuel nozzle) were tested on both DF-1 and M85 fuel at various fuel nozzle atomizing air pressures. One burner configuration was installed into an engine installed in a test-bed vehicle and exhaust emissions were measured on an EPA test cycle on a vehicle dynamometer.

Gasifier Transient Behavior. An integral part of rig and engine testing under the ATTAP durability schedule is the acceleration of the gasifier from idle to peak gasifier speeds. In order to provide consistent acceleration rates between different engine builds, gasifier acceleration tests were run with an all-metal engine to determine the factors that affect the gasifier's transient behavior. Control software routines, fuel pump hardware and electronics, and engine hardware effects were all noted. Important factors are now monitored and controlled to provide consistent gasifier accelerations between different engine and rig builds.

Engine Configuration Optimization. Testing has been performed to determine the optimum parameters desirable for ceramic component operation such as best available compressor diffuser geometry, best air intake geometry and best impeller tip clearance. While these tests were not exhaustive, they were designed to help select the best available hardware to use when engine testing ceramic components.

Engine testing continued in 1991 to determine the best compressor diffuser geometry for overall engine efficiency and surge-free operation. A 24-vane diffuser with modified geometry was tested in a test-bed engine for comparison with the 24-vane and 18-vane diffusers tested in 1990. The modified 24-vane diffuser had performance characteristics very similar to the 18-vane diffuser. The engine utilizing the modified 24-vane diffuser did not surge during gasifier accelerations while the engine assembled with the standard 24-vane diffuser in 1990 had surged. Further testing to determine compressor diffuser effects on engine surge characteristics were discontinued in order to pursue testing in a compressor rig. Compressor rig testing allows the whole operating range of the diffuser and impeller to be evaluated while allowing additional instrumentation to be added with much less difficulty than in an engine.

Air inlet geometry effects on engine operation continued to be evaluated in 1991. Previous test experience with the test-bed engine has shown that air filter orientation can affect engine performance. In order to provide more consistent inlet flow conditions, an inlet housing was fabricated with stationary inlet guide vanes and installed in a test-bed engine. The air inlet filters were rotated to determine the position that most significantly affected engine performance, although the decrease in engine performance was not as great as had been experienced in previous testing. With this filter orientation, back-to-back tests were run with the fixed inlet guide vanes and the standard inlet geometry.

There has been a significant number of impeller tip rubs when testing ceramic and metal components during ATTAP. In order to obtain more information on allowable impeller tip clearances, an impeller shroud was fabricated with wear pegs and installed in an all-metal gasifier assembly. Gasifier accelerations were run from idle to full speed. The impeller did not rub during the testing and the post-test wear peg measurements provided information used in later compressor builds.

Ceramic Regenerator Disk Pressure Drop Test. Test-bed engine tests were carried out to compare the effect on engine performance between Corning wrapped ceramic regenerator disks and NGK extruded, segmented disks. Both sets of regenerator disks were installed into a engine and a baseline power test was run. There was no measurable effect on engine performance between the two tests with different ceramic disks. A baseline test was run with metal regenerators that confirmed the lower pressure drop with metal disks that had been documented in the 1990 Annual Report.

Table XVII.
Total test hours.

	Test hours		
	Pre-1991	1991	Cumulative
Engine test hours	1592	128	1720
Hot rig test hours	852	719	1571
Totals	2444	847	3291

Test-Bed Vehicle Engine Testing. A test-bed engine ran a baseline test in the dynamometer test cell prior to installation in the test-bed vehicle. No problems were noted during the test to peak engine operating temperatures and speeds. After delivery to the vehicle the engine was utilized to check the vehicle modifications made for the turbine engine and to check out the engine and vehicle wiring systems. Several problems with the vehicle/engine plumbing systems and some wiring problems were discovered and resolved. The vehicle and engine then were used to display turbine technology at the 1991 Contractors Coordination Meeting. Total test time in 1991 is shown in Table XVII.

APPENDIX

List of Acronyms

AES	Advanced Engineering Staff
AGT	automotive gas turbine/Advanced Gas Turbine
α	alpha
AS	alumino-silicate
ATTAP	Advanced Turbine Technology Applications Project
BALCO	The Balancing Company
β	beta
BOT	burner outlet temperature
BSFC	brake specific fuel consumption
BU	buildup
CAD	computer-aided design
CBO	The Carborundum Company
C/C	carbon/carbon
CF	centrifugal force
CFD	computational fluid dynamics
CIP	cold isostatic pressing
CNC	computer numerical control
CO	carbon monoxide
CPS	Ceramics Process Systems
CPU	central processing unit
CTAHE	Ceramic Technology for Advanced Heat Engines
CY	calendar year
DFMA	design for manufacturability and assembly
dwg	drawing
DOE	U.S. Department of Energy
DTM	desktop manufacturing
E	elastic modules
EDM	electronic development module (engine controller)
EPA	Environmental Protection Agency
FCM	function control module
FEM	finite element method
FOD	foreign object damage
FPI	fluorescent penetrant inspection
GCC	Garrett Ceramic Components
GM	General Motors
gm/mi	grams per mile
GT	gasifier turbine
GTE	GTE Laboratories Inc.
HC	hydrocarbon
HIP	hot isostatic pressing
hp	horsepower
HP	Hewlett Packard
HTML	High Temperature Materials Laboratory
Hz	Hertz (cycle/second)
I.D.	inner diameter
IEA	International EnergyAgency
I/O	input/output
krpm	thousands of revolutions per minute
ksi	kilopounds per square inch
K_t	theoretical stress concentration factor
kW	kilowatt
LAS	lithium alumino-silicate
LCF	low cycle fatigue
LeRC	NASA Lewis Research Center
ℓ	liter
MAS	magnesium alumino silicate
MAT	mullite aluminum titanate
MOR	modules of rupture
MPa	megapascal
MR	magnetoresistive
NDE	nondestructive evaluation
NGK	NGK-Locke, Inc.
N_1	gasifier speed
NO_x	oxides of nitrogen
N/TRW	Norton/TRW Ceramics
NZP	zirconium phosphate
O.D.	outer diameter
ODS	oxide dispersion strengthen
ORNL	Oak Ridge National Laboratory
POS	probability of survival
ppm	parts per million
psi	pounds per square inch
RDS	see VMS
RIT	rotor inlet temperature
RPD	reference powertrain design
rpm	revolutions per minute
SiC	silicon carbide
Si_3N_4	silicon nitride
SEM	scanning electron microscope
SENB	single edge notched beam
SLS	selective laser sintering
S/N	serial number
Spec	specification
3-D	three-dimensional
TIT	turbine inlet temperature
2-D	two-dimensional
UHC	unburned hydrocarbons
ULEV	ultra low emissions vehicle
VBG	variable burner geometry
VMS	Vehicular Electronic Controller Instrumentation System

v/o	volume percent
V/Vc	surface velocity/critical velocity
w	omega, frequency
WBS	work breakdown structure
x/Cs	blade axial distance/blade axial chord
XEDA	X-ray Energy Dispersive Analysis

1. Report No.	2. Government Accession No.	3. Recipient's Catalog No.
NASA CR-195367		

4. Title and Subtitle
Advanced Turbine Technology Applications Project (ATTAP)--
1991 Annual Report

5. Report Date
December 1992

6. Performing Organization Code

7. Author(s)
Engineering Department, Allison Gas Turbine Division
Advanced Engineering Staff, General Motors Technical Center

8. Performing Organization Report No.
EDR 16624

9. Performing Organization Name and Address
Allison Gas Turbine Division
General Motors Corporation
P.O. Box 420
Indianapolis, IN 46206-0420

10. Work Unit No.

11. Contract or Grant No.
DEN 4-336

12. Sponsoring Agency Name and Address
U.S. Department of Energy
Conservation and Renewable Energy
Office of Transportation Technologies

13. Type of Report and Period Covered
Contractor Report
January - December 1991

14. Sponsoring Agency Code
DOE/NASA

15. Supplementary Notes
Annual Report, prepared under Interagency Agreement DE-A101-85CE50111.
Project Manager P. T. Kerwin, Propulsion Systems Division,
NASA Lewis Research Center, Cleveland, OH 44135

16. Abstract

ATTAP activities during the past year included test-bed engine design and development, ceramic component design, materials and component characterization, ceramic component process development and fabrication, ceramic component rig testing, and test-bed engine fabrication and testing. Significant technical challenges remain, but all areas exhibited progress. Test-bed engine design and development included engine mechanical design, combustion system design, alternate aerodynamic designs of gasifier scrolls, and engine system integration aimed at upgrading the AGT-5 from a 1038°C (1900°F) metal engine to a durable 1372°C (2500°F) structural ceramic component test-bed engine. ATTAP-defined ceramic and associated ceramic/metal component design activities completed include the ceramic gasifier turbine static structure, the ceramic gasifier turbine rotor, ceramic combustors, the ceramic regenerator disk, the ceramic power turbine rotors, the ceramic/metal power turbine static structure. The material and component characterization efforts included the testing and evaluation of seven candidate materials and three development components. Ceramic component process development and fabrication proceeded for the gasifier turbine rotor, gasifier turbine scroll, gasifier turbine vanes and vane platform, extruded regenerator disks, and thermal insulation. Component rig activities included the development of both rigs and the necessary test procedures, and conduct of rig testing of the ceramic components and assemblies. Test-bed engine fabrication, testing, and development supported improvements in ceramic component technology that permit the achievement of both program performance and durability goals. Total test time in 1991 amounted to 847 hours, of which 128 hours were engine testing, and 719 were hot rig testing.

17. Key Words (Suggested by Author(s))
automotive gas turbine, ceramic components,
structural ceramics, engine configuration rotors,
alternate propulsion systems, vehicular propulsion,
alternate fuels, emissions, improved fuel economy

18. Distribution Statement
Unclassified, unlimited

19. Security Classif. (of this report)	20. Security Classif. (of this page)	21. No. of Pages	22. Price*
Unclassified	Unclassified	90	

*For sale by the National Technical Information Service, Springfield, Virginia 22151

REPORT DOCUMENTATION PAGE

Form Approved
OMB No. 0704-0188

1. AGENCY USE ONLY (*Leave blank*)

2. REPORT DATE
DECEMBER 1992

3. REPORT TYPE AND DATES COVERED
Final Contractor Report

4. TITLE AND SUBTITLE
Advanced Turbine Technology Applications Project (ATTAP) 1991 Annual Report

5. FUNDING NUMBERS
WU-778-32-21
DEN3-336

6. AUTHOR(S)
Engineering Department

7. PERFORMING ORGANIZATION NAME(S) AND ADDRESS(ES)
Allison Engine Company
P.O. Box 420
Indianapolis, Indiana 46206–0420

8. PERFORMING ORGANIZATION REPORT NUMBER
E–9037

9. SPONSORING/MONITORING AGENCY NAME(S) AND ADDRESS(ES)
National Aeronautics and Space Administration
Lewis Research Center
Cleveland, Ohio 44135–3191

10. SPONSORING/MONITORING AGENCY REPORT NUMBER
NASA CR–195367
DOE/NASA/0336–4

11. SUPPLEMENTARY NOTES
Project Manager, Paul T. Kerwin, Propulsion Systems Division, NASA Lewis Research Center, organization code 2703, (216) 433–3409.

12a. DISTRIBUTION/AVAILABILITY STATEMENT
Unclassified - Unlimited
Subject Category N/A
DOE Category

12b. DISTRIBUTION CODE

13. ABSTRACT (*Maximum 200 words*)

ATTAP activities during the past year included test-bed engine design and development, ceramic component design, materials and component characterization, ceramic component process development and fabrication, ceramic component rig testing, and test-bed engine fabrication and testing. Significant technical challenges remain, but all areas exhibited progress. Test-bed engine design and development included engine mechanical design, combustion system design, alternate aerodynamic designs of gasifier scrolls, and engine system integration aimed at upgrading the AGT-5 from a 1038°C (1900°F) metal engine to a durable 1372°C (2500°F) structural ceramic component test-bed engine. ATTAP-defined ceramic and associated ceramic/metal component design activities completed include the ceramic gasifier turbine static structure, the ceramic gasifier turbine rotor, ceramic combustors, the ceramic regenerator disk, the ceramic power turbine rotors, the ceramic/metal power turbine static structure. The material and component characterization efforts included the testing and evaluation of seven candidate materials and three development components. Ceramic component process development and fabrication proceeded for the gasifier turbine rotor, gasifier turbine scroll, gasifier turbine vanes and vane platform, extruded regenerator disks, and thermal insulation. Component rig activities included the development of both rigs and the necessary test procedures, and conduct of rig testing of the ceramic components and assemblies. Test-bed engine fabrication, testing, and development supported improvements in ceramic component technology that permit the achievement of both program performance and durability goals. Total test time in 1991 amounted to 847 hours, of which 128 hours were engine testing, and 719 were hot rig testing.

14. SUBJECT TERMS
Automotive; Small gas turbine; Ceramic components; Structural ceramics; Alternative fuels; Emissions

15. NUMBER OF PAGES
96

16. PRICE CODE
A05

17. SECURITY CLASSIFICATION OF REPORT	18. SECURITY CLASSIFICATION OF THIS PAGE	19. SECURITY CLASSIFICATION OF ABSTRACT	20. LIMITATION OF ABSTRACT
Unclassified	Unclassified	Unclassified	